A detailed kinetic modeling study of aromatics formation in laminar premixed acetylene and ethylene flames

ARTICLE *in* COMBUSTION AND FLAME · JULY 1997

Impact Factor: 3.08 · DOI: 10.1016/S0010-2180(97)00068-0

2 AUTHORS, INCLUDING:

Hai Wang
Stanford University
163 PUBLICATIONS **6,431** CITATIONS

A Detailed Kinetic Modeling Study of Aromatics Formation in Laminar Premixed Acetylene and Ethylene Flames

HAI WANG*

Department of Mechanical Engineering, University of Delaware, Newark, DE 19716-3140

and

MICHAEL FRENKLACH*

Department of Mechanical Engineering, University of California at Berkeley, Berkeley, CA 94720-1740

A computational study was performed for the formation and growth of polycyclic aromatic hydrocarbons (PAHs) in laminar premixed acetylene and ethylene flames. A new detailed reaction mechanism describing fuel pyrolysis and oxidation, benzene formation, and PAH mass growth and oxidation is presented and critically tested. It is shown that the reaction model predicts reasonably well the concentration profiles of major and intermediate species and aromatic molecules in a number of acetylene and ethylene flames reported in the literature. It is demonstrated that reactions of n-C_4H_x + C_2H_2 leading to the formation of one-ring aromatics are as important as the propargyl recombination, and hence must be included in kinetic modeling of PAH formation in hydrocarbon flames. It is further demonstrated that the mass growth of PAHs can be accounted for by the previously proposed H-abstraction–C_2H_2-addiction mechanism.

INTRODUCTION

Considerable progress has been made in recent years on the detailed reaction kinetics of aromatics formation, growth, and oxidation in hydrocarbon combustion [1–28]. Due to its fundamental and practical importance, the mechanism of benzene formation in particular has been intensely studied [e.g., 19, 20, 23, 24, 29–31]. Despite many uncertainties concerning detailed reaction pathways, it is now possible to predict benzene production in hydrocarbon flames with a reasonable degree of accuracy. On the other hand, the mass growth of aromatic species from benzene to polycyclic aromatic hydrocarbons (PAHs) has received considerably less attention. Because PAHs are known products of fuel-rich combustion and are the most likely precursors to soot [1, 32], a basic understanding of PAH growth kinetics is of significant interest from both fundamental and practical standpoints. In this paper, we report a detailed reaction mechanism of PAH formation and growth. The reported reaction mechanism was developed based on the knowledge built upon the previous shock-tube [9–11, 13] and flame [12, 16–19, 23] modeling studies, and a set of recently evaluated or theoretically calculated *self-consistent* thermodynamic [33], transport [34], and chemical kinetic [24] data of aromatic species.

The reaction mechanism is tested against the PAH concentration profiles in a number of sooting or near-sooting laminar burner-stabilized flat flames. These flames include a 20-torr near-sooting acetylene flame [19], a 90-torr sooting acetylene flame [3], and an atmospheric sooting ethylene flame [15, 16]. It will also be shown that the proposed reaction mechanism is capable of predicting quantitatively or near quantitatively the formation and growth of PAHs in these flames. Based on the numerical analysis, we demonstrate that both $C_2 + C_4$ and $C_3H_3 + C_3H_3$ channels to aromatics are feasible, depending on particular flame conditions. In addition, the reversibility of the $C_3H_3 + C_3H_3$ reactions leading to benzene or phenyl is discussed with indication that these reactions are unlikely to be elementary steps at high temperatures. We will also address several other important issues, including remaining uncertainties in the flame chemistry of aromatics.

*Corresponding author.

COMBUSTION AND FLAME 110: 173–221 (1997)

Published by Elsevier Science Inc.

0010-2180/97/$17.00
PII S0010-2180(97)00068-0

COMPUTER MODEL

The detailed reaction mechanism consists of 527 reactions and 99 chemical species. The reactions and their forward rate coefficients are given in Table 1. The species nomenclature is essentially the same as that reported in Refs. 9 and 10. The subsequent minor modifications are documented in Table 1 of Ref. 24. For a limited number of PAH species, there exist radical isomers that differ by the position of the radical site in the aromatic structure. Because such radical isomers often have different thermochemical properties [33] and exhibit different reactivity [24], they are differentiated in the present reaction mechanism. For such cases, an additional integer is attached to the species name which specifies the radical position. For example, A_3-*i* is a phenanthryl radical with the unpaired electron located at the *i*th carbon atom. The numbering system follows the IUPAC nomenclature as documented in Fig. 2 of Ref. 33.

The reverse rate coefficients were calculated via equilibrium constants. The thermodynamic data were taken from GRI-Mech 1.2 [35], and for species not included their properties are presented in Table 2. Details concerning the sources and methods of estimation of the thermodynamic data can be found in our previous publications [24, 33]. Every effort was made to ensure self-consistency of the reaction rate coefficients and thermodynamic data used in the present reaction mechanism.

The rate coefficients were either taken from literature or estimated based upon analogous reactions. The sources of the rate coefficient expressions are provided in the last column of Table 1. The pressure dependence of the reaction rate coefficients was carefully taken into account. The rate coefficients of most unimolecular reactions are given in Troe's fall-off form [66]. The rate coefficients of other unimolecular reactions, along with the bimolecular chemically activated reactions, are given at several pressure values of interest. Below, the key points concerning the reaction mechanism are discussed.

C_1H_x and C_2H_x Reactions

The H/O, C_1H_x, and C_2H_x submechanism (reactions R1–R171) was taken from GRI-Mech 1.2 [35]. Because the GRI-Mech was optimized for natural-gas combustion, the following minor modifications were made to better describe acetylene and ethylene oxidation in flames. First, the product channel of the reaction $CH_2 + O_2$ was changed from HCO + OH to $CO_2 + H + H$ to improve the H-atom prediction in the 20-torr acetylene flame of Westmoreland et al. [19]. Second, the rate coefficient of reaction $C_2H + H_2 \rightleftharpoons C_2H_2 + H$ (R50) was updated on the basis of newly reported experimental data [36, 37]. Third, based on the QRRK analysis of Bozzelli and Dean [38], three product channels were assigned to the reaction $C_2H_3 + O_2$, including $C_2H_2 + HO_2$ (R154), $C_2H_3O + O$ (R155), and HCO + CH_2O (R156), with their rate coefficient expressions also taken from Ref. 38.

Additional C_1H_x and C_2H_x reactions were included in the reaction mechanism. The C_2O chemistry was taken from Miller and Bowman [44]. The chemistry of the vinyoxy (C_2H_3O) radicals is practically unknown. To avoid severe C_2H_3O buildup, its unimolecular dissociation (−R177) and its reactions with H, O, and OH (R178–181) were included and their rate parameters estimated.

Reactions of Nonaromatic Species

The following reactions are included in the reaction mechanism to account for C_3H_2 and C_3H_3 radical production:

$$C_2H_2 + CH \rightleftharpoons C_3H_2 + H, \quad \text{(R185)}$$

$$C_2H_2 + CH_2 \rightleftharpoons C_3H_3 + H, \quad \text{(R186)}$$

$$C_2H_2 + CH_2^* \rightleftharpoons C_3H_3 + H, \quad \text{(R187)}$$

where CH_2 and CH_2^* are the triplet and singlet methylenes, respectively. The rate coefficients of reactions

$$C_2H_2 + C_2H \rightleftharpoons n\text{-}C_4H_3, \quad \text{(R191)}$$

$$C_2H_2 + C_2H \rightleftharpoons i\text{-}C_4H_3, \quad \text{(R192)}$$

$$C_4H_2 + H \rightleftharpoons n\text{-}C_4H_3, \quad \text{(R241)}$$

TABLE 1

Reaction Mechanism

No.	Reactions[b]	$k = AT^n \exp(-E/RT)$[a] A	n	E	Comments/ References
	Reactions of H_2/O_2				
1	$H + O_2 \rightleftharpoons O + OH$	8.30(+13)		14.413	[35]
2	$O + H_2 \rightleftharpoons H + OH$	5.00(+4)	2.67	6.29	[35]
3	$OH + H_2 \rightleftharpoons H + H_2O$	2.16(+8)	1.51	3.43	[35]
4	$OH + OH \rightleftharpoons O + H_2O$	3.57(+4)	2.40	−2.11	[35]
5	$H + H + M \rightleftharpoons H_2 + M$	1.00(+18)	−1.0		*c*,[35]
6	$H + OH + M \rightleftharpoons H_2O + M$	2.20(+22)	−2.0		*d*,[35]
7	$O + H + M \rightleftharpoons OH + M$	5.00(+17)	−1.0		*e*,[35]
8	$O + O + M \rightleftharpoons O_2 + M$	1.20(+17)	−1.0		*f*,[35]
9	$H + O_2 + M \rightleftharpoons HO_2 + M$	2.80(+18)	−0.86		*g*,[35]
10	$OH + OH(+M) \rightleftharpoons H_2O_2(+M)$	7.40(+13)	−0.37		k_∞,[35]
		2.30(+18)	−0.9	−1.7	$k_0/[M']$, *h*
	$a = 0.7346, T^{***} = 94, T^* = 1756, T^{**} = 5182$				*i*
	Reactions of HO_2				
11	$HO_2 + H \rightleftharpoons O + H_2O$	3.97(+12)		0.671	[35]
12	$OH_2 + H \rightleftharpoons O_2 + H_2$	2.80(+13)		1.068	[35]
13	$HO_2 + H \rightleftharpoons OH + OH$	1.34(+14)		0.635	[35]
14	$HO_2 + O \rightleftharpoons OH + O_2$	2.00(+13)			[35]
15	$HO_2 + OH \rightleftharpoons O_2 + H_2O$	2.90(+13)		−0.5	[35]
16	$HO_2 + HO_2 \rightleftharpoons O_2 + H_2O_2$	1.30(+11)		−1.63	[35]
17	$HO_2 + HO_2 \rightleftharpoons O_2 + H_2O_2$	4.20(+14)		12.0	[35]
	Reactions of H_2O_2				
18	$H_2O_2 + H \rightleftharpoons HO_2 + H_2$	1.21(+7)	2.0	5.2	[35]
19	$H_2O_2 + H \rightleftharpoons OH + H_2O$	1.00(+13)		3.6	[35]
20	$H_2O_2 + O \rightleftharpoons OH + HO_2$	9.63(+6)	2.0	4.0	[35]
21	$H_2O_2 + OH \rightleftharpoons HO_2 + H_2O$	1.75(+12)		0.32	[35]
22	$H_2O_2 + OH \rightleftharpoons HO_2 + H_2O$	5.80(+14)		9.56	[35]
	Reactions of CO/CO_2				
23	$CO + O + M \rightleftharpoons CO_2 + M$	6.02(+14)		3.0	*j*,[35]
24	$CO + OH \rightleftharpoons CO_2 + H$	4.76(+7)	1.228	0.07	[35]
25	$CO + H_2(+M) \rightleftharpoons CH_2O(+M)$	4.30(+7)	1.5	79.6	k_∞,[35]
		5.07(+27)	−3.42	84.35	$k_0/[M']$, *h*
	$a = 0.9320, T^{***} = 197, T^* = 1540, T^{**} = 10.3$				*i*
26	$CO + O_2 \rightleftharpoons CO_2 + O$	2.50(+12)		47.8	[35]
27	$CO + HO_2 \rightleftharpoons CO_2 + OH$	1.50(+14)		23.6	[35]
	Reactions of C				
28	$C + OH \rightleftharpoons CO + H$	5.00(+13)			[35]
29	$C + O_2 \rightleftharpoons CO + O$	5.80(+13)		0.576	[35]
	Reactions of CH				
30	$CH + H \rightleftharpoons C + H_2$	1.10(+14)			[35]
31	$CH + O \rightleftharpoons CO + H$	5.70(+13)			[35]
32	$CH + OH \rightleftharpoons HCO + H$	3.00(+13)			[35]
33	$CH + H_2 \rightleftharpoons CH_2 + H$	1.10(+8)	1.79	1.67	[35]
34	$CH + H_2O \rightleftharpoons CH_2O + H$	5.71(+12)		−0.755	[35]
35	$CH + O_2 \rightleftharpoons HCO + O$	3.30(+13)			[35]
36	$CH + CO(+M) \rightleftharpoons HCCO(+M)$	5.00(+13)			k_∞,[35]
		2.69(+28)	−3.74	1.936	$k_0/[M']$, *h*
	$a = 0.5757, T^{***} = 237, T^* = 1652, T^{**} = 5069$				*i*
37	$CH + CO_2 \rightleftharpoons HCO + CO$	3.40(+12)		0.69	[35]

TABLE 1 (Continued)

Reaction Mechanism

c No.	Reactions[b]	$k = AT^n \exp(-E/RT)$[a] A	n	E	Comments/ References
	Reactions of HCO				
38	$HCO + H(+M) \rightleftharpoons CH_2O(+M)$	1.09(+12)	0.48	−0.26	k_∞,[35]
		1.35(+24)	−2.57	1.425	k_0/[M'], *h*
	$a = 0.7824, T^{***} = 271, T^* = 2755, T^{**} = 6570$				*i*
39	$HCO + H \rightleftharpoons CO + H_2$	7.34(+13)			[35]
40	$HCO + O \rightleftharpoons CO + OH$	3.00(+13)			[35]
41	$HCO + O \rightleftharpoons CO_2 + H$	3.00(+13)			[35]
42	$HCO + OH \rightleftharpoons CO + H_2O$	5.00(+13)			[35]
43	$HCO + M \rightleftharpoons CO + H + M$	1.87(+17)	−1.0	17.0	*e*,[35]
44	$HCO + O_2 \rightleftharpoons CO + HO_2$	7.60(+12)		0.4	[35]
	Reactions of CH_2				
45	$CH_2 + H(+M) \rightleftharpoons CH_3(+M)$	2.50(+16)	−0.8		k_∞,[35]
		3.20(+27)	−3.14	1.23	k_0/[M'], *h*
	$a = 0.68, T^{***} = 78, T^* = 1995, T^{**} = 5590$				*i*
46	$CH_2 + O \rightleftharpoons HCO + H$	8.00(+13)			[35]
47	$CH_2 + OH \rightleftharpoons CH_2O + H$	2.00(+13)			[35]
48	$CH_2 + OH \rightleftharpoons CH + H_2O$	1.13(+7)	2.0	3.0	[35]
49	$CH_2 + H_2 \rightleftharpoons H + CH_3$	5.00(+5)	2.0	7.23	[35]
50	$CH_2 + O_2 \rightleftharpoons CO_2 + H + H$	1.32(+13)		1.5	*k*,[35]
51	$CH_2 + HO_2 \rightleftharpoons CH_2O + OH$	2.00(+13)			[35]
52	$CH_2 + C \rightleftharpoons C_2H + H$	5.00(+13)			[35]
53	$CH_2 + CO(+M) \rightleftharpoons CH_2CO(+M)$	8.10(+11)	0.5	4.51	k_∞,[35]
		2.69(+33)	−5.11	7.095	k_0/[M'], *h*
	$a = 0.5907, T^{***} = 275, T^* = 1226, T^{**} = 5185$				*i*
54	$CH_2 + CH \rightleftharpoons C_2H_2 + H$	4.00(+13)			[35]
55	$CH_2 + CH_2 \rightleftharpoons C_2H_2 + H_2$	3.20(+13)			[35]
	Reactions of CH_2*				
56	$CH_2^* + N_2 \rightleftharpoons CH_2 + N_2$	1.50(+13)		0.6	[35]
57	$CH_2^* + Ar \rightleftharpoons CH_2 + Ar$	9.00(+12)		0.6	[35]
58	$CH_2^* + H \rightleftharpoons CH + H_2$	3.00(+13)			[35]
59	$CH_2^* + O \rightleftharpoons CO + H_2$	1.50(+13)			[35]
60	$CH_2^* + O \rightleftharpoons HCO + H$	1.50(+13)			[35]
61	$CH_2^* + OH \rightleftharpoons CH_2O + H$	3.00(+13)			[35]
62	$CH_2^* + H_2 \rightleftharpoons CH_3 + H$	7.00(+13)			[35]
63	$CH_2^* + O_2 \rightleftharpoons H + OH + CO$	2.80(+13)			[35]
64	$CH_2^* + O_2 \rightleftharpoons CO + H_2O$	1.20(+13)			[35]
65	$CH_2^* + H_2O(+M) \rightleftharpoons CH_3OH(+M)$	2.00(+13)			k_∞,[35]
		2.70(+38)	−6.3	3.1	k_0/[M'], *l*
	$a = 0.1507, T^{***} = 134, T^* = 2383, T^{**} = 7265$				*i*
66	$CH_2^* + H_2O \rightleftharpoons CH_2 + H_2O$	3.00(+13)			[35]
67	$CH_2^* + CO \rightleftharpoons CH_2 + CO$	9.00(+12)			[35]
68	$CH_2^* + CO_2 \rightleftharpoons CH_2 + CO_2$	7.00(+12)			[35]
69	$CH_2^* + CO_2 \rightleftharpoons CH_2O + CO$	1.40(+13)			[35]
	Reactions of CH_2O				
70	$CH_2O + H(+M) \rightleftharpoons CH_2OH(+M)$	5.40(+11)	0.454	3.6	k_∞,[35]
		1.27(+32)	−4.820	6.53	k_0/[M'], *l*
	$a = 0.7187, T^{***} = 103, T^* = 1291, T^{**} = 4160$				*i*
71	$CH_2O + H(+M) \rightleftharpoons CH_3O(+M)$	5.40(+11)	0.454	2.6	k_∞,[35]
		2.20(+30)	−4.8	5.56	k_0/[M'], *l*
	$a = 0.758, T^{***} = 94, T^* = 1555, T^{**} = 4200$				*i*

TABLE 1 (Continued)

Reaction Mechanism

No.	Reactions[b]	$k = AT^n \exp(-E/RT)$[a] A	n	E	Comments/ References
72	$CH_2O + H \rightleftharpoons HCO + H_2$	2.30(+10)	1.05	3.275	[35]
73	$CH_2O + O \rightleftharpoons HCO + OH$	3.90(+13)		3.54	[35]
74	$CH_2O + OH \rightleftharpoons HCO + H_2O$	3.43(+9)	1.18	−0.447	[35]
75	$CH_2O + O_2 \rightleftharpoons HCO + HO_2$	1.00(+14)		40.0	[35]
76	$CH_2O + HO_2 \rightleftharpoons HCO + H_2O_2$	1.00(+12)		8.0	[35]
77	$CH_2O + CH \rightleftharpoons CH_2CO + H$	9.46(+13)		−0.515	[35]
	Reactions of CH_3				
78	$CH_3 + H(+M) \rightleftharpoons CH_4(+M)$	1.27(+16)	−0.63	0.383	k_∞, [35]
		2.477(+33)	−4.760	2.44	$k_0/[M']$, *h*
	$a = 0.783$, $T^{***} = 74$, $T^* = 2941$, $T^{**} = 6964$				*i*
79	$CH_3 + O \rightleftharpoons CH_2O + H$	8.43(+13)			[35]
80	$CH_3 + OH(+M) \rightleftharpoons CH_3OH(+M)$	6.30(+13)			k_∞, [35]
		2.70(+38)	−6.3	3.1	$k_0/[M']$, *l*
	$a = 0.2105$, $T^{***} = 83.5$, $T^* = 5398$, $T^{**} = 8370$				*i*
81	$CH_3 + OH \rightleftharpoons CH_2 + H_2O$	5.60(+7)	1.6	5.42	[35]
82	$CH_3 + OH \rightleftharpoons CH_2^* + H_2O$	2.50(+13)			[35]
83	$CH_3 + O_2 \rightleftharpoons O + CH_3O$	2.68(+13)		28.8	[35]
84	$CH_3 + O_2 \rightleftharpoons OH + CH_2O$	3.60(+10)		8.94	[35]
85	$CH_3 + HO_2 \rightleftharpoons CH_4 + O_2$	1.00(+12)			[35]
86	$CH_3 + HO_2 \rightleftharpoons CH_3O + OH$	2.00(+13)			[35]
87	$CH_3 + H_2O_2 \rightleftharpoons CH_4 + HO_2$	2.45(+4)	2.47	5.18	[35]
88	$CH_3 + C \rightleftharpoons C_2H_2 + H$	5.00(+13)			[35]
89	$CH_3 + CH \rightleftharpoons C_2H_3 + H$	3.00(+13)			[35]
90	$CH_3 + HCO \rightleftharpoons CH_4 + CO$	2.65(+13)			[35]
91	$CH_3 + CH_2O \rightleftharpoons CH_4 + HCO$	3.32(+3)	2.81	5.86	[35]
92	$CH_3 + CH_2 \rightleftharpoons C_2H_4 + H$	4.00(+13)			[35]
93	$CH_3 + CH_2^* \rightleftharpoons C_2H_4 + H$	1.20(+13)		−0.57	[35]
94	$CH_3 + CH_3(+M) \rightleftharpoons C_2H_6(+M)$	2.12(+16)	−0.97	0.62	k_∞, [35]
		1.77(+50)	−9.67	6.22	$k_0/[M']$, *h*
	$a = 0.5325$, $T^{***} = 151$, $T^* = 1038$, $T^{**} = 4970$				*i*
95	$CH_3 + CH_3 \rightleftharpoons H + C_2H_5$	4.99(+12)	0.1	10.6	[35]
	Reactions of CH_3O/CH_2OH				
96	$CH_3O + H(+M) \rightleftharpoons CH_3OH(+M)$	5.00(+13)			k_∞, [35]
		8.60(+28)	−4.0	3.025	$k_0/[M']$, *l*
	$a = 0.8902$, $T^{***} = 144$, $T^* = 2838$, $T^{**} = 45{,}569$				*i*
97	$CH_3O + H \rightleftharpoons CH_2OH + H$	3.40(+6)	1.6		[35]
98	$CH_3O + H \rightleftharpoons CH_2O + H_2$	2.00(+13)			[35]
99	$CH_3O + H \rightleftharpoons CH_3 + OH$	3.20(+13)			[35]
100	$CH_3O + H \rightleftharpoons CH_2^* + H_2O$	1.60(+13)			[35]
101	$CH_3O + O \rightleftharpoons CH_2O + OH$	1.00(+13)			[35]
102	$CH_3O + OH \rightleftharpoons CH_2O + H_2O$	5.00(+12)			[35]
103	$CH_3O + O_2 \rightleftharpoons CH_2O + HO_2$	4.28(−13)	7.6	−3.53	[35]
104	$CH_2OH + H(+M) \rightleftharpoons CH_3OH(+M)$	1.80(+13)			k_∞, [35]
		3.00(+31)	−4.8	3.3	$k_0/[M']$, *l*
	$a = 0.7679$, $T^{***} = 338$, $T^* = 1812$, $T^{**} = 5081$				*i*
105	$CH_2OH + H \rightleftharpoons CH_2O + H_2$	2.00(+13)			[35]
106	$CH_2OH + H \rightleftharpoons CH_3 + OH$	1.20(+13)			[35]
107	$CH_2OH + H \rightleftharpoons CH_2^* + H_2O$	6.00(+12)			[35]
108	$CH_2OH + O \rightleftharpoons CH_2O + OH$	1.00(+13)			[35]
109	$CH_2OH + OH \rightleftharpoons CH_2O + H_2O$	5.00(+12)			[35]
110	$CH_2OH + O_2 \rightleftharpoons CH_2O + HO_2$	1.80(+13)		0.9	[35]

TABLE 1 (Continued)

Reaction Mechanism

No.	Reactions[b]	$k = AT^n \exp(-E/RT)$[a] A	n	E	Comments/ References
	Reactions of CH_4				
111	$CH_4 + H \rightleftharpoons CH_3 + H_2$	6.60(+8)	1.62	10.84	[35]
112	$CH_4 + O \rightleftharpoons CH_3 + OH$	1.02(+9)	1.5	8.6	[35]
113	$CH_4 + OH \rightleftharpoons CH_3 + H_2O$	1.00(+8)	1.6	3.12	[35]
114	$CH_4 + CH \rightleftharpoons C_2H_4 + H$	6.00(+13)			[35]
115	$CH_4 + CH_2 \rightleftharpoons CH_3 + CH_3$	2.46(+6)	2.0	8.27	[35]
116	$CH_4 + CH_2^* \rightleftharpoons CH_3 + CH_3$	1.60(+13)		−0.57	[35]
	Reactions of CH_3OH				
117	$CH_3OH + H \rightleftharpoons CH_2OH + H_2$	1.70(+7)	2.1	4.87	[35]
118	$CH_3OH + H \rightleftharpoons CH_3O + H_2$	4.20(+6)	2.1	4.87	[35]
119	$CH_3OH + O \rightleftharpoons CH_2OH + OH$	3.88(+5)	2.5	3.1	[35]
120	$CH_3OH + O \rightleftharpoons CH_3O + OH$	1.30(+5)	2.5	5.0	[35]
121	$CH_3OH + OH \rightleftharpoons CH_2OH + H_2O$	1.44(+6)	2.0	−0.84	[35]
122	$CH_3OH + OH \rightleftharpoons CH_3O + H_2O$	6.30(+6)	2.0	1.5	[35]
123	$CH_3OH + CH_3 \rightleftharpoons CH_2OH + CH_4$	3.00(+7)	1.5	9.94	[35]
124	$CH_3OH + CH_3 \rightleftharpoons CH_3O + CH_4$	1.00(+7)	1.5	9.94	[35]
	Reactions of C_2H				
125	$C_2H + H(+M) \rightleftharpoons C_2H_2(+M)$	1.00(+17)	−1.0		k_∞, [35]
		3.75(+33)	−4.8	1.9	$k_0/[M']$, *h*
	$a = 0.6464, T^{***} = 132, T^* = 1315, T^{**} = 5566$				*i*
126	$C_2H + O \rightleftharpoons CH + CO$	5.00(+13)			[35]
127	$C_2H + OH \rightleftharpoons H + HCCO$	2.00(+13)			[35]
128	$C_2H + O_2 \rightleftharpoons HCO + CO$	5.00(+13)		1.5	[35]
129	$C_2H + H_2 \rightleftharpoons H + C_2H_2$	4.90(+5)	2.5	0.56	*m*
	Reactions of HCCO				
130	$HCCO + H \rightleftharpoons CH_2^* + CHO$	1.00(+14)			[35]
131	$HCCO + O \rightleftharpoons H + CO + CO$	1.00(+14)			[35]
132	$HCCO + O_2 \rightleftharpoons OH + CO + CO$	1.60(+12)		0.854	[35]
133	$HCCO + CH \rightleftharpoons C_2H_2 + CO$	5.00(+13)			[35]
134	$HCCO + CH_2 \rightleftharpoons C_2H_3 + CO$	3.00(+13)			[35]
135	$HCCO + HCCO \rightleftharpoons C_2H_2 + CO + CO$	1.00(+13)			[35]
	Reactions of C_2H_2				
136	$C_2H_2 + H(+M) \rightleftharpoons C_2H_3(+M)$	5.60(+12)		2.4	k_∞, [35]
		3.80(+40)	−7.27	7.22	$k_0/[M']$, *h*
	$a = 0.7507, T^{***} = 98.5, t^* = 1302, T^{**} = 4167$				*i*
137	$C_2H_2 + O \rightleftharpoons HCCO + H$	1.02(+7)	2.0	1.9	[35]
138	$C_2H_2 + O \rightleftharpoons C_2H + OH$	4.60(+19)	−1.41	28.95	[35]
139	$C_2H_2 + O \rightleftharpoons CH_2 + CO$	1.02(+7)	2.0	1.9	[35]
140	$C_2H_2 + OH \rightleftharpoons CH_2CO + H$	2.18(−4)	4.5	−1.0	[35]
141	$C_2H_2 + OH \rightleftharpoons HCCOH + H$	5.04(+5)	2.3	13.5	[35]
142	$C_2H_2 + OH \rightleftharpoons C_2H + H_2O$	3.37(+7)	2.0	14.0	[35]
143	$C_2H_2 + OH \rightleftharpoons CH_3 + CO$	4.83(−4)	4.0	−2.0	[35]
	Reactions of $CH_2CO/HCCOH$				
144	$CH_2CO + H \rightleftharpoons HCCO + H_2$	5.00(+13)		8.0	[35]
145	$CH_2CO + H \rightleftharpoons CH_3 + CO$	1.13(+13)		3.428	[35]
146	$CH_2CO + O \rightleftharpoons HCCO + OH$	1.00(+13)		8.0	[35]
147	$CH_2CO + O \rightleftharpoons CH_2 + CO_2$	1.75(+12)		1.35	[35]
148	$CH_2CO + OH \rightleftharpoons HCCO + H_2O$	7.50(+12)		2.0	[35]
149	$HCCOH + H \rightleftharpoons CH_2CO + H$	1.00(+13)			[35]

TABLE 1 (Continued)

Reaction Mechanism

No.	Reactions[b]	$k = AT^n \exp(-E/RT)$[a] A	n	E	Comments/ References
		Reactions of C_2H_3			
150	$C_2H_3 + H(+M) \rightleftharpoons C_2H_4(+M)$	6.08(+12)	0.27	0.28	k_∞, [35]
		1.40(+30)	−3.86	3.32	$k_0/[M']$, *h*
	$a = 0.7820, T^{***} = 207.5, T^* = 2663, T^{**} = 6095$				*i*
151	$C_2H_3 + H \rightleftharpoons C_2H_2 + H_2$	3.00(+13)			[35]
152	$C_2H_3 + O \rightleftharpoons CH_2CO + H$	3.00(+13)			[35]
153	$C_2H_3 + OH \rightleftharpoons C_2H_2 + H_2O$	5.00(+12)			[35]
154	$C_2H_3 + O_2 \rightleftharpoons C_2H_2 + HO_2$	1.66(+14)	−0.83	2.54	[38]
155	$C_2H_3 + O_2 \rightleftharpoons C_2H_3O + O$	2.50(+12)	0.057	0.95	20, 90 torr, [38]
		1.24(+13)	−0.12	1.696	760 torr
156	$C_2H_3 + O_2 \rightleftharpoons HCO + CH_2O$	1.64(+21)	−2.78	2.523	20, 90 torr, [38]
		8.60(+21)	−2.97	3.32	760 torr
		Reactions of C_2H_4			
157	$C_2H_4(+M) \rightleftharpoons H_2 + C_2H_2(+M)$	8.00(+12)	0.44	88.77	k_∞, [35]
		7.00(+50)	−9.31	99.86	$k_0/[M']$, *h*
	$a = 0.7345, T^{***} = 180, T^* = 1035, t^{**} = 5417$				*i*
158	$C_2H_4 + H(+M) \rightleftharpoons C_2H_5(+M)$	1.08(+12)	0.454	1.82	k_∞, [35]
		1.20(+42)	−7.62	6.97	$k_0/[M']$, *h*
	$a = 0.9753, T^{***} = 210, T^* = 987, T^{**} = 4374$				
159	$C_2H_4 + H \rightleftharpoons C_2H_3 + H_2$	1.33(+6)	2.53	12.24	[35]
160	$C_2H_4 + O \rightleftharpoons CH_3 + HCO$	1.92(+7)	1.83	0.22	[35]
161	$C_2H_4 + OH \rightleftharpoons C_2H_3 + H_2O$	3.60(+6)	2.0	2.5	[35]
162	$C_2H_4 + CH_3 \rightleftharpoons C_2H_3 + CH_4$	2.27(+5)	2.0	9.2	[35]
		Reactions of C_2H_5			
163	$C_2H_5 + H(+M) \rightleftharpoons C_2H_6(+M)$	5.21(+17)	−0.99	1.58	k_∞, [35]
		1.99(+41)	−7.08	6.685	$k_0/[M']$, *h*
	$a = 0.8422, T^{***} = 125, T^* = 2219, T^{**} = 6882$				*i*
164	$C_2H_5 + H \rightleftharpoons C_2H_4 + H_2$	2.00(+12)			[35]
165	$C_2H_5 + O \rightleftharpoons CH_3 + CH_2O$	1.32(+14)			[35]
166	$C_2H_5 + O_2 \rightleftharpoons C_2H_4 + HO_2$	8.40(+11)		3.875	[35]
		Reactions of C_2H_6			
167	$C_2H_6 + H \rightleftharpoons C_2H_5 + H_2$	1.15(+8)	1.9	7.53	[35]
168	$C_2H_6 + O \rightleftharpoons C_2H_5 + OH$	8.98(+7)	1.92	5.69	[35]
169	$C_2H_6 + OH \rightleftharpoons C_2H_5 + H_2O$	3.54(+6)	2.12	0.87	[35]
170	$C_2H_6 + CH_2^* \rightleftharpoons C_2H_5 + CH_3$	4.00(+13)		−0.55	[35]
171	$C_2H_6 + CH_3 \rightleftharpoons C_2H_5 + CH_4$	6.14(+6)	1.74	10.45	[35]
		Reactions of C_2O			
172	$HCCO + OH \rightleftharpoons C_2O + H_2O$	3.00(+13)			[23]
173	$C_2O + H \rightleftharpoons CH + CO$	5.00(+13)			[23]
174	$C_2O + O \rightleftharpoons CO + CO$	5.00(+13)			[23]
175	$C_2O + OH \rightleftharpoons CO + CO + H$	2.00(+13)			[23]
176	$C_2O + O_2 \rightleftharpoons CO + CO + O$	2.00(+13)			[23]
		Reactions of C_2H_3O			
177	$CH_2CO + H \rightleftharpoons C_2H_3O$	5.40(+11)	0.454	1.82	$k_{177} = 0.5 \times k_{\infty,158}$
178	$C_2H_3O + H \rightleftharpoons CH_2CO + H_2$	1.00(+13)			*n*
179	$C_2H_3O + O \rightleftharpoons CH_2O + HCO$	9.60(+6)	1.83	0.22	$k_{179} = 0.5 \times k_{160}$
180	$C_2H_3O + O \rightleftharpoons CH_2CO + OH$	1.00(+13)			*n*
181	$C_2H_3 + OH \rightleftharpoons CH_2CO + H_2O$	5.00(+12)			*n*

TABLE 1 (Continued)

Reaction Mechanism

No.	Reactions[b]	$k = AT^n \exp(-E/RT)$[a]			Comments/ References
		A	n	E	
	Additional Reactions of C_1H_x *and* C_2H_x *Species*				
182	$CH_3 + HCCO \rightleftharpoons C_2H_4 + CO$	5.00(+13)			*n*
183	$CH_3 + C_2H \rightleftharpoons C_3H_3 + H$	2.41(+13)			[39]
184	$CH_4 + C_2H \rightleftharpoons C_2H_2 + CH_3$	1.81(+12)		0.5	[39]
185	$C_2H_2 + CH \rightleftharpoons C_3H_2 + H$	3.00(+13)			[40]
186	$C_2H_2 + CH_2 \rightleftharpoons C_3H_3 + H$	1.20(+13)		6.62	[41]
187	$C_2H_2 + CH_2^* \rightleftharpoons C_3H_3 + H$	2.00(+13)			*n*
188	$C_2H_2 + CH_3 \rightleftharpoons a\text{-}C_3H_4 + H$	2.87(+21)	−2.74	24.8	20, 90 torr, [42]
		5.72(+20)	−2.36	31.5	760 torr
189	$C_2H_2 + CH_3 \rightleftharpoons p\text{-}C_3H_4 + H$	1.00(+13)	−0.53	13.4	20, 90 torr, [42]
		2.72(+18)	−1.97	20.2	760 torr
190	$C_2H_2 + C_2H \rightleftharpoons C_4H_2 + H$	9.60(+13)			*o*
191	$C_2H_2 + C_2H \rightleftharpoons n\text{-}C_4H_3$	1.10(+30)	−6.30	2.79	20 torr, [43]
		1.30(+30)	−6.12	2.51	90 torr
		4.50(+37)	−7.68	7.10	760 torr
192	$C_2H_2 + C_2H \rightleftharpoons i\text{-}C_4H_3$	4.10(+33)	−7.31	4.60	20 torr, [43]
		1.60(+34)	−7.28	4.83	90 torr
		2.60(+44)	−9.47	14.65	760 torr
193	$C_2H_2 + C_2H_3 \rightleftharpoons C_4H_4 + H$	5.00(+14)	−0.71	6.7	20 torr, [24]
		4.60(+16)	−1.25	8.4	90 torr
		2.00(+18)	−1.68	10.6	760 torr
194	$C_2H_2 + C_2H_3 \rightleftharpoons n\text{-}C_4H_5$	1.10(+32)	−7.33	6.2	20 torr, [24]
		2.40(+31)	−6.95	5.6	90 torr
		9.30(+38)	−8.76	12.0	760 torr
195	$C_2H_2 + C_2H_3 \rightleftharpoons i\text{-}C_4H_5$	2.10(+36)	−8.78	9.1	20 torr, [24]
		1.00(+37)	−8.77	9.8	90 torr
		1.60(+46)	−10.98	18.6	760 torr
196	$C_2H_4 + C_2H \rightleftharpoons C_4H_4 + H$	1.20(+13)			[39]
197	$C_2H_4 + C_2H_3 \rightleftharpoons 1,3\text{-}C_4H_6 + H$	7.40(+14)	−0.66	8.42	20 torr, *p*
		1.90(+17)	−1.32	10.60	90 torr
		2.80(+21)	−2.44	14.72	760 torr
198	$C_2H_2 + HCCO \rightleftharpoons C_3H_3 + CO$	1.00(+11)		3.0	[44]
199	$C_2H_4 + O_2 \rightleftharpoons C_2H_3 + HO_2$	4.22(+13)		60.8	*q*
200	$C_2H_3 + H_2O_2 \rightleftharpoons C_2H_4 + HO_2$	1.21(+10)		−0.596	[39]
201	$C_2H_3 + HCO \rightleftharpoons C_2H_4 + CO$	2.50(+13)			*n*
202	$C_2H_3 + CH_3 \rightleftharpoons C_2H_2 + CH_4$	3.92(+11)			[39]
203	$C_2H_3 + C_2H_3 \rightleftharpoons 1,3\text{-}C_4H_6$	7.00(+57)	−13.82	17.6	20 torr, *p*
		1.50(+52)	−11.97	16.1	90 torr
		1.50(+42)	−8.84	12.5	760 torr
204	$C_2H_3 + C_2H_3 \rightleftharpoons i\text{-}C_4H_5 + H$	1.50(+30)	−4.95	13.0	20 torr, *p*
		7.20(+28)	−4.49	14.3	90 torr
		1.20(+22)	−2.44	13.7	760 torr
205	$C_2H_3 + C_2H_3 \rightleftharpoons n\text{-}C_4H_5 + H$	1.10(+24)	−3.28	12.4	20 torr, *p*
		4.60(+24)	−3.38	14.7	90 torr
		2.40(+20)	−2.04	15.4	760 torr
	Reactions of C_3H_x				
206	$C_3H_2 + O \rightleftharpoons C_2H_2 + CO$	6.80(+13)			[40]
207	$C_3H_2 + OH \rightleftharpoons HCO + C_2H_2$	6.80(+13)			[40]
208	$C_3H_2 + O_2 \rightleftharpoons HCCO + CO + H$	5.00(+13)			[23]
209	$C_3H_2 + CH \rightleftharpoons C_4H_2 + H$	5.00(+13)			*n*
210	$C_3H_2 + CH_2 \rightleftharpoons n\text{-}C_4H_3 + H$	5.00(+13)			*n*
211	$C_3H_2 + CH_3 \rightleftharpoons C_4H_4 + H$	5.00(+12)			*n*
212	$C_3H_2 + HCCO \rightleftharpoons n\text{-}C_4H_3 + CO$	1.00(+13)			*n*

TABLE 1 (Continued)

Reaction Mechanism

No.	Reactions[b]	$k = AT^n \exp(-E/RT)$[a] A	n	E	Comments/ References
213	$C_3H_3 + H(+M) \rightleftharpoons a\text{-}C_3H_4(+M)$	3.00(+13)			k_∞, r
		1.40(+31)	−5.0	−6.0	$k_0/[M']$, e
	$a = 0.5$, $T^{***} = 2000$, $T^* = 10$, $T^{**} = 10{,}000$				i
214	$C_3H_3 + H(+M) \rightleftharpoons p\text{-}C_3H_4(+M)$	3.00(+13)			k_∞, r
		1.40(+31)	−5.0	−6.0	$k_0/[M']$, e
	$a = 0.5$, $T^{***} = 2000$, $T^* = 10$, $T^{**} = 10{,}000$				i
215	$C_3H_3 + O \rightleftharpoons CH_2O + C_2H$	2.00(+13)			[44]
216	$C_3H_3 + OH \rightleftharpoons C_3H_2 + H_2O$	2.00(+13)			[44]
217	$C_3H_3 + OH \rightleftharpoons C_2H_3 + HCO$	4.00(+13)			n
218	$C_3H_3 + O_2 \rightleftharpoons CH_2CO + HCO$	3.00(+10)		2.878	[49]
219	$C_3H_3 + HO_2 \rightleftharpoons a\text{-}C_3H_4 + O_2$	1.00(+12)			n
220	$C_3H_3 + HO_2 \rightleftharpoons p\text{-}C_3H_4 + O_2$	1.00(+12)			n
221	$C_3H_3 + HCO \rightleftharpoons a\text{-}C_3H_4 + CO$	2.50(+13)			n
222	$C_3H_3 + HCO \rightleftharpoons p\text{-}C_3H_4 + CO$	2.50(+13)			n
223	$C_3H_3 + CH \rightleftharpoons i\text{-}C_4H_3 + H$	5.00(+13)			n
224	$C_3H_3 + CH_2 \rightleftharpoons C_4H_4 + H$	2.00(+13)			n
225	$i\text{-}C_4H_5 + H \rightleftharpoons C_3H_3 + CH_3$	2.00(+13)		2.0	n
226	$C_3H_3 + CH_3(+M) \rightleftharpoons 1,2\text{-}C_4H_6(+M)$	1.50(+13)			k_∞, s
		2.60(+58)	−11.94	9.77	$k_0/[M']$
	$a = 0.175$, $T^{***} = 1340$, $T^* = 60{,}000$, $T^{**} = 9770$				i
227	$C_3H_3 + C_3H_3 \rightarrow A_1$	1.00(+11)			20 torr; see text
		1.00(+12)			90 torr
		2.00(+12)			760 torr
228	$a\text{-}C_3H_4 + H \rightleftharpoons C_3H_3 + H_2$	1.15(+8)	1.9	7.53	$k_{228} = k_{232}$
229	$a\text{-}C_3H_4 + O \rightleftharpoons CH_2CO + CH_2$	2.00(+7)	1.8	1.0	t
230	$a\text{-}C_3H_4 + OH \rightleftharpoons C_3H_3 + H_2O$	5.30(+6)	2.0	2.0	u
231	$a\text{-}C_3H_4 + C_2H \rightleftharpoons C_2H_2 + C_3H_3$	1.00(+13)			n
232	$p\text{-}C_3H_4 + H \rightleftharpoons C_3H_3 + H_2$	1.15(+8)	1.9	7.53	$k_{232} = k_{167}$
233	$p\text{-}C_3H_4 + H \rightleftharpoons CH_3 + C_2H_2$	1.30(+5)	2.5	1.0	[48]
234	$p\text{-}C_3H_4 + OH \rightleftharpoons C_3H_3 + H_2O$	3.54(+6)	2.12	0.87	$k_{234} = k_{169}$
235	$p\text{-}C_3H_4 + C_2H \rightleftharpoons C_2H_2 + C_3H_3$	1.00(+13)			n
	Reactions of C_4H *and* C_4H_2				
236	$C_4H + H(+M) \rightleftharpoons C_4H_2(+M)$	1.00(+17)	−1.0		k_∞, $k_{236} = k_{125}$
		3.75(+33)	−4.8	1.9	$k_0/[M']$, e
	$a = 0.6464$, $T^{***} = 132$, $T^* = 1315$, $T^{**} = 5566$				i
237	$C_4H + C_2H_2 \rightleftharpoons C_6H_2 + H$	9.60(+13)			$k_{237} = k_{190}$
238	$C_4H + O \rightleftharpoons C_2H + C_2O$	5.00(+13)			$k_{238} = k_{126}$
239	$C_4H + O_2 \rightleftharpoons HCCO + C_2O$	5.00(+13)		1.5	$k_{239} = k_{128}$
240	$C_4H + H_2 \rightleftharpoons H + C_4H_2$	4.90(+5)	2.5	0.56	$k_{240} = k_{129}$
241	$C_4H_2 + H \rightleftharpoons n\text{-}C_4H_3$	1.70(+49)	−11.67	12.80	20 torr, p
		3.30(+50)	−11.80	15.01	90 torr
		1.10(+42)	−8.72	15.30	760 torr
242	$C_4H_2 + H \rightleftharpoons i\text{-}C_4H_3$	4.30(+45)	−10.15	13.25	20 torr, p
		2.60(+46)	−10.15	15.50	90 torr
		1.10(+30)	-4.92	10.80	760 torr
243	$C_4H_2 + O \rightleftharpoons C_3H_2 + CO$	2.70(+13)		1.72	[52]
244	$C_4H_2 + OH \rightleftharpoons H_2C_4O + H$	6.60(+12)		−0.41	[53]
245	$C_4H_2 + OH \rightleftharpoons C_4H + H_2O$	3.37(+7)	2.0	14.0	$k_{245} = k_{142}$
246	$C_4H_2 + CH \rightleftharpoons C_5H_2 + H$	5.00(+13)			n
247	$C_4H_2 + CH_2 \rightleftharpoons C_5H_3 + H$	1.30(+13)		6.62	$k_{247} = k_{186}$
248	$C_4H_2 + CH_2^* \rightleftharpoons C_5H_3 + H$	2.00(+13)			n
249	$C_4H_2 + C_2H \rightleftharpoons C_6H_2 + H$	9.60(+13)			$k_{249} = k_{190}$
250	$C_4H_2 + C_2H \rightleftharpoons C_6H_3$	1.10(+30)	−6.30	2.79	20 torr, $k_{250} = k_{191}$
		1.30(+30)	−6.12	2.51	90 torr
		4.50(+37)	−7.68	7.10	760 torr

TABLE 1 (Continued)

Reaction Mechanism

No.	Reactions[b]	$k = AT^n \exp(-E/RT)$[a]			Comments/ References
		A	n	E	
251	$H_2C_4O + H \rightleftharpoons C_2H_2 + HCCO$	5.00(+13)		3.0	[23]
252	$H_2C_4O + OH \rightleftharpoons CH_2CO + HCCO$	1.00(+7)	2.0	2.0	[23]
253	$H_2C_4O + O \rightleftharpoons CH_2CO + C_2O$	2.00(+7)	1.9	0.2	n
	Reactions of C_4H_3 *and* C_4H_4				
254	$n\text{-}C_4H_3 \rightleftharpoons i\text{-}C_4H_3$	3.70(+61)	−15.81	54.89	20 torr, p
		1.00(+51)	−12.45	51.00	90 torr
		4.10(+43)	−9.49	53.00	760 torr
255	$n\text{-}C_4H_3 + H \rightleftharpoons i\text{-}C_4H_3 + H$	2.40(+11)	0.79	2.41	20 torr, p
		9.20(+11)	0.63	2.99	90 torr
		2.50(+20)	−1.67	10.80	760 torr
256	$n\text{-}C_4H_3 + H \rightleftharpoons C_2H_2 + c_2H_2$	1.60(+19)	−1.60	2.22	20 torr, p
		1.30(+20)	−1.85	2.96	90 torr
		6.30(+25)	−3.34	10.01	760 torr
257	$i\text{-}C_4H_3 + H \rightleftharpoons C_2H_2 + C_2H_2$	2.40(+19)	−1.60	2.80	20 torr, p
		3.70(+22)	−2.50	5.14	90 torr
		2.80(+23)	−2.55	10.78	760 torr
258	$n\text{-}C_4H_3 + H \rightleftharpoons C_4H_4$	1.10(+42)	−9.65	7.00	20 torr, p
		1.10(+42)	−9.65	7.00	90 torr
		2.00(+47)	−10.26	13.07	760 torr
259	$i\text{-}C_4H_3 + H \rightleftharpoons C_4H_4$	4.20(+44)	−10.27	7.89	20 torr, p
		5.30(+46)	−10.68	9.27	90 torr
		3.40(+43)	−9.01	12.12	760 torr
260	$n\text{-}C_4H_3 + H \rightleftharpoons C_4H_2 + H_2$	1.50(+13)			$k_{260} = 0.5 \times k_{151}$
261	$i\text{-}C_4H_3 + H \rightleftharpoons C_4H_2 + H_2$	3.00(+13)			$k_{261} = k_{151}$
262	$n\text{-}C_4H_3 + OH \rightleftharpoons C_4H_2 + H_2O$	2.50(+12)			$k_{262} = 0.5 \times k_{153}$
263	$i\text{-}C_4H_3 + OH \rightleftharpoons C_4H_2 + H_2O$	5.00(+12)			$k_{263} = k_{153}$
264	$i\text{-}C_4H_3 + O_2 \rightleftharpoons HCCO + CH_2CO$	7.86(+16)	−1.80		[54]
265	$n\text{-}C_4H_3 + C_2H_2 \rightleftharpoons l\text{-}C_6H_4 + H$	3.70(+16)	−1.21	11.1	20 torr, [24]
		1.80(+19)	−1.95	13.2	90 torr
		2.50(+14)	−0.56	10.6	760 torr
266	$n\text{-}C_4H_3 + C_2H_2 \rightleftharpoons n\text{-}C_6H_5$	6.00(+33)	−7.37	13.7	20 torr, [24]
		4.10(+33)	−7.12	13.7	90 torr
		2.70(+36)	−7.62	16.2	760 torr
267	$n\text{-}C_4H_3 + C_2H_2 \rightleftharpoons A_1\text{-}$	2.30(+68)	−17.65	24.4	20 torr, [24]
		9.80(+68)	−17.58	26.5	90 torr
		9.60(+70)	−17.77	31.3	760 torr
268	$n\text{-}C_4H_3 + C_2H_2 \rightleftharpoons c\text{-}C_6H_4 + H$	1.90(+36)	−7.21	17.9	20 torr, [24]
		3.50(+41)	−8.63	23.0	90 torr
		6.90(+46)	−10.01	30.1	760 torr
269	$C_4H_4 + H \rightleftharpoons n\text{-}C_4H_5$	4.20(+50)	−12.34	12.5	20 torr, [24]
		1.10(+50)	−11.94	13.4	90 torr
		1.30(+51)	−11.92	16.5	760 torr
270	$C_4H_4 + H \rightleftharpoons i\text{-}C_4H_5$	9.60(+52)	−12.85	14.3	20 torr, [24]
		2.10(+52)	−12.44	15.5	90 torr
		4.90(+51)	−11.92	17.7	760 torr
271	$C_4H_4 + H \rightleftharpoons n\text{-}C_4H_3 + H_2$	6.65(+5)	2.53	12.24	$k_{271} = 0.5 \times k_{159}$
272	$C_4H_4 + H \rightleftharpoons i\text{-}C_4H_3 + H_2$	3.33(+5)	2.53	9.24	v
273	$C_4H_4 + OH \rightleftharpoons n\text{-}C_4H_3 + H_2O$	3.10(+6)	2.0	3.43	$k_{273} = 0.5 \times k_{293}$
274	$C_4H_4 + OH \rightleftharpoons i\text{-}C_4H_3 + H_2O$	1.55(+6)	2.0	0.43	$k_{274} = 0.5 \times k_{294}$
275	$C_4H_4 + O \rightleftharpoons p\text{-}C_3H_4 + CO$	2.70(+13)		1.72	$k_{275} = k_{243}$
276	$C_4H_4 + C_2H_3 \rightleftharpoons l\text{-}C_6H_6 + H$	7.40(+14)	−0.66	8.42	20 torr, $k_{276} = k_{197}$
		1.90(+17)	−1.32	10.60	90 torr
		2.80(+21)	−2.44	14.72	760 torr

TABLE 1 (Continued)

Reaction Mechanism

No.	Reactions[b]	$k = AT^n \exp(-E/RT)$[a] A	n	E	Comments/ References
	Reactions of C_4H_5 *and* $1,3\text{-}C_4H_6$				
277	$n\text{-}C_4H_5 \rightleftharpoons i\text{-}C_4H_5$	1.30(+62)	−16.38	49.6	20 torr, [24]
		4.90(+66)	−17.26	55.4	90 torr
		1.50(+67)	−16.89	59.1	760 torr
278	$n\text{-}C_4H_5 + H \rightleftharpoons i\text{-}C_4H_5 + H$	1.00(+36)	−6.26	17.5	20 torr, p
		1.00(+34)	−5.61	18.5	90 torr
		3.10(+26)	−3.35	17.4	760 torr
279	$1,3\text{-}C_4H_6 \rightleftharpoons i\text{-}C_4H_5 + H$	8.20(+51)	−10.92	118.4	20 torr, p
		3.30(+45)	−8.95	115.9	90 torr
		5.70(+36)	−6.27	112.4	760 torr
280	$1,3\text{-}C_4H_6 \rightleftharpoons n\text{-}C_4H_5 + H$	3.50(+61)	−13.87	129.7	20 torr, p
		8.50(+54)	−11.78	127.5	90 torr
		5.30(+44)	−8.62	123.6	760 torr
281	$n\text{-}C_4H_5 + H \rightleftharpoons C_4H_4 + H_2$	1.50(+13)			$k_{281} = 0.5 \times k_{151}$
282	$i\text{-}C_4H_5 + H \rightleftharpoons C_4H_4 + H_2$	3.00(+13)			$k_{282} = k_{151}$
283	$n\text{-}C_4H_5 + OH \rightleftharpoons C_4H_4 + H_2O$	2.50(+12)			$k_{283} = 0.5 \times k_{153}$
284	$i\text{-}C_4H_5 + OH \rightleftharpoons C_4H_4 + H_2O$	5.00(+12)			$k_{284} = 0.5 \times k_{153}$
285	$n\text{-}C_4H_5 + O_2 \rightarrow C_2H_4 + CO + HCO$	4.16(+10)		2.5	[55]
286	$i\text{-}C_4H_5 + O_2 \rightleftharpoons CH_2CO + C_2H_3O$	7.86(+16)	−1.8		$k_{286} = k_{264}$
287	$n\text{-}C_4H_5 + C_2H_2 + M \rightleftharpoons n\text{-}C_6H_7 + M$	4.50(+26)	−3.28	10.2	20, 90 torr, [24]
	$n\text{-}C_4H_5 + C_2H_2 \rightleftharpoons n\text{-}C_6H_7$	1.10(+14)	−1.27	2.9	760 torr
288	$n\text{-}C_4H_5 + C_2H_2 + M \rightleftharpoons c\text{-}C_6H_7 + M$	5.20(+25)	−4.21	4.0	20, 90 torr, [24]
	$n\text{-}C_4H_5 + C_2H_2 \rightleftharpoons c\text{-}C_6H_7$	5.00(+24)	−5.46	4.6	760 torr
289	$n\text{-}C_4H_5 + C_2H_2 \rightleftharpoons l\text{-}C_6H_6 + H$	5.80(+8)	1.02	10.9	20, 90, 760 torr, [24]
290	$n\text{-}C_4H_5 + C_2H_2 \rightleftharpoons A_1 + H$	2.10(+15)	−1.07	4.8	20, 90 torr, [24]
		1.60(+16)	−1.33	5.4	760 torr
291	$1,3\text{-}C_4H_6 + H \rightleftharpoons n\text{-}C_4H_5 + H_2$	1.33(+6)	2.53	12.24	$k_{291} = k_{159}$
292	$1,3\text{-}C_4H_6 + H \rightleftharpoons i\text{-}C_4H_5 + H_2$	6.65(+5)	2.53	9.24	w
293	$1,3\text{-}C_4H_6 + OH \rightleftharpoons n\text{-}C_4H_5 + H_2O$	6.20(+6)	2.0	3.43	x
294	$1,3\text{-}C_4H_6 + OH \rightleftharpoons i\text{-}C_4H_5 + H_2O$	3.10(+6)	2.0	0.43	y
295	$1,3\text{-}C_4H_6 + C_2H_3 \rightleftharpoons C_6H_8 + H$	7.40(+14)	−0.66	8.42	20 torr, $k_{295} = k_{197}$
		1.90(+17)	−1.32	10.60	90 torr
		2.80(+21)	−2.44	14.72	760 torr
	Reactions of $1,2\text{-}C_4H_6$				
296	$1,2\text{-}C_4H_6 + H \rightleftharpoons 1,3\text{-}C_4H_6 + H$	2.00(+13)		4.0	n
297	$1,2\text{-}C_4H_6 + H \rightleftharpoons i\text{-}C_4H_5 + H_2$	1.70(+5)	2.5	2.49	z
298	$1,2\text{-}C_4H_6 + H \rightleftharpoons a\text{-}C_3H_4 + CH_3$	2.00(+13)		2.0	n
299	$1,2\text{-}C_4H_6 + O \rightleftharpoons CH_2CO + C_2H_4$	1.20(+8)	1.65	0.327	z
300	$1,2\text{-}C_4H_6 + O \rightleftharpoons i\text{-}C_4H_5 + OH$	1.80(+11)	0.7	5.88	z
301	$1,2\text{-}C_4H_6 + OH \rightleftharpoons i\text{-}C_4H_5 + H_2O$	3.10(+6)	2.0	−0.298	z
	Reactions of C_5H_2 *and* C_5H_3				
302	$C_5H_2 + OH \rightarrow C_4H_2 + H + CO$	2.00(+13)			n
303	$C_5H_2 + CH \rightleftharpoons C_6H_2 + H$	5.00(+13)			n
304	$C_5H_2 + O_2 \rightleftharpoons H_2C_4O + CO$	1.00(+12)			n
305	$C_5H_3 + OH \rightleftharpoons C_5H_2 + H_2O$	1.00(+13)			n
306	$C_5H_3 + CH \rightleftharpoons C_6H_2 + H + H$	5.00(+13)			n
307	$C_5H_3 + CH_2 \rightleftharpoons l\text{-}C_6H_4 + H$	5.00(+13)			n
308	$C_5H_3 + O_2 \rightleftharpoons H_2C_4O + HCO$	1.00(+12)			n
	Reactions of C_6H *and* C_6H_2				
309	$C_6H + H(+M) \rightleftharpoons C_6H_2(+M)$	1.00(+17)	−1.0		k_∞, $k_{309} = k_{125}$
		3.75(+33)	−4.8	1.9	$k_0/[M']^h$, e
	$a = 0.6464$, $T^{***} = 132$, $T^* = 1315$, $T^{**} = 5566$				i

TABLE 1 (Continued)

Reaction Mechanism

No.	Reactions[b]	$k = AT^n \exp(-E/RT)$[a]			Comments/ References
		A	n	E	
310	$C_6H_2 + H \rightleftharpoons C_6H_3$	4.30(+45)	−10.15	13.25	20 torr, $k_{310} = k_{242}$
		2.60(+46)	−10.15	15.50	90 torr
		1.10(+30)	−4.92	10.80	760 torr
311	$C_6H + O \rightleftharpoons C_4H + C_2O$	5.00(+13)			$k_{311} = k_{126}$
312	$C_6H + H_2 \rightleftharpoons H + C_6H_2$	4.90(+5)	2.5	0.56	$k_{312} = k_{129}$
313	$C_6H_2 + O \rightleftharpoons C_5H_2 + CO$	2.70(+13)		1.72	$k_{313} = k_{243}$
314	$C_6H_2 + OH \rightarrow C_2H + C_2H_2 + C_2O$	6.60(+12)		−0.41	$k_{314} = k_{244}$
315	$C_6H_2 + OH \rightleftharpoons C_6H + H_2O$	3.37(+7)	2.0	14.0	$k_{315} = k_{142}$
	Reactions of C_6H_3 *and* C_6H_4				
316	$C_6H_3 + H \rightleftharpoons C_4H_2 + C_2H_2$	2.40(+19)	−1.60	2.80	20 torr, $k_{316} = k_{257}$
		3.70(+22)	−2.50	5.14	90 torr
		2.80(+23)	−2.55	10.78	760 torr
317	$C_6H_3 + H \rightleftharpoons l\text{-}C_6H_4$	4.20(+44)	−10.27	7.89	20 torr, $k_{317} = k_{259}$
		5.30(+46)	−10.68	9.27	90 torr
		3.40(+43)	−9.01	12.12	760 torr
318	$C_6H_3 + H \rightleftharpoons C_6H_2 + H_2$	3.00(+13)			$k_{318} = k_{151}$
319	$C_6H_3 + OH \rightleftharpoons C_6H_2 + H_2O$	5.00(+12)			$k_{319} = k_{153}$
320	$C_6H_3 + O_2 \rightarrow CO + C_3H_2 + HCCO$	5.00(+11)			n
321	$l\text{-}C_6H_4 + H \rightleftharpoons n\text{-}C_6H_5$	3.30(+44)	−10.04	18.8	20 torr, [24]
		2.60(+43)	−9.53	18.1	90 torr
		5.90(+39)	−8.25	15.6	760 torr
322	$l\text{-}C_6H_4 + H \rightleftharpoons A_1\text{-}$	3.60(+77)	−20.09	28.1	20 torr, [24]
		4.70(+78)	−20.10	29.5	90 torr
		1.70(+78)	−19.72	31.4	760 torr
323	$l\text{-}C_6H_4 + H \rightleftharpoons c\text{-}C_6H_4 + H$	2.20(+47)	−9.98	24.0	20 torr, [24]
		9.70(+48)	−10.37	27.0	90 torr
		1.40(+54)	−11.70	34.5	760 torr
324	$l\text{-}C_6H_4 + H \rightleftharpoons C_6H_3 + H_2$	6.65(+6)	2.53	9.24	$k_{324} = k_{292}$
325	$l\text{-}C_6H_4 + OH \rightleftharpoons C_6H_3 + H_2O$	3.10(+6)	2.0	0.43	$k_{325} = k_{294}$
326	$c\text{-}C_6H_4 + H \rightleftharpoons A_1\text{-}$	1.20(+77)	−18.77	36.3	20 torr, [24]
		1.00(+71)	−16.88	34.2	90 torr
		2.40(+60)	−13.66	29.5	760 torr
	Reactions of C_6H_5 *and* $l\text{-}C_6H_6$				
327	$n\text{-}C_6H_5 \rightleftharpoons A_1\text{-}$	1.30(+62)	−15.94	35.8	20 torr, [24]
		1.30(+59)	−14.78	35.6	90 torr
		5.10(+54)	−13.11	35.7	760 torr
328	$n\text{-}C_6H_5 \rightleftharpoons c\text{-}C_6H_4 + H$	2.70(+65)	−15.93	59.7	20 torr, [24]
		1.50(+64)	−15.32	61.5	90 torr
		1.30(+59)	−13.56	62.0	760 torr
329	$n\text{-}C_6H_5 + H \rightleftharpoons i\text{-}C_6H_5 + H$	2.40(+11)	0.79	2.41	20 torr, $k_{329} = k_{255}$
		9.20(+11)	0.63	2.99	90 torr
		2.50(+20)	−1.67	10.80	760 torr
330	$n\text{-}C_6H_5 + H \rightleftharpoons C_4H_4 + C_2H_2$	1.60(+19)	−1.60	2.22	20 torr, $k_{330} = k_{256}$
		1.30(+20)	−1.85	2.96	90 torr
		6.30(+25)	−3.34	10.01	760 torr
331	$i\text{-}C_6H_5 + H \rightleftharpoons C_4H_4 + C_2H_2$	2.40(+19)	−1.60	2.80	20 torr, $k_{331} = k_{257}$
		3.70(+22)	−2.50	5.14	90 torr
		2.80(+23)	−2.55	10.78	760 torr
332	$n\text{-}C_6H_5 + H \rightleftharpoons l\text{-}C_6H_6$	1.10(+42)	−9.65	7.00	20 torr, $k_{332} = k_{258}$
		1.10(+42)	−9.65	7.00	90 torr
		2.00(+47)	−10.26	13.07	760 torr
333	$i\text{-}C_6H_5 + H \rightleftharpoons l\text{-}C_6H_6$	4.20(+44)	−10.27	7.89	20 torr, $k_{332} = k_{259}$
		5.30(+46)	−10.68	9.27	90 torr
		3.40(+43)	−9.01	12.12	760 torr

TABLE 1 (Continued)

Reaction Mechanism

No.	Reactions[b]	$k = AT^n \exp(-E/RT)$[a] A	n	E	Comments/ References
334	$n\text{-}C_6H_5 + H \rightleftharpoons l\text{-}C_6H_4 + H_2$	1.50(+13)			$k_{334} = 0.5 \times k_{151}$
335	$i\text{-}C_6H_5 + H \rightleftharpoons l\text{-}C_6H_4 + H_2$	3.00(+13)			$k_{335} = k_{151}$
336	$n\text{-}C_6H_5 + OH \rightleftharpoons l\text{-}C_6H_4 + H_2O$	2.50(+12)			$k_{336} = 0.5 \times k_{153}$
337	$i\text{-}C_6H_5 + OH \rightleftharpoons l\text{-}C_6H_4 + H_2O$	5.00(+12)			$k_{337} = k_{153}$
338	$n\text{-}C_6H_5 + O_2 \rightarrow C_4H_4 + CO + HCO$	4.16(+10)		2.5	$k_{338} = k_{285}$
339	$i\text{-}C_6H_5 + O_2 \rightarrow CH_2CO + CH_2CO + C_2H$	7.86(+16)	−1.80		$k_{339} = k_{264}$
340	$l\text{-}C_6H_6 + H + M \rightleftharpoons n\text{-}C_6H_7 + M$	2.90(+17)	−0.52	1.0	20, 90 torr, [24]
	$l\text{-}C_6H_6 + H \rightleftharpoons n\text{-}C_6H_7$	1.50(+16)	−1.69	1.6	760 torr
341	$l\text{-}C_6H_6 + H + M \rightleftharpoons c\text{-}C_6H_7 + M$	1.70(+28)	−4.72	2.8	20, 90 torr, [24]
	$l\text{-}C_6H_6 + H \rightleftharpoons c\text{-}C_6H_7$	4.70(+27)	−6.11	3.8	760 torr
342	$l\text{-}C_6H_6 + H \rightleftharpoons A_1 + H$	8.70(+16)	−1.34	3.5	20, 90 torr, [24]
		2.00(+18)	−1.73	4.5	760 torr
343	$l\text{-}C_6H_6 + H \rightleftharpoons n\text{-}C_6H_5 + H_2$	6.65(+5)	2.53	12.24	$k_{343} = 0.5 \times k_{159}$
344	$l\text{-}C_6H_6 + H \rightleftharpoons i\text{-}C_6H_5 + H_2$	3.33(+5)	2.53	9.24	$k_{344} = 0.5 \times k_{292}$
345	$l\text{-}C_6H_6 + OH \rightleftharpoons n\text{-}C_6H_5 + H_2O$	6.20(+6)	2.0	3.43	$k_{345} = k_{293}$
346	$l\text{-}C_6H_6 + OH \rightleftharpoons i\text{-}C_6H_5 + H_2O$	3.10(+6)	2.0	0.43	$k_{346} = k_{294}$
	Reactions of C_6H_7 *and* C_6H_8				
347	$n\text{-}C_6H_7 \rightleftharpoons c\text{-}C_6H_7$	4.10(+24)	−7.11	3.9	20 torr, [24]
		3.60(+27)	−7.54	5.8	90 torr
		1.20(+31)	−7.95	8.9	760 torr
348	$n\text{-}C_6H_7 \rightleftharpoons A_1 + H$	8.40(+21)	−4.22	11.3	20 torr, [24]
		8.80(+24)	−4.86	13.4	90 torr
		3.20(+26)	−4.99	15.5	760 torr
349	$n\text{-}C_6H_7 + H \rightleftharpoons i\text{-}C_6H_7 + H$	4.00(+41)	−8.09	19.2	20 torr
		1.60(+42)	−8.18	21.8	90 torr
		2.40(+49)	−10.72	15.1	760 torr
350	$i\text{-}C_6H_7 + H \rightleftharpoons C_6H_8$	1.20(+60)	−13.86	21.0	20 torr
		1.40(+55)	−12.32	19.3	90 torr
		1.80(+39)	−7.62	11.0	760 torr
351	$n\text{-}C_6H_7 + H \rightleftharpoons C_6H_8$	8.70(+69)	−17.01	24.0	20 torr
		6.70(+65)	−15.64	23.2	90 torr
		5.60(+48)	−10.54	14.7	760 torr
352	$n\text{-}C_6H_7 + H \rightleftharpoons l\text{-}C_6H_6 + H_2$	1.50(+13)			$k_{352} = 0.5 \times k_{151}$
353	$i\text{-}C_6H_7 + H \rightleftharpoons l\text{-}C_6H_6 + H_2$	3.00(+13)			$k_{353} = k_{151}$
354	$n\text{-}C_6H_7 + OH \rightleftharpoons l\text{-}C_6H_6 + H_2O$	2.50(+12)			$k_{354} = 0.5 \times k_{153}$
355	$i\text{-}C_6H_7 + OH \rightleftharpoons l\text{-}C_6H_6 + H_2O$	5.00(+12)			$k_{355} = k_{153}$
356	$n\text{-}C_6H_7 + O_2 \rightarrow 1,3\text{-}C_4H_6 + CO + HCO$	4.16(+10)		2.5	$k_{356} = k_{285}$
357	$i\text{-}C_6H_7 + O_2 \rightarrow 2CH_2CO + C_2H_3$	7.86(+16)	−1.80		$k_{357} = k_{264}$
358	$C_6H_8 + H \rightleftharpoons n\text{-}C_6H_7 + H_2$	1.33(+6)	2.53	12.24	$k_{358} = k_{159}$
359	$C_6H_8 + H \rightleftharpoons i\text{-}C_6H_7 + H_2$	6.65(+5)	2.53	9.24	$k_{359} = k_{292}$
360	$C_6H_8 + OH \rightleftharpoons n\text{-}C_6H_7 + H_2O$	6.20(+6)	2.0	3.43	$k_{360} = k_{293}$
361	$C_6H_8 + OH \rightleftharpoons i\text{-}C_6H_7 + H_2O$	3.10(+6)	2.0	0.43	$k_{361} = k_{294}$
	Reactions of Benzene (A_1) *and Phenyl* (A_1-)				
362	$A_1 + H \rightleftharpoons c\text{-}C_6H_7$	6.60(+25)	−5.41	−5.3	20 torr, [24]
		4.80(+30)	−6.54	−0.9	90 torr
		2.00(+38)	−8.32	6.4	760 torr
363	$A_1 + H \rightleftharpoons A_1\text{-} + H_2$	2.50(+14)		16.0	[57]
364	$A_1 + OH \rightleftharpoons A_1\text{-} + H_2O$	1.60(+8)	1.42	1.45	[58]
365	$A_1\text{-} + H(+M) \rightleftharpoons A_1(+M)$	1.00(+14)			k_∞, p
		6.60(+75)	−16.3	7.0	$k_0/[M']$, e
	$a = 1.0$, $T^{***} = 0.1$, $T^* = 585$, $T^{**} = 6113$				i

TABLE 1 (Continued)

Reaction Mechanism

No.	Reactions[b]	$k = AT^n \exp(-E/RT)$[a] A	n	E	Comments/ References
	Formation and Reactions of Phenylacetylene (A_1C_2H)				
366	n-$C_4H_3 + C_4H_2 \rightleftharpoons A_1C_2H$-	2.30(+68)	−17.65	24.4	20 torr, $k_{366} = k_{267}$
		9.80(+68)	−17.58	26.5	90 torr
		9.60(+70)	−17.77	31.3	760 torr
367	$A_1 + C_2H \rightleftharpoons A_1C_2H + H$	5.00(+13)			n
368	A_1-$+ C_2H_2 \rightleftharpoons n$-$A_1C_2H_2$	7.70(+40)	−9.19	13.4	20 torr, [24]
		9.90(+41)	−9.26	15.7	90 torr
		7.00(+38)	−8.02	16.4	760 torr
369	A_1-$+ C_2H_2 \rightleftharpoons A_1C_2H + H$	7.50(+26)	−3.96	17.1	20 torr, [24]
		9.90(+30)	−5.07	21.1	90 torr
		3.30(+33)	−5.70	25.5	760 torr
370	$A_1C_2H + H \rightleftharpoons n$-$A_1C_2H_2$	1.00(+54)	−12.76	17.2	20 torr, [24]
		1.20(+51)	−11.69	17.3	90 torr
		3.00(+43)	−9.22	15.3	760 torr
371	$A_1C_2H + H \rightleftharpoons i$-$A_1C_2H_2$	1.00(+54)	−12.76	17.2	20 torr, $k_{371} = k_{370}$
		1.20(+51)	−11.69	17.3	90 torr
		3.00(+43)	−9.22	15.3	760 torr
372	$A_1C_2H + H \rightleftharpoons A_1C_2H^* + H_2$	2.50(+14)		16.0	$k_{372} = k_{363}$
373	$A_1C_2H + H \rightleftharpoons A_1C_2H$-$+ H_2$	2.50(+14)		16.0	$k_{373} = k_{363}$
374	$A_1C_2H + OH \rightleftharpoons A_1C_2H^* + H_2O$	1.60(+8)	1.42	1.45	$k_{374} = k_{364}$
375	$A_1C_2H + OH \rightleftharpoons A_1C_2H$-$+ H_2O$	1.60(+8)	1.42	1.45	$k_{375} = k_{364}$
376	A_1C_2H-$+ H(+M) \rightleftharpoons A_1C_2H(+M)$	1.00(+14)			k_∞, $k_{376} = k_{365}$
		6.60(+75)	−16.3	7.0	$k_0/[M']$, e
	$a = 1.0$, $T^{***} = 0.1$, $T^* = 585$, $T^{**} = 6113$				i
377	$A_1C_2H^* + H(+M) \rightleftharpoons A_1C_2H(+M)$	1.00(+14)			k_∞, $k_{377} = k_{365}$
		6.60(+75)	−16.3	7.0	$k_0/[M']$, e
	$a = 1.0$, $T^{***} = 0.1$, $T^* = 585$, $T^{**} = 6113$				i
	Formation and Reactions of Phenylvinyl ($A_1C_2H_2$) *and Styrene* ($A_1C_2H_3$)				
378	$A_1 + C_2H_3 \rightleftharpoons A_1C_2H_3 + H$	7.90(+11)		6.4	[59]
379	A_1-$+ C_2H_4 \rightleftharpoons A_1C_2H_3 + H$	2.51(+12)		6.19	[59]
380	A_1-$+ C_2H_3 \rightleftharpoons A_1C_2H_3$	1.90(+48)	−10.52	17.5	20 torr, p
		3.90(+38)	−7.63	12.9	90 torr
		1.20(+27)	−4.22	7.2	760 torr
381	A_1-$+ C_2H_3 \rightleftharpoons i$-$A_1C_2H_2 + H$	1.80(+31)	−4.63	31.7	20 torr, p
		5.80(+18)	−1.00	26.8	90 torr
		8.50(−2)	4.71	18.4	760 torr
382	A_1-$+ C_2H_3 \rightleftharpoons n$-$A_1C_2H_2 + H$	1.50(+32)	−4.91	35.5	20 torr, p
		5.10(+20)	−1.56	31.4	90 torr
		9.40(+0)	4.14	23.2	760 torr
383	$A_1C_2H_3 \rightleftharpoons i$-$A_1C_2H_2 + H$	1.20(+46)	−9.07	118.3	20 torr, p
		3.80(+37)	−6.55	114.2	90 torr
		5.30(+27)	−3.63	109.3	760 torr
384	$A_1C_2H_3 \rightleftharpoons n$-$A_1C_2H_2 + H$	1.90(+54)	−11.39	130.2	20 torr, p
		1.30(+44)	−8.36	125.4	90 torr
		1.10(+32)	−4.77	119.5	760 torr
385	$A_1C_2H_3 + H \rightleftharpoons A_1C_2H_3^* + H_2$	2.50(+14)		16.0	$k_{385} = k_{363}$
386	$A_1C_2H_3 + OH \rightleftharpoons A_1C_2H_3^* + H_2O$	1.60(+8)	1.42	1.45	$k_{386} = k_{364}$
387	$A_1C_2H_3^* + H(+M) \rightleftharpoons A_1C_2H_3(+M)$	1.00(+14)			k_∞, $k_{387} = k_{365}$
		6.60(+75)	−16.3	7.0	$k_0/[M']$, e
	$a = 1.0$, $T^{***} = 0.1$, $T^* = 585$, $T^{**} = 6113$				i
388	$A_1C_2H_3 + H \rightleftharpoons n$-$A_1C_2H_2 + H_2$	6.65(+6)	2.53	12.24	$k_{388} = 0.5 \times k_{159}$
389	$A_1C_2H_3 + H \rightleftharpoons i$-$A_1C_2H_2 + H_2$	3.33(+5)	2.53	9.24	$k_{389} = 0.5 \times k_{292}$
390	$A_1C_2H_3 + OH \rightleftharpoons n$-$A_1C_2H_2 + H_2O$	3.10(+6)	2.0	3.43	$k_{390} = k_{294}$

TABLE 1 (Continued)

Reaction Mechanism

No.	Reactions[b]	$k = AT^n \exp(-E/RT)$[a] A	n	E	Comments/ References
391	$A_1C_2H_3 + OH \rightleftharpoons i\text{-}A_1C_2H_2 + H_2O$	1.55(+6)	2.0	0.43	$k_{391} = k_{295}$
392	$n\text{-}A_1C_2H_2 + H \rightleftharpoons A_1C_2H + H_2$	1.50(+13)			$k_{392} = 0.5 \times k_{151}$
393	$i\text{-}A_1C_2H_2 + H \rightleftharpoons A_1C_2H + H_2$	3.00(+13)			$k_{393} = k_{151}$
394	$n\text{-}A_1C_2H_2 + H \rightleftharpoons i\text{-}A_1C_2H_2 + H$	2.30(+37)	−6.00	35.2	20 torr, p
		1.20(+25)	−2.42	30.5	90 torr
		9.90(+4)	3.37	22.0	760 torr
395	$n\text{-}A_1C_2H_2 + OH \rightleftharpoons A_1C_2H + H_2O$	2.50(+12)			$k_{395} = 0.5 \times k_{153}$
396	$i\text{-}A_1C_2H_2 + OH \rightleftharpoons A_1C_2H + H_2O$	5.00(+12)			$k_{396} = k_{153}$
	Formation and Reactions of Naphthalene (A_2)				
397	$A_1C_2H^* + C_2H_2 \rightleftharpoons A_2\text{-}1$	5.20(+72)	−18.11	33.9	20 torr, [24]
		2.00(+72)	−17.74	36.6	90 torr
		1.10(+62)	−14.56	33.1	760 torr
398	$A_1C_2H^* + C_2H_2 \rightleftharpoons A_1C_2H)_2 + H$	5.50(+32)	−5.46	27.6	20 torr, [24]
		4.80(+29)	−4.59	26.0	90 torr
		1.80(+19)	−1.67	18.8	760 torr
399	$A_1C_2H^* + C_2H_2 \rightleftharpoons$ naphthyne + H	2.30(+58)	−12.87	44.6	20 torr, [24]
		5.20(+64)	−14.54	52.2	90 torr
		5.70(+64)	−14.41	57.0	760 torr
400	$A_1C_2H)_2 + H \rightleftharpoons A_2\text{-}1$	2.00(+82)	−20.23	36.9	20 torr, [24]
		2.00(+75)	−18.06	34.5	90 torr
		6.90(+63)	−14.57	29.9	760 torr
401	$A_1C_2H)_2 + H \rightleftharpoons$ naphthyne + H	3.90(+74)	−16.91	53.7	20 torr, [24]
		2.70(+76)	−17.32	58.2	90 torr
		1.90(+73)	−16.30	60.9	760 torr
402	Naphthyne + $H \rightleftharpoons A_2\text{-}1$	3.30(+65)	−16.79	37.4	20 torr, [24]
		5.90(+61)	−15.42	36.5	90 torr
		4.90(+52)	−12.43	33.0	760 torr
403	$A_1C_2H + C_2H \rightleftharpoons A_1C_2H)_2 + H$	5.00(+13)			n
404	$A_1C_2H_3^* + C_2H_2 \rightleftharpoons A_2 + H$	2.10(+15)	−1.07	6.0	20, 90 torr, *aa*
		1.60(+16)	−1.33	6.6	760 torr
405	$n\text{-}A_1C_2H_2 + C_2H_2 \rightleftharpoons A_2 + H$	2.10(+15)	−1.07	4.8	20, 90 torr, $k_{405} = k_{290}$
		1.60(+16)	−1.33	5.4	760 torr
406	$A_2 + H \rightleftharpoons A_2\text{-}1 + H_2$	2.50(+14)		16.0	$k_{406} = k_{363}$
407	$A_2 + H \rightleftharpoons A_2\text{-}2 + H_2$	2.50(+14)		16.0	$k_{407} = k_{363}$
408	$A_2 + OH \rightleftharpoons A_2\text{-}1 + H_2O$	1.60(+8)	1.42	1.45	$k_{408} = k_{364}$
409	$A_2 + OH \rightleftharpoons A_2\text{-}2 + H_2O$	1.60(+8)	1.42	1.45	$k_{409} = k_{364}$
410	$A_2\text{-}1 + H(+M) \rightleftharpoons A_2(+M)$	1.00(+14)			k_∞, p
		3.8(+127)	−31.434	18.7	$k_0/[M']$, e
	$a = 0.2$, $T^{***} = 123$, $T^* = 478$, $T^{**} = 5412$				i
411	$A_2\text{-}2 + H(+M) \rightleftharpoons A_2(+M)$	1.00(+14)			k_∞, p
		9.5(+129)	−32.132	18.8	$k_0/[M']$, e
	$a = 0.87$, $T^{***} = 493$, $T^* = 118$, $T^{**} = 5652$				i
412	$A_2\text{-}1 + H \rightleftharpoons A_2\text{-}2 + H$	8.80(+58)	−11.68	61.0	20 torr, p
		6.50(+45)	−7.90	55.5	90 torr
		2.40(+24)	−1.81	45.3	760 torr
	Formation and Reactions of Ethynylnaphthalene (A_2C_2H)				
t + 413	$A_2 + C_2H \rightleftharpoons A_2C_2HA + H$	5.00(+13)			n
414	$A_2 + C_2H \rightleftharpoons A_2C_2HB + H$	5.00(+13)			n
415	$A_2\text{-}1 + C_2H_2 \rightleftharpoons A_2C_2H_2$	4.50(+39)	−8.71	14.3	20 torr, [24]
		3.40(+43)	−9.56	18.2	90 torr
		1.70(+43)	−9.12	21.1	760 torr
416	$A_2\text{-}1 + C_2H_2 \rightleftharpoons A_2C_2HA + H$	1.40(+22)	−2.64	17.4	20 torr, [24]
		9.10(+24)	−3.39	20.4	90 torr
		1.30(+24)	−3.06	22.6	760 torr

TABLE 1 (Continued)

Reaction Mechanism

No.	Reactions[b]	$k = AT^n \exp(-E/RT)$[a] A	n	E	Comments/ References
417	$A_2C_2HA + H \rightleftharpoons A_2C_2H_2$	1.90(+50)	−11.63	16.2	20 torr, [24]
		3.30(+51)	−11.72	18.9	90 torr
		5.90(+46)	−10.03	19.1	760 torr
418	$A_2C_2H_2 + H \rightleftharpoons A_2C_2HA + H_2$	1.50(+13)			n
419	$A_2C_2H_2 + OH \rightleftharpoons A_2C_2HA + H_2O$	2.50(+12)			n
420	$A_2C_2HA + H \rightleftharpoons A_2C_2HA^* + H_2$	2.50(+14)		16.0	$k_{420} = k_{363}$
421	$A_2C_2HB + H \rightleftharpoons A_2C_2HB^* + H_2$	2.50(+14)		16.0	$k_{421} = k_{363}$
422	$A_2C_2HA + OH \rightleftharpoons A_2C_2HA^* + H_2O$	1.60(+8)	1.42	1.45	$k_{422} = k_{364}$
423	$A_2C_2HB + OH \rightleftharpoons A_2C_2HB^* + H_2O$	1.60(+8)	1.42	1.45	$k_{423} = k_{364}$
424	$A_2C_2HB^* + H(+M) \rightleftharpoons A_2C_2HB(+M)$	1.00(+14)			k_∞, $k_{424} = k_{410}$
		3.8(+127)	−31.434	18.7	k_0/[M′], e
	$a = 0.2$, $T^{***} = 123$, $T^* = 478$, $T^{**} = 5412$				i
425	$A_2C_2HA^* + H(+M) \rightleftharpoons A_2C_2HA(+M)$	1.00(+14)			k_∞, $k_{425} = k_{411}$
		9.5(+129)	−32.132	18.8	k_0/[M′], e
	$a = 0.87$, $T^{***} = 493$, $T^* = 118$, $T^{**} = 5652$				i
	Formation and Reactions of Phenanthrene (A_3)				
426	$A_2C_2HB^* + C_2H_2 \rightleftharpoons A_3$-1	5.20(+72)	−18.11	33.9	20 torr, $k_{426} = k_{397}$
		2.00(+72)	−17.74	36.6	90 torr
		1.10(+62)	−14.56	33.1	760 torr
427	$A_2C_2HB^* + C_2H_2 \rightleftharpoons A_2C_2H)_2 + H$	5.50(+32)	−5.46	27.6	20 torr, $k_{427} = k_{398}$
		4.80(+29)	−4.59	26.0	90 torr
		1.80(+19)	−1.67	18.8	760 torr
428	$A_2C_2H)_2 + H \rightleftharpoons A_3$-1	2.00(+82)	−20.23	36.9	20 torr, $k_{428} = k_{400}$
		2.00(+75)	−18.06	34.5	90 torr
		6.90(+63)	−14.57	29.9	760 torr
429	$A_2C_2HA^* + C_2H_2 \rightleftharpoons A_3$-4	5.20(+72)	−18.11	33.9	20 torr, $k_{429} = k_{397}$
		2.00(+72)	−17.74	36.6	90 torr
		1.10(+62)	−14.56	33.1	760 torr
430	$A_2C_2HA^* + C_2H_2 \rightleftharpoons A_2C_2H)_2 + H$	5.50(+32)	−5.46	27.6	20 torr, $k_{430} = k_{398}$
		4.80(+29)	−4.59	26.0	90 torr
		1.80(+19)	−1.67	18.8	760 torr
431	$A_2C_2H)_2 + H \rightleftharpoons A_3$-4	2.00(+82)	−20.23	36.9	20 torr, $k_{431} = k_{399}$
		2.00(+75)	−18.06	34.5	90 torr
		6.90(+63)	−14.57	29.9	760 torr
432	$A_2C_2HA + C_2H \rightleftharpoons A_2C_2\ H)_2 + H$	5.00(+13)			n
433	$A_2C_2HB + C_2H \rightleftharpoons A_2C_2\ H)_2 + H$	5.00(+13)			n
434	$A_3 + H \rightleftharpoons A_3$-1 $+ H_2$	2.50(+14)		16.0	$k_{434} = k_{363}$
435	$A_3 + H \rightleftharpoons A_3$-4 $+ H_2$	2.50(+14)		16.0	$k_{435} = k_{363}$
436	$A_3 + OH \rightleftharpoons A_3$-1 $+ H_2O$	1.60(+8)	1.42	1.45	$k_{436} = k_{364}$
437	$A_3 + OH \rightleftharpoons A_3$-4 $+ H_2O$	1.60(+8)	1.42	1.45	$k_{437} = k_{364}$
438	A_3-1 $+ H(+M) \rightleftharpoons A_3(+M)$	1.00(14)			k_∞, p
		4.0(+148)	−37.51	20.6	k_0/[M′], e
	$a = 1$, $T^{***} = 1$, $T^* = 145$, $T^{**} = 5633$				i
439	A_3-4 $+ H(+M) \rightleftharpoons A_3(+M)$	1.00(+14)			k_∞, p
		2.1(+139)	−34.80	18.4	k_0/[M′], e
	$a = 1$, $T^{***} = 1$, $T^* = 171$, $T^{**} = 4993$				i
440	A_3-1 $+ H \rightleftharpoons A_3$-4 $+ H$	1.70(+72)	−15.22	77.2	20 torr, p
		9.30(+58)	−11.45	71.1	90 torr
		3.80(+40)	−6.31	61.8	760 torr
	Formation and Reactions of Pyrene (A_4)				
441	$A_3 + C_2H \rightleftharpoons A_3C_2H + H$	5.00(+13)			n
442	A_3-4 $+ C_2H_2 \rightleftharpoons A_3C_2H_2$	6.70(+45)	−10.55	21.2	20 torr, [24]
		6.50(+53)	−12.59	26.9	90 torr
		8.00(+61)	−14.50	34.8	760 torr

TABLE 1 (Continued)

Reaction Mechanism

No.	Reactions[b]	$k = AT^n \exp(-E/RT)$[a] A	n	E	Comments/ References
443	$A_3\text{-}4 + C_2H_2 \rightleftharpoons A_3C_2H + H$	8.00(+17)	−1.21	22.6	20 torr, [24]
		3.40(+12)	0.34	19.7	90 torr
		1.20(+26)	−3.44	30.2	760 torr
444	$A_3\text{-}4 + C_2H_2 \rightleftharpoons A_4 + H$	4.00(+23)	−3.20	14.4	20 torr, [24]
		8.90(+24)	−3.56	15.9	90 torr
		3.30(+24)	−3.36	17.8	760 torr
445	$A_3C_2H + H \rightleftharpoons A_3C_2H_2$	5.20(+47)	−11.05	14.7	20 torr, [24]
		1.40(+56)	−13.21	21.0	90 torr
		1.90(+64)	−15.12	29.3	760 torr
446	$A_3C_2H + H \rightleftharpoons A_4 + H$	6.80(+26)	−4.07	9.5	20 torr, [24]
		4.20(+27)	−4.25	10.9	90 torr
		9.00(+38)	−7.39	20.7	760 torr
447	$A_3C_2H_2 \rightleftharpoons A_4 + H$	7.30(+48)	−11.86	28.1	20 torr, [24]
		6.30(+59)	−14.70	36.9	90 torr
		2.00(+63)	−15.28	43.2	760 torr
448	$A_4 + H \rightleftharpoons A_4\text{-} + H_2$	2.50(+14)		16.0	$k_{448} = k_{363}$
449	$A_4 + OH \rightleftharpoons A_4\text{-} + H_2O$	1.60(+8)	1.42	1.45	$k_{449} = k_{364}$
450	$A_4\text{-} + H \rightleftharpoons A_4$	1.00(+14)			n
	Formation and Reactions of Biphenyl (P_2)				
451	$A_1 + A_1\text{-} = P_2 + H$	5.60(+12)	−0.074	7.55	20 torr, p
		1.50(+14)	−0.45	8.92	90 torr
		1.10(+23)	−2.92	15.89	760 torr
452	$A_1 + A_1\text{-} \rightleftharpoons P_2\text{-}H$	8.10(+36)	−8.62	9.13	20 torr, p
		2.20(+36)	−8.21	9.92	90 torr
		3.70(+32)	−6.74	9.87	760 torr
453	$P_2 + H \rightleftharpoons P_2\text{-}H$	1.16(+41)	−9.51	10.83	20 torr, p
		2.40(+40)	−9.06	11.57	90 torr
		6.82(+35)	−7.37	11.23	760 torr
454	$A_1\text{-} + A_1\text{-} \rightleftharpoons P_2$	3.80(+31)	−5.75	7.95	20 torr, p
		6.10(+25)	−4.00	5.59	90 torr
		2.00(+19)	−2.05	2.90	760 torr
455	$A_1\text{-} + A_1\text{-} \rightleftharpoons P_2\text{-} + H$	7.00(+23)	−2.33	38.54	20 torr, p
		8.60(+13)	0.50	34.82	90 torr
		2.30(−1)	4.62	28.95	760 torr
456	$P_2 \rightleftharpoons P_2\text{-} + H$	9.00(+37)	−6.63	119.58	20 torr, p
		8.10(+31)	−4.79	117.12	90 torr
		1.10(+25)	−2.72	114.27	760 torr
457	$P_2 + H \rightleftharpoons P_2\text{-} + H_2$	2.50(+14)		16.0	$k_{457} = k_{363}$
458	$P_2 + OH \rightleftharpoons P_2\text{-} + H_2O$	1.60(+8)	1.42	1.45	$k_{458} = k_{364}$
459	$P_2\text{-} + C_2H_2 \rightleftharpoons A_3 + H$	4.60(+6)	1.97	7.3	$k_{459} = k_{\infty,442}$
	Benzene Oxidation				
460	$A_1 + O \rightleftharpoons C_6H_5O + H$	2.20(+13)		4.53	[58]
461	$A_1 + OH \rightleftharpoons C_6H_5OH + H$	1.30(+13)		10.6	[58]
462	$A_1\text{-} + O_2 \rightleftharpoons C_6H_5O + O$	2.10(+12)		7.47	[60]; see text
463	$C_6H_5O \rightleftharpoons CO + C_5H_5$	2.50(+11)		43.9	[60]
464	$C_6H_5O + H(+M) \rightleftharpoons C_6H_5OH(+M)$	2.50(+14)			k_∞, [28]
		1.00(+94)	−21.84	13.9	$k_0/[M']$, e
	$a = 0.043$, $T^{***} = 304$, $T^* = 60{,}000$, $T^{**} = 5896$				i
465	$C_6H_5O + H \rightleftharpoons CO + C_5H_6$	3.00(+13)			n
466	$C_6H_5O + O \rightarrow HCO + 2C_2H_2 + CO$	3.00(+13)			n
467	$C_6H_5OH + H \rightleftharpoons C_6H_5O + H_2$	1.15(+14)		12.4	[61]
468	$C_6H_5OH + O \rightleftharpoons C_6H_5O + OH$	2.80(+13)		7.35	[62]
469	$C_6H_5OH + OH \rightleftharpoons C_6H_5O + H_2O$	6.00(+12)			[61]

TABLE 1 (Continued)

Reaction Mechanism

No.	Reactions[b]	$k = AT^n \exp(-E/RT)$[a] A	n	E	Comments/ References
470	$C_5H_5 + H(+M) \rightleftharpoons C_5H_6(+M)$	1.00(+14)			k_∞,[28]
		4.40(+80)	−18.28	13.0	k_0/[M'], *e*
	$a = 0.068, T^{***} = 401, T^* = 4136, T^{**} = 5502$				*i*
471	$C_5H_5 + O \rightleftharpoons n\text{-}C_4H_5 + CO$	1.00(+14)			[62]
472	$C_5H_5 + OH \rightleftharpoons C_5H_4OH + H$	5.00(+12)			*n*
473	$C_5H_5 + HO_2 \rightleftharpoons C_5H_5O + OH$	3.00(+13)			[62]
474	$C_5H_6 + H \rightleftharpoons C_5H_5 + H_2$	2.20(+8)	1.77	3.0	[62]
475	$C_5H_6 + O \rightleftharpoons C_5H_5 + OH$	1.80(+13)		3.08	[62]
476	$C_5H_6 + OH \rightleftharpoons C_5H_5 + H_2O$	3.43(+9)	1.18	−0.447	[62]
477	$C_5H_5O \rightleftharpoons n\text{-}C_4H_5 + CO$	2.50(+11)		43.9	[62]
478	$C_5H_5O + H \rightleftharpoons CH_2O + 2C_2H_2$	3.00(+13)			*n*
479	$C_5H_5O + O \rightleftharpoons CO_2 + n\text{-}C_4H_5$	3.00(+13)			*n*
480	$C_5H_4OH \rightleftharpoons C_5H_4O + H$	2.10(+13)		48.0	[62]
481	$C_5H_4OH + H \rightleftharpoons CH_2O + 2C_2H_2$	3.00(+13)			*n*
482	$C_5H_4OH + O \rightleftharpoons CO_2 + n\text{-}C_4H_5$	3.00(+13)			*n*
483	$C_5H_4O \rightleftharpoons CO + C_2H_2 + C_2H_2$	1.00(+15)		78.0	[62]
484	$C_5H_4O + O \rightleftharpoons CO_2 + 2C_2H_2$	3.00(+13)			*n*
	PAH Oxidation by OH				
485	$A_1C_2H + OH \rightarrow A_1\text{-} + CH_2CO$	2.18(−4)	4.5	−1.0	$k_{485} = k_{139}$
486	$A_1C_2H)_2 + OH \rightarrow A_1C_2H\text{-} + CH_2CO$	2.18(−4)	4.5	−1.0	$k_{486} = k_{139}$
487	$A_2C_2HA + OH \rightarrow A_2\text{-}1 + CH_2CO$	2.18(−4)	4.5	−1.0	$k_{487} = k_{139}$
488	$A_2C_2HB + OH \rightarrow A_2\text{-}2 + CH_2CO$	2.18(−4)	4.5	−1.0	$k_{488} = k_{139}$
489	$A_3C_2H + OH \rightarrow A_3\text{-}4 + CH_2CO$	2.18(−4)	4.5	−1.0	$k_{489} = k_{139}$
490	$A_1C_2H + OH \rightarrow C_6H_5O + C_2H_2$	1.30(+13)		10.6	$k_{490} = k_{461}$
491	$A_1C_2H_3 + OH \rightarrow C_6H_5O + C_2H_4$	1.30(+13)		10.6	$k_{491} = k_{461}$
492	$A_1C_2H)_2 + OH \rightarrow C_4H_2 + C_6H_5O$	1.30(+13)		10.6	$k_{492} = k_{461}$
493	$A_2 + OH \rightarrow A_1C_2H + CH_2CO + H$	1.30(+13)		10.6	$k_{493} = k_{461}$
494	$A_2C_2HA + OH \rightarrow A_1C_2H + H_2C_4O + H$	1.30(+13)		10.6	$k_{494} = k_{461}$
495	$A_2C_2HB + OH \rightarrow A_1C_2H + H_2C_4O + H$	1.30(+13)		10.6	$k_{495} = k_{461}$
496	$A_3 + OH \rightarrow A_2C_2HB + CH_2CO + H$	6.50(+12)		10.6	$k_{496} = 0.5 \times k_{461}$
497	$A_3 + OH \rightarrow A_2C_2HA + CH_2CO + H$	6.50(+12)		10.6	$k_{497} = 0.5 \times k_{461}$
498	$A_3C_2H + OH \rightarrow A_2C_2HA + H_2C_4O + H$	6.50(+12)		10.6	$k_{498} = 0.5 \times k_{461}$
499	$A_3C_2H + OH \rightarrow A_2C_2HB + H_2C_4O + H$	6.50(+12)		10.6	$k_{499} = 0.5 \times k_{461}$
500	$A_4 + OH \rightarrow A_3\text{-}4 + CH_2CO$	1.30(+13)		10.6	$k_{500} = k_{461}$
	PAH Oxidation by O				
501	$A_1C_2H + O \rightarrow HCCO + A_1\text{-}$	2.04(+7)	2.0	1.9	$k_{501} = k_{137} + k_{139}$
502	$A_1C_2H)_2 + O \rightarrow HCCO + A_1C_2H\text{-}$	2.04(+7)	2.0	1.9	$k_{502} = k_{137} + k_{139}$
503	$A_1C_2H_3 + O \rightarrow A_1\text{-} + CH_3 + CO$	1.92(+7)	1.83	0.22	$k_{503} = k_{160}$
504	$A_2C_2HA + O \rightarrow HCCO + A_2\text{-}1$	2.04(+7)	2.0	1.9	$k_{504} = k_{137} + k_{139}$
505	$A_2C_2HB + O \rightarrow HCCO + A_2\text{-}2$	2.04(+7)	2.0	1.9	$k_{505} = k_{137} + k_{139}$
506	$A_1C_2H + O \rightarrow C_2H + C_6H_5O$	2.20(+13)		4.53	$k_{506} = k_{460}$
507	$A_1C_2H_3 + O \rightarrow C_2H_3 + C_6H_5O$	2.20(+13)		4.53	$k_{507} = k_{460}$
508	$A_1C_2H)_2 + O \rightarrow C_6H_5O + C_4H$	2.20(+13)		4.53	$k_{508} = k_{460}$
509	$A_2 + O \rightarrow CH_2CO + A_1C_2H$	2.20(+13)		4.53	$k_{509} = k_{460}$
510	$A_2C_2HA + O \rightarrow A_1C_2H)_2 + CH_2CO$	2.20(+12)		4.53	$k_{510} = k_{460}$
511	$A_2C_2HB + O \rightarrow A_1C_2H)_2 + CH_2CO$	2.20(+13)		4.53	$k_{511} = k_{460}$
512	$A_3 + O \rightarrow A_2C_2HA + CH_2CO$	1.10(+13)		4.53	$k_{512} = 0.5 \times k_{460}$
513	$A_3 + O \rightarrow A_2C_2HB + CH_2CO$	1.10(+13)		4.53	$k_{513} = 0.5 \times k_{460}$
514	$A_3C_2H + O \rightarrow A_2C_2HA + H_2C_4O$	1.10(+13)		4.53	$k_{514} = 0.5 \times k_{460}$
515	$A_3C_2H + O \rightarrow A_2C_2HB + H_2C_4O$	1.10(+13)		4.53	$k_{515} = 0.5 \times k_{460}$
516	$A_4 + O \rightarrow A_3\text{-}4 + HCCO$	2.20(+13)		4.53	$k_{516} = k_{460}$

TABLE 1 (Continued)

Reaction Mechanism

No.	Reactions[b]	$k = AT^n \exp(-E/RT)$[a] A	n	E	Comments/ References
	PAH Oxidation by O_2				
517	$A_1C_2H^* + O_2 \rightarrow l\text{-}C_6H_4 + CO + HCO$	2.10(+12)		7.47	$k_{517} = k_{462}$
518	$A_1C_2H\text{-} + O_2 \rightarrow l\text{-}C_6H_4 + CO + HCO$	2.10(+12)		7.47	$k_{518} = k_{462}$
519	$A_1C_2H_3^* + O_2 \rightarrow l\text{-}C_6H_6 + CO + HCO$	2.10(+12)		7.47	$k_{519} = k_{462}$
520	$n\text{-}A_1C_2H_2 + O_2 \rightarrow A_1\text{-} + CO + CH_2O$	1.00(+11)			n
521	$A_2\text{-}1 + O_2 \rightarrow A_1C_2H + HCO + CO$	2.10(+12)		7.47	$k_{521} = k_{462}$
522	$A_2\text{-}2 + O_2 \rightarrow A_1C_2H + HCO + CO$	2.10(+12)		7.47	$k_{522} = k_{462}$
523	$A_2C_2HA^* + O_2 \rightarrow A_2\text{-}1 + CO + CO$	2.10(+12)		7.47	$k_{523} = k_{462}$
524	$A_2C_2HB^* + O_2 \rightarrow A_2\text{-}2 + CO + CO$	2.10(+12)		7.47	$k_{524} = k_{462}$
525	$A_3\text{-}4 + O_2 \rightarrow A_2C_2HB + HCO + CO$	2.10(+12)		7.47	$k_{525} = k_{462}$
526	$A_3\text{-}1 + O_2 \rightarrow A_2C_2HA + HCO + CO$	2.10(+12)		7.47	$k_{526} = k_{462}$
527	$A_4\text{-} + O_2 \rightarrow A_3\text{-}4 + CO + CO$	2.10(+12)		7.47	$k_{527} = k_{462}$

[a] The units are mole, centimeter, second, and kilocalorie. Numbers in parentheses denote powers of 10. The reverse rate coefficients were calculated via equilibrium constants.

[b] Reactions with the sign " $\rightleftharpoons$ " are reversible and those with " $\rightarrow$ " are irreversible.

[c] Third-body enhancement factors: $H_2 = 0.096T^{0.4}$, $H_2O = 60T^{-0.25}$, $CH_4 = 2$, $CO_2 = 550T^{-1.0}$, $C_2H_6 = 3$, and Ar = 0.63.

[d] Third-body enhancement factors: $H_2 = 0.73$, $H_2O = 3.65$, $CH_4 = 2.0$, $C_2H_6 = 3.0$, and Ar = 0.38.

[e] Third-body enhancement factors: $H_2 = 2$, $H_2O = 6$, $CH_4 = 2$, CO = 1.5, $CO_2 = 2$, $C_2H_6 = 3$, and Ar = 0.7.

[f] Third-body enhancement factors: $H_2 = 2.4$, $H_2O = 15.4$, $CH_4 = 2$, CO = 1.75, $CO_2 = 3.6$, $C_2H_6 = 3$, and Ar = 0.83.

[g] Third-body enhancement factors: $O_2 = 107T^{-0.86}$, $H_2O = 3.35T^{0.1}$, CO = 0.75, $CO_2 = 1.5$, $C_2H_6 = 1.5$, $N_2 = 134T^{-0.86}$, and Ar = $0.25T^{0.06}$.

[h] $[M'] = \Sigma_i \beta_i C_i$, where β_i is the third-body enhancement factor with its value given in comment *e* and C_i is the concentration of species *i*.

[i] Troe's broadening factor, $F_c(T) = (1 - a)\exp(-T/T^{***}) + a\exp(-T/T^*) + \exp(-T^{**}/T)$.

[j] Third-body enhancement factors: $H_2 = 2$, $O_2 = 6$, $H_2O = 6$, $CH_4 = 2$, CO = 1.5, $CO_2 = 3.5$, $C_2H_6 = 3$, and Ar = 0.5.

[k] Products modified from HCO + OH in Ref. 35 to CO + H + H (see text).

[l] [M'] is defined in comment *h*. Third-body enhancement factors: $H_2 = 2$, $H_2O = 6$, $CH_4 = 2$, CO = 1.5, $CO_2 = 2$, and $C_2H_6 = 3$.

[m] Evaluated based on the rate data reported in Refs. 36 and 37.

[n] Estimated.

[o] Average of the rate coefficients report in Refs. 36 and 37.

[p] See Appendix.

[q] The rate coefficient expression was taken from Ref. 39 with 3.2 kcal/mol added to the activation energy to account for the difference in $\Delta_f H^0_{298}$ of C_2H_3 between the present study and Ref. 39.

[r] k_∞ was obtained by averaging the rate coefficients reported in Refs. 45 and 46. k_0 and F_c were obtained by fitting the high-temperature data reported in Refs. 47 and 48.

[s] Assumed to be equal to that of $C_2H_3 + CH_3(+M) \rightleftharpoons C_3H_6(+M)$. k_∞, k_0, and the fall-off parameters were obtained by fitting the RRKM results of Ref. 39 with $\langle E_{down} \rangle = 600$ cm^{-1}. [M'] is defined in comment *h*. The third-body enhancement factors are given in comment *e*.

[t] Estimated based on a theoretical study [50].

[u] The rate coefficient expression was obtained by fitting the rate data reported in Ref. 51, assuming that the temperature exponent is equal to 2 (see text).

[v] The *A* factor was assumed to be equal to half of that for k_{271} and *E* reduced by 3 kcal/mol to account for the energy difference between $n\text{-}C_4H_3$ and $i\text{-}C_4H_3$ (see text).

[w] The *A* factor was assumed to be equal to half of that for k_{291} and *E* reduced by 3 kcal/mol to account for the energy difference between $n\text{-}C_4H_5$ and $i\text{-}C_4H_5$ (see text).

[x] The *A* factor was assumed to be equal to that of k_{294} and *E* increased by 3 kcal/mol to account for the energy difference between $n\text{-}C_4H_5$ and $i\text{-}C_4H_5$ (see text).

[y] The rate coefficient expression was obtained by fitting the rate data reported in Ref. 51, assuming that the temperature exponent is equal to 2 (see text).

[z] The rate coefficients were assumed to be equal to those of the analogous reactions of C_3H_6. The latter were taken from Ref. 56.

[aa] The rate coefficient expression is the same as that of the analogous reaction 290, but with 1.2 kcal/mol added to the activation energy to account for the energy barrier difference between C_2H_2 addition to $n\text{-}C_4H_5$ and to phenyl [24].

$$C_4H_2 + H \rightleftharpoons i\text{-}C_4H_3, \quad \text{(R242)}$$

$$n\text{-}C_4H_3 \rightleftharpoons i\text{-}C_4H_3, \quad \text{(R254)}$$

were obtained by a Rice–Ramsperger–Kassel–Marcus (RRKM) analysis [43], treating them as chemically activated processes. The RRKM parameters were obtained from *ab initio* quantum mechanical calculation on the i.e., MP4/6-31G**//HF/6-31G** level. The computed rate coefficient of the related reaction

$$C_2H_2 + C_2H \rightleftharpoons C_4H_2 + H \quad \text{(R190)}$$

is in close agreement with the average of the data reported in Refs. 36 and 37, and hence the rate parameters obtained from our RRKM analysis are consistent with the assignment of k_{190} in the reaction model. It was assumed that the difference in the enthalpies of formation between n-C_4H_3 and i-C_4H_3 is 8 kcal/mol, based on our *ab initio* calculations at the MP4/6-31G**//HF/6-31G** level [43]. We note that the 8-kcal/mol difference compares favorable to the literature data, e.g., 6–7 kcal/mol assigned in the work of Kiefer and von Drasek [67], and Stein's estimate of 8 kcal/mol based on the upper limit of the resonant energy in the propargyl radical (see Ref. 68 for a review on the enthalpy of formation of C_4H_3).

The formation and destruction of vinylacetylene (C_4H_4) and 1,3-butadiene ($1,3$-C_4H_6) were described by reactions between C_1 and C_3 and between C_2 and C_2. Specifically, C_4H_4 is produced/destroyed mainly through reactions

$$C_2H_3 + C_2H_2 \rightleftharpoons C_4H_4 + H, \quad \text{(R193)}$$

$$C_3H_3 + CH_2 \rightleftharpoons C_4H_4 + H. \quad \text{(R224)}$$

For 1,3-butadiene, the following major reactions were assigned:

$$C_2H_4 + C_2H_3 \rightleftharpoons 1,3\text{-}C_4H_6 + H, \quad \text{(R197)}$$

$$C_3H_3 + CH_3 \rightleftharpoons 1,2\text{-}C_4H_6, \quad \text{(R226)}$$

$$1,2\text{-}C_4H_6 + H \rightleftharpoons 1,3\text{-}C_4H_6 + H. \quad \text{(R296)}$$

The rate coefficient of (R197) was obtained in the present study through an RRKM calculation (see Appendix).

Miller and Melius [23] suggested that in rich flames the n-C_4H_3 (H–C≡C–CH=$\dot{C}$H) radical is rapidly consumed to form its resonantly stabilized i-C_4H_3 (H–C≡C–$\dot{C}$=CH_2) radical via

$$n\text{-}C_4H_3 + H \rightleftharpoons i\text{-}C_4H_3 + H. \quad \text{(R255)}$$

In their analysis, a rate coefficient value of 5×10^{13} cm^3 mol^{-1} s^{-1} was assumed for k_{255}. We note that (R255) is a typical chemically activated reaction and hence its rate coefficient must exhibit a pressure dependence. We performed an RRKM analysis for this multichannel chemically activated/unimolecular reaction system, including the stabilization, isomerization, or dissociation of the hot adduct, leading to C_4H_4, $C_4H_2 + H_2$, $C_2H_2 + C_2H_2$, and i-$C_4H_3 + H$ (see Appendix). Our RRKM calculations suggest that under combustion temperatures, the rate coefficient of

$$n\text{-}C_4H_3 + H \rightleftharpoons C_2H_2 + C_2H_2 \quad \text{(R256)}$$

is larger than k_{255}, but $k_{255} + k_{256} \approx 10^{14}$ cm^3 mol^{-1} s^{-1}. These RRKM results are incorporated into the present reaction mechanism. Thus, the total destruction rate of n-C_4H_3 in the present reaction model is larger than that assumed in Ref. 23. Similar RRKM calculations were performed for reaction systems involving n-$C_4H_5 + H$ and n-$A_1C_2H_2 + H$ (see Appendix).

The rate coefficient expression for the H abstraction of $1,3$-C_4H_6 by OH (R294) was obtained by fitting the rate data reported in Ref. 51, assuming that the temperature exponent is equal to 2 to take into account the non-Arrhenius behavior typical for this type of reactions. The primary products of the H-abstraction reaction are assumed to be the resonantly stabilized i-C_4H_5 and H_2O. For reaction (R293), $1,3$-$C_4H_6 + OH \rightarrow n$-$C_4H_5 + H_2O$, we assume that k_{293} differs from k_{294} in the activation energy with E_{293} being 3 kcal/mol larger than E_{294}, as in Ref. 23. For other analogous H-abstraction reactions by OH, similar rate coefficient expressions were assigned but with corrections to the A factor to account for the reaction path degeneracy.

TABLE 2

Thermochemical Properties

Species[a]	$\Delta_f H°_{298}$ (kcal/mol)	$S°_{298}$ (cal/mol K)	$C°_p(T)$ (cal/mol K) 300	500	1000	1500	2000	2500	References/ Comments
C_2O	68.5	55.68	10.3	11.7	13.7	14.6	15.2	15.4	[63]
C_2H_3O	6.1	64.28	13.9	20.5	23.4	26.4	28.2	29.1	[64]
C_3H_2	106.5	56.22	13.2	17.0	21.6	24.1	25.8	26.7	[63]
C_3H_3	83.1	61.48	15.8	19.5	25.0	27.5	29.2	30.1	[63]
a-C_3H_4	45.2	54.89	14.1	19.8	28.0	32.0	34.2	35.3	[63]
p-C_3H_4	44.0	49.49	14.6	19.7	27.7	31.8	34.0	35.2	[63]
C_4H	192.9	63.47	16.0	18.9	22.4	24.1	25.2	25.7	*b*
C_4H_2	112.0	61.18	17.7	21.9	26.6	29.0	30.5	31.2	*c*
H_2C_4O	54.6	66.43	17.3	21.8	28.7	31.5	33.3	34.2	[63]
n-C_4H_3	127.1	67.98	17.7	23.3	30.1	33.4	35.0	35.9	[24]
i-C_4H_3	119.1	70.18	19.9	24.5	30.6	33.6	35.2	36.0	*d*
C_4H_4	68.0	66.57	17.5	24.5	33.7	38.0	40.2	41.3	[24]
n-C_4H_5	85.4	69.46	18.8	26.5	37.1	42.3	45.1	46.4	[24]
i-C_4H_5	77.4	68.46	18.1	26.0	37.0	42.2	45.2	46.5	[24]
1,3-C_4H_6	26.3	66.40	18.3	27.3	40.5	46.8	50.2	51.8	[24]
1,2-C_4H_6	39.3	69.71	19.3	27.5	40.1	45.6	49.5	51.3	[64]
C_5H_2	165.3	63.69	19.9	26.0	32.8	35.4	36.9	37.6	[63]
C_5H_3	135.4	70.53	21.0	27.0	34.9	38.5	40.6	41.7	[63]
C_5H_4O	11.0	67.14	18.4	28.9	43.3	49.0	51.8	53.4	[64]
C_5H_5	63.5	66.79	18.4	29.6	42.8	48.1	51.1	52.7	[64]
C_5H_5O	19.3	73.53	21.6	33.5	48.1	53.7	57.0	58.7	[64]
C_5H_4OH	19.2	74.08	23.0	34.5	47.6	52.9	55.9	57.6	[64]
C_5H_6	31.9	65.49	18.2	30.2	45.8	52.1	55.8	57.7	[64]
C_6H	250.4	75.97	22.0	27.0	32.1	34.2	35.5	36.3	*e*
C_6H_2	169.5	74.35	24.8	30.7	37.0	39.8	41.5	42.4	*f*
C_6H_3	174.7	78.76	24.9	32.3	41.1	44.9	46.7	47.8	*d*
l-C_6H_4	123.5	76.82	25.2	34.0	44.8	49.5	52.0	53.1	[24]
c-C_6H_4	106.0	67.85	19.3	30.0	43.3	48.7	51.6	52.7	[24]
n-C_6H_5	140.9	80.50	26.2	35.9	48.3	53.9	57.0	58.3	[24]
i-C_6H_5	132.9	78.77	24.9	35.0	48.0	53.8	57.2	58.2	*d*
C_6H_5O	11.4	73.56	22.7	35.7	52.2	58.5	62.3	64.3	[63]
C_6H_5OH	−23.0	75.24	24.9	38.6	55.6	62.4	66.5	68.7	[63]
l-C_6H_6	81.8	78.91	25.8	36.9	51.7	58.4	62.2	63.6	[24]
c-C_6H_7	49.9	72.00	21.7	35.7	54.5	62.6	67.2	68.7	[24]
n-C_6H_7	99.3	82.08	27.3	39.0	55.2	62.7	67.2	68.7	[24]
i-C_6H_7	91.3	79.57	25.5	37.7	54.7	62.6	67.1	68.7	*d*
C_6H_8	40.2	79.83	26.7	39.7	58.5	67.2	72.4	74.0	[24]
A_1·	78.6	68.62	18.5	30.6	46.3	52.8	56.4	57.8	[24, 33]
A_1	20.0	64.40	19.6	32.7	50.1	57.5	61.7	63.2	[24, 33]
A_1C_2H*	133.2	78.03	26.5	40.4	57.5	64.4	68.5	69.5	[24, 33]
A_1C2H-	132.7	78.06	26.5	40.5	57.6	64.6	68.1	69.8	[24, 33]
A_1C_2H	73.8	76.41	27.9	43.1	61.8	69.5	73.7	75.2	[24, 33]
n-$A_1C_2H_2$	94.5	86.02	28.0	43.6	63.9	72.5	77.7	79.1	[24, 33]
i-$A_1C_2H_2$	86.5	81.30	28.0	43.8	64.6	73.5	78.5	80.2	*d*
$A_1C_2H_3$*	92.4	84.52	26.5	42.3	63.4	72.5	77.1	79.3	*g*
$A_1C_2H_3$	35.4	81.33	28.5	45.4	68.2	78.0	83.8	85.4	*g*
$A_1C_2H)_2$	129.0	84.50	35.5	52.5	72.7	80.8	85.7	86.7	[24, 33]
Naphthyne	119.7	82.17	30.6	48.4	70.9	79.8	85.1	86.2	[23]
A_2-1	94.7	83.13	30.4	49.7	74.5	84.4	90.2	91.6	[24, 33]
A_2-2	94.3	83.33	30.8	49.8	74.5	84.4	90.2	91.6	*g*
A_2	35.8	80.26	31.8	52.1	78.4	89.2	95.4	97.1	[24, 33]
A_2C_2HA*	149.6	91.34	38.5	59.7	85.8	96.1	101.9	103.6	*h, i*
A_2C_2HB*	149.2	91.68	38.5	59.8	85.8	96.1	102.1	103.4	*h, j*
A_2C_2HA	90.6	91.21	39.7	62.1	89.7	100.8	107.4	108.8	*h, k*

TABLE 2 (Continued)

Thermochemical Properties

Species[a]	$\Delta_f H°_{298}$ (kcal/mol)	$S°_{298}$ (cal/mol K)	$C°_p(T)$ (cal/mol K) 300	500	1000	1500	2000	2500	References/ Comments
A_2C_2HB	89.6	91.28	39.9	62.1	89.7	101.0	106.6	109.3	*h, l*
$A_2C_2H_2$	112.3	100.77	40.1	62.9	92.1	104.2	111.1	113.2	[24]
$A_2C_2H)_2$	176.2	102.67	49.2	73.0	101.6	113.1	118.7	121.3	*h*
A_3-1	108.5	97.30	45.9	69.2	102.8	116.1	123.8	125.6	*g*
A_3-4	107.5	97.05	42.7	69.2	102.8	116.1	123.9	125.5	[24, 33]
A_3	49.6	95.74	43.9	71.4	106.7	120.8	129.1	130.9	*g*
A_3C_2H	109.1	105.28	52.2	81.5	118.1	132.5	140.7	142.9	[24, 33]
$A_3C_2H_2$	130.4	125.84	52.0	82.1	120.4	135.9	144.5	147.2	[24]
A_4-	112.4	99.56	46.8	76.1	113.0	127.4	134.4	137.7	*g*
A_4	53.9	95.79	48.7	79.2	117.3	132.2	140.7	142.7	[24, 33]
P_2-1	102.0	96.70	37.1	61.0	91.6	103.9	111.1	113.0	*g*
P_2	43.4	93.75	38.2	63.1	95.4	108.6	116.5	118.3	*g*
P_2-H	79.0	100.12	39.7	65.9	99.8	113.7	121.6	124.1	*h*

[a] The thermodynamic data for O, O_2, H, H_2, OH, H_2O, HO_2, H_2O_2, C, CH, CH_2, CH_2*, CH_3, CH_4, CO, CO_2, HCO, CH_2O, CH_2OH, CH_3O, CH_3OH, C_2H, C_2H_2, C_2H_3, C_2H_4, C_2H_5, C_2H_6, CH_2CO, HCCO, and HCCOH were taken from the GRI-Mech 1.2 [35].

[b] $\Delta_f H°_{298}$ was calculated with the ethylenic C–H bond dissociation energy (at 298 K) of 132.9 kcal/mol, consistent with the assignments for C_2H_2 and C_2H. The $S°_{298}$ and $C°_p$ data were taken from Ref. 43.

[c] $\Delta_f H°_{298}$ was taken from Ref. 65. The $S°_{298}$ and $C°_p$ data were taken from Ref. 64.

[d] $\Delta_f H°_{298}$ values of the resonantly stabilized radicals were calculated based on the ethylenic C–H bond dissociation energy (at 298 K) of 111.1 kcal/mol (consistent with the assignments of C_2H_3 and C_2H_4) minus 8 kcal/mol of resonance stabilization energy (see text). The $S°_{298}$ and $C°_p$ data were obtained using the method described in Ref. 24.

[e] Derived from the data of C_2H and C_4H and a "complete additivity" relation $P(C_6H) = 2P(C_4H) - P(C_2H)$.

[f] Derived from the data of C_2H_2 and C_4H_2 and a "complete additivity" relation $P(C_6H_2) = 2P(C_4H_2) - P(C_2H_2)$.

[g] $\Delta_f H°_{298}$ was taken from Ref. 33. The $S°_{298}$ and $C°_p$ data were obtained using the method described in Ref. 24.

[h] $\Delta_f H°_{298}$ was calculated using the AM1-GC method described in Ref. 33. The $S°_{298}$ and $C°_p$ data were obtained using the method described in Ref. 24.

[i] 1-Ethynyl-2-naphthyl.

[j] 2-Ethynyl-1-naphthyl.

[k] 1-Ethynylnaphthalene.

[l] 2-Ethynylnaphthalene.

There is no direct experimental measurement for the H abstraction of C_4H_4 and 1,3-C_4H_6 by the H atom. The rate coefficient of reaction

$$1,3\text{-}C_4H_6 + H \rightleftharpoons n\text{-}C_4H_5 + H_2 \qquad \text{(R291)}$$

was assumed to be equal to that of $C_2H_4 + H \rightleftharpoons C_2H_3 + H_2$ (R159). For the i-$C_4H_5 + H_2$ channel (R292), the activation energy of k_{291} was reduced by 3 kcal/mol, consistent with the H abstraction by OH discussed previously. Again, the rate coefficients of the analogous reactions were assigned with the same expressions as k_{291} and k_{292}, but corrections were made to the A factors to account for the reaction path degeneracy.

Formation and Reactions of Aromatic Species

The aromatics submechanism describes PAH formation and growth up to pyrene. It was suggested in the work of Frenklach and Warnatz [12] that the first aromatic ring is mainly produced by

$$n\text{-}C_4H_3 + C_2H_2 \rightarrow n\text{-}C_6H_5 \rightarrow \text{phenyl},$$

$$n\text{-}C_4H_5 + C_2H_2 \rightarrow n\text{-}C_6H_7 \rightarrow \text{benzene} + H.$$

Subsequently, the direct chemically activated pathways

$$n\text{-}C_4H_3 + C_2H_2 \rightleftharpoons \text{phenyl}, \qquad \text{(R267)}$$

$$n\text{-}C_4H_5 + C_2H_2 \rightleftharpoons \text{benzene} \qquad \text{(R290)}$$

were suggested by Westmoreland et al. [19] for benzene and phenyl formation in a near-soot-

ing acetylene flame. Recently, Miller and Melius [23] suggested that n-C_4H_3 and n-C_4H_5 could not be in concentrations large enough to form benzene or phenyl, because these radicals transform rapidly to resonantly stabilized isomers i-C_4H_3 and i-C_4H_5, respectively, via

$$n\text{-}C_4H_3 + H \rightleftharpoons i\text{-}C_4H_3 + H, \qquad \text{(R255)}$$

$$n\text{-}C_4H_5 + H \rightleftharpoons i\text{-}C_4H_5 + H. \qquad \text{(R278)}$$

They suggested that the recombination channels of propargyl radicals

$$C_3H_3 + C_3H_3 \rightleftharpoons \text{benzene}, \qquad \text{(R227)}$$

$$C_3H_3 + C_3H_3 \rightleftharpoons \text{phenyl} + H \qquad \text{(R227}'\text{)}$$

are more important sources of the first aromatic ring in flames. Because the preceding reactions require extensive internal rearrangements steps before the nonaromatic C_6H_6 adduct can isomerize to hot benzene molecule and subsequently be stabilized or dissociate to phenyl and H, the extent of benzene and phenyl production from a single-step reaction is uncertain, particularly under the present flame conditions.

Furthermore, we note that the assignment of k_{227} or $k_{227'} = 1 \times 10^{13}$ cm^3 mol^{-1} s^{-1} as in the work of Miller and Melius [23] is unreasonable at flame temperatures. Specifically, if $k_{227'} = 1 \times 10^{13}$ cm^3 mol^{-1} s^{-1}, the reverse rate coefficients are calculated, respectively, to be 2.0×10^{14} and 1.4×10^{15} cm^3 mol^{-1} s^{-1} at temperatures of 1500 and 1800 K, which are apparently too high. Similarly, if $k_{227} = 1 \times 10^{13}$ cm^3 mol^{-1} s^{-1}, the rate coefficient at, say, 1 atm and 1500 K for the reverse reaction is much larger than that of benzene dissociation to phenyl and H,

$$A_1 \rightleftharpoons A_{1^-} + H, \qquad \text{(-R365)}$$

which is 35 kcal/mol less endothermic than reaction (R227) and thus more favored under almost all conditions.

The difficulties with the propargyl recombination route to aromatics have been discussed by us previously [22, 69]. Similar difficulties were also noted in Refs. 25 and 27 in the context of benzene oxidation. Nonetheless, in view of the experimental observations of benzene production by the reaction of propargyl radicals [20, 30] and enhanced soot production in shock-tube pyrolysis of allene [13], it appears evident that propargyl recombination does ultimately lead to benzene. However, it is likely that such a process involves several elementary reaction steps. For example, the recombination of propargyl radicals may lead to stabilized linear (nonaromatic) C_6H_6 adducts, which may subsequently isomerize or react with other reactive species to form benzene. If so, in a flame environment the nonaromatic C_6H_6 adducts should be susceptible to thermal decomposition and oxidation, perhaps more readily than benzene. Hence reactions (R227) and (R227′) represent essentially global reaction steps, and their rate coefficients may be considerable lower than 2×10^{13} cm^3 mol^{-1} s^{-1}, the value determined by the overall disappearance rate of propargyl radicals [30].

Substantial uncertainties also exist for phenyl oxidation. A recent shock-tube study [70] of the reaction

$$A_{1^-} + O_2 \rightleftharpoons C_6H_5O + O \qquad \text{(R462)}$$

yielded a considerably larger rate coefficient than a previous measurement [60] and suggested a second product channel, i.e., phenyl + $O_2 \rightleftharpoons$ p-benzoquinone + H. Recently, Lin and coworkers [71, 72] performed experimental and theoretical studies for the phenyl + O_2 reaction. Their *ab initio* molecular orbital calculations failed to identify the p- and o-benzoquinone radicals as being energetically stable. However, using the RRKM approach, Yu and Lin [71] reproduced the total rate coefficient reported in Ref. 70 and reconciled the same data with their own low-temperature rate data of the phenyl and O_2 addition reaction.

In view of the lack of conclusive experimental evidence to support the reported rate data in one way or the other, we adopted in our base case calculation the rate coefficient of Lin and Lin [60] for reaction (R462), assigned (R227) to be irreversible and the only benzene formation channel from propargyl recombination, and varied k_{227} to fit the experimentally

determined peak concentration of benzene. In addition to the propargyl recombination reaction and the reactions of n-C_4H_3 and n-C_4H_5 with C_2H_2, i.e., (R267) and (R290), the following elementary reactions were also considered:

$$l\text{-}C_6H_4 + H \rightleftharpoons A_{1^-}, \quad \text{(R322)}$$

$$c\text{-}C_6H_4 + H \rightleftharpoons A_{1^-}, \quad \text{(R326)}$$

$$n\text{-}C_6H_5 \rightleftharpoons A_{1^-}, \quad \text{(R327)}$$

$$l\text{-}C_6H_6 + H \rightleftharpoons A_1 + H, \quad \text{(R342)}$$

$$n\text{-}C_6H_7 \rightleftharpoons A_1 + H, \quad \text{(R348)}$$

$$c\text{-}C_6H_7 \rightleftharpoons A_1 + H. \quad \text{(-R362)}$$

The rate coefficients of the preceding reactions were taken from our previous RRKM calculation [24]. For n-C_6H_5 and n-C_6H_7, reactions similar to (R255) and (R278) were included to account for their conversion to resonantly stabilized i-C_6H_5 and i-C_6H_7 isomers. The oxidation mechanism of benzene and phenyl is taken primarily from Ref. 62.

A number of computational cases were tested, in which k_{227} and k_{462} were assigned expressions different from those in the base case. The tested cases are summarized in Table 3. We will discuss in more detail these particular cases in a later section, except to mention that the k_{462} expression shown in Table 3 for Cases 2 and 4 is the total rate coefficient of the phenyl reaction with O_2, leading to C_6H_5O + O and benzoquinone + H, taken from Frank et al. [70]. Unless otherwise indicated, all computational results reported here were obtained with the base case reaction mechanism.

The rate coefficients of the H-abstraction from benzene by H and OH were taken from the work of Kiefer et al. [57] and Baulch et al. [58], respectively. The pressure-dependent rate coefficient of reaction

$$A_{1^-} + H(+M) \rightleftharpoons A_1(+M) \quad \text{(R365)}$$

was obtained through an RRKM calculation with details given in the Appendix. It was found

TABLE 3

Case Study—First Aromatic Ring Formation[a]

No.	Reactions[c]	$k = AT^n \exp(-E/RT)^b$ A	n	E	Comments/ References
Base case					
227	$C_3H_3 + C_3H_3 \rightarrow A_1$	1.00(+11)			20 torr
		1.00(+12)			90 torr
462	$A_{1^-} + O_2 \rightleftharpoons C_6H_5O + O$	2.10(+12)		7.47	[60]
Case 1					
227	$C_3H_3 + C_3H_3 \rightleftharpoons A_1$	1.00(+11)			20 torr
		1.00(+12)			90 torr
462	$A_{1^-} + O_2 \rightleftharpoons C_6H_5O + O$	2.10(+12)		7.47	[60]
Case 2					
227	$C_3H_3 + C_3H_3 \rightarrow A_1$	1.00(+11)			20 torr
		1.00(+12)			90 torr
462	$A_{1^-} + O_2 \rightleftharpoons C_6H_5O + O$	2.70(+12)	0.35	5.97	*d*
Case 3					
227	$C_3H_3 + C_3H_3 \rightarrow A_1$	0.0			
462	$A_{1^-} + O_2 \rightleftharpoons C_6H_5O + O$	2.10(+12)		7.47	[60]
Case 4					
227	$C_3H_3 + C_3H_3 \rightleftharpoons A_{1^-} + H$	1.00(+13)			[23]
462	$A_{1^-} + O_2 \rightleftharpoons C_6H_5O + O$	2.10(+12)		7.47	[60]

[a] See text and Table 1 for the reactions of C_4H_x with C_2H_y species leading to phenyl and benzene formation.

[b] The units are mole, centimeter, second, and kilocalorie. Numbers in parentheses denote powers of 10.

[c] Reactions with the " $\rightleftharpoons$ " are reversible and those with " $\rightarrow$ " are irreversible.

[d] Sum of the rate coefficient expressions of two channels (C_6H_5O + O, benzoquinone + H) reported by Frank et al. [70].

that the RRKM calculation yielded rate coefficients in close agreement with the experimental data of Hsu et al. [73] and Kiefer et al. [57] (see Appendix) and that the pressure fall-off of k_{365} is significant under the conditions of the tested flames. These results then prompted us to calculate the rate coefficients of the combination reactions of H and larger aromatic radicals, including napthyl radicals (A_2-1 and A_2-2) and phenanthryl (A_3-1 and A_3-4). The resulting rate coefficient expressions are fitted into Troe's fall-off formula and are provided in Table 1.

The growth of PAH species follows essentially the H-abstraction–C_2H_2-addition mechanism [9, 10, 12]. The H-abstraction reactions of PAH species by H and OH were assigned the same rate coefficients as those of benzene. The pressure-dependent rate coefficients of aromatic radical reactions with C_2H_2 were taken from our previous RRKM calculation [24]. In addition to the first direct acetylene addition and ring formation, the reaction sequence shown in Scheme 1 was also considered [24]. We also included the reactions of PAH molecules with ethynyl radical, i.e.,

$$A_i + C_2H \rightleftharpoons A_iC_2H + H.$$

The rate parameters of PAH oxidation by OH, O, and O_2 are not known. However, it is expected that the rate coefficients of these reactions are not significantly different from those of the analogous reactions of benzene and phenyl. Hence, three classes of reactions were assigned, including PAH molecule oxidation by OH (R485–500) and O (R501–516), and PAH radical oxidation by O_2 (R517–527) with their rate coefficients assumed to be equal to those of the benzene/phenyl reactions.

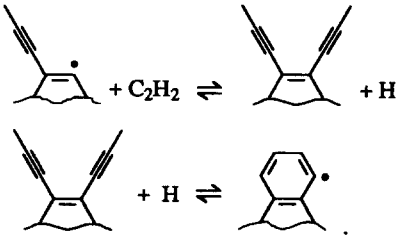

Scheme 1.

Computational Procedures

All computations were performed using CHEMKIN II [74] and the Sandia premixed flame code [75]. The transport properties of nonaromatic species were taken from Ref. 76 and those of aromatic species from Ref. 34. Flame computations were performed with windward differencing on the convective terms, and multicomponent diffusion formulas, and include H and H_2 thermal diffusion [75].

RESULTS: NUMERICAL PREDICTIONS

A summary of the conditions of the three well-studied burner-stabilized laminar premixed flames simulated in the present study is given in Table 4. All three flames are fuel-rich, with flame 1 being near-sooting and flames 2 and 3 being sooting. In the following text, we shall discuss briefly the main flame structures, followed by a discussion of benzene formation and PAH growth.

Main Flame Structures

The experimental and computed mole fraction profiles of the major species in flames 1–3 are shown in Figs. 1–3, respectively. It is seen that the model predicts reasonably well the mole fraction profiles of the major species. It is evident, however, that the computed concentrations of CO in the postflame zone for all

TABLE 4

Flame Conditions

No.	Composition in Argon	Equivalence Ratio	Pressure (torr)	T_{max} (K)	Unburned Gas Velocity (cm/s)	References
1	0.465 C_2H_2–0.485 O_2	2.4	20	1901	50	[19]
2	0.236 C_2H_2–0.214 O_2	2.76	90	1988	20.4	[3]
3	0.165 C_2H_4–0.179 O_2	2.76	760	1901	7.8	[16]

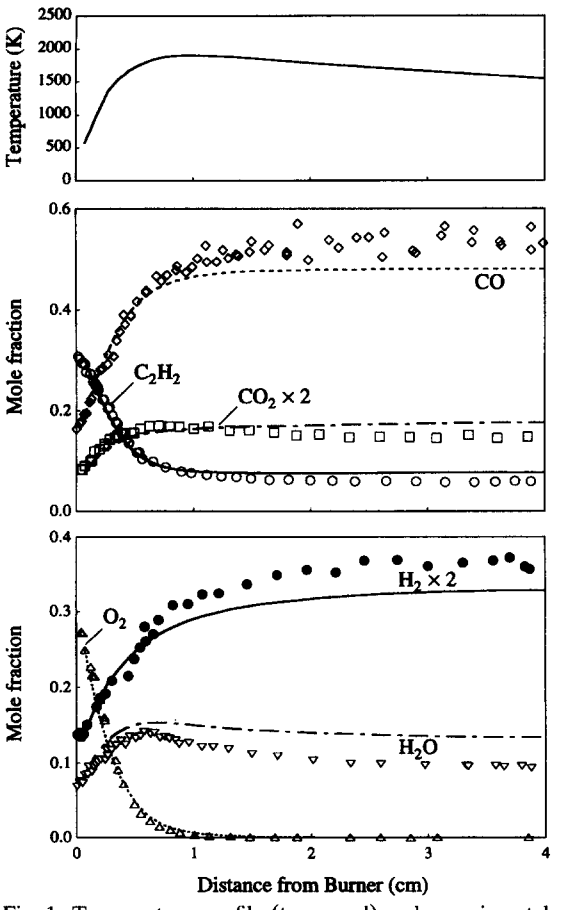

Fig. 1. Temperature profile (top panel) and experimental (symbols) [19] and computed (lines) mole fraction profiles of major species in flame 1.

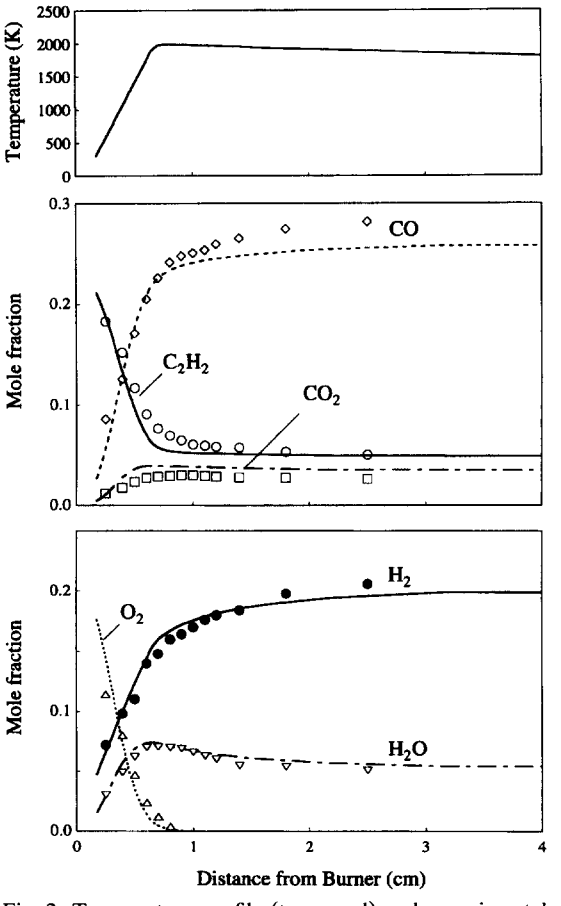

Fig. 2. Temperature profile (top panel) and experimental (symbols) [3] and computed (lines) mole fraction profiles of major species in flame 2.

flames and of H_2 for flames 1 and 3 are persistently lower than the experimental data. Such a discrepancy is caused by the fact that while the model predicts larger OH concentrations, it underpredicts the H-atom concentrations as will be discussed later. Because in the postflame zone the reactions

$$H_2 + OH \rightleftharpoons H_2O + H \qquad (R3)$$

$$CO + OH \rightleftharpoons CO_2 + H \qquad (24)$$

are in partial equilibrium, a larger OH concentration and a lower H-atom concentration inevitably shift the equilibrium to disfavor H_2 and CO. We note that the same observation was also made by Miller and Melius [23] in the analysis of a 20-torr acetylene flame of Bastin et al. [18].

Minor Species Concentrations

The experimental and computed mole fraction profiles of H, OH, HO_2, HCO + C_2H_5, and CH_2O + C_2H_6 in flame 1 are presented in Fig. 4, of CH_2, CH_3, CH_4, C_2H_3, C_2H_4, and C_3H_3 in Fig. 5, and of C_4H_2, C_4H_3, C_4H_4, C_4H_5, and C_4H_6 in Fig. 6. The mole fraction profiles of C_2H_4, C_4H_2, and C_6H_2 of flame 2 are presented in Fig. 7, and those of CH_4, C_2H_2, C_4H_2, C_4H_4, and C_4H_6 of flame 3 are presented in Fig. 8. It is seen that in general the key intermediate species concentration profiles are well reproduced by the reaction model. In most cases, the peak radical concentrations are predicted within a factor of 2 or better, which is probably to within the experimental uncertainty.

The peak H-atom concentration computed for flame 1 is somewhat lower than the experi-

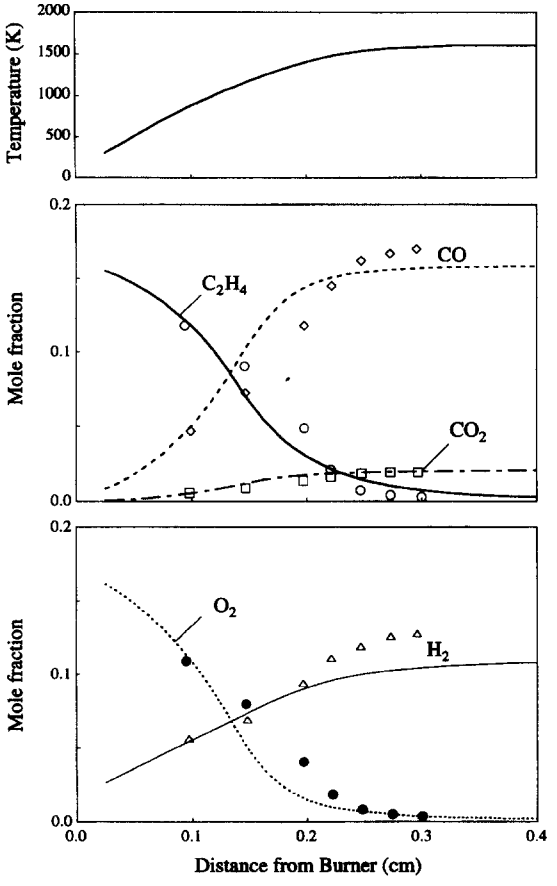

Fig. 3. Temperature profile (top panel) and experimental (symbols) [16] and computed (lines) mole fraction profiles of major species in flame 3.

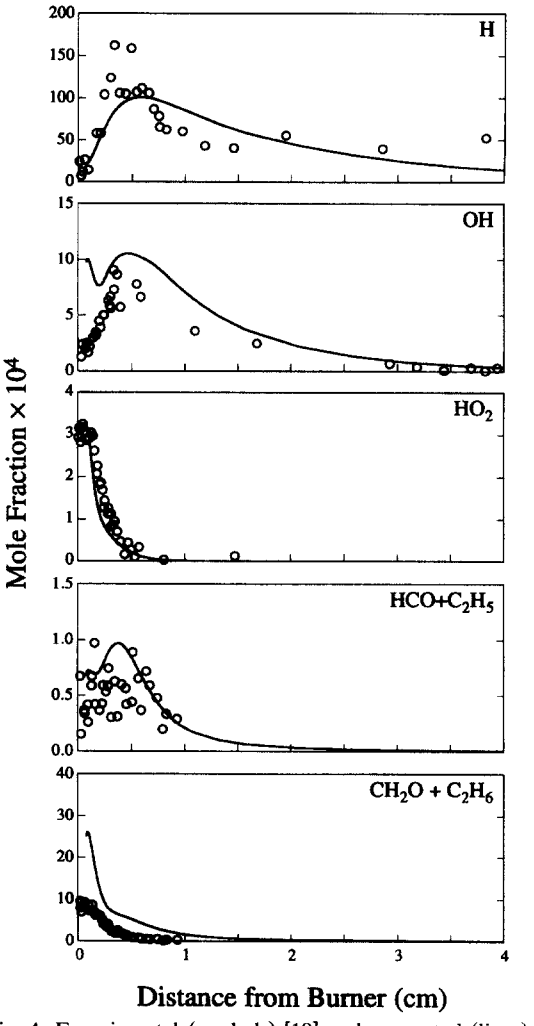

Fig. 4. Experimental (symbols) [19] and computed (lines) mole fraction profiles of selected intermediate species in flame 1.

mental data. We note that by reassigning the products of the reaction $CH_2 + O_2$ to $CO_2 + 2H$ as discussed in the Reaction Model section, the peak H-atom mole fraction computed for flame 1 is elevated by about 30%, and hence the prediction has already been improved over the original GRI-Mech. An additional sensitivity test by changing the branching ratio of the $C_2H_2 + O$ reaction did not improve the H-atom prediction. Further sensitivity and flux analyses suggest that within the framework of the present understanding of acetylene oxidation chemistry, it is unlikely that the computed peak H-atom mole fraction can be brought to the level determined by experiment.

The peak OH radical concentration of flame 1 is reasonably well reproduced as seen in Fig. 4. However, a secondary maximum near the burner was predicted by the model. It was found that the OH radicals near the burner are produced mainly by the reaction

$$HO_2 + H \rightleftharpoons OH + OH. \qquad \text{(R13)}$$

Because the concentrations of H and HO_2 are not overpredicted as seen in Fig. 4, there may be additional channels responsible for OH removal near the burner surface. Including the potential low-temperature OH consumption channel

$$C_2H_2 + OH \rightleftharpoons C_2H_2OH$$

did not resolve the problem. Although the dou-

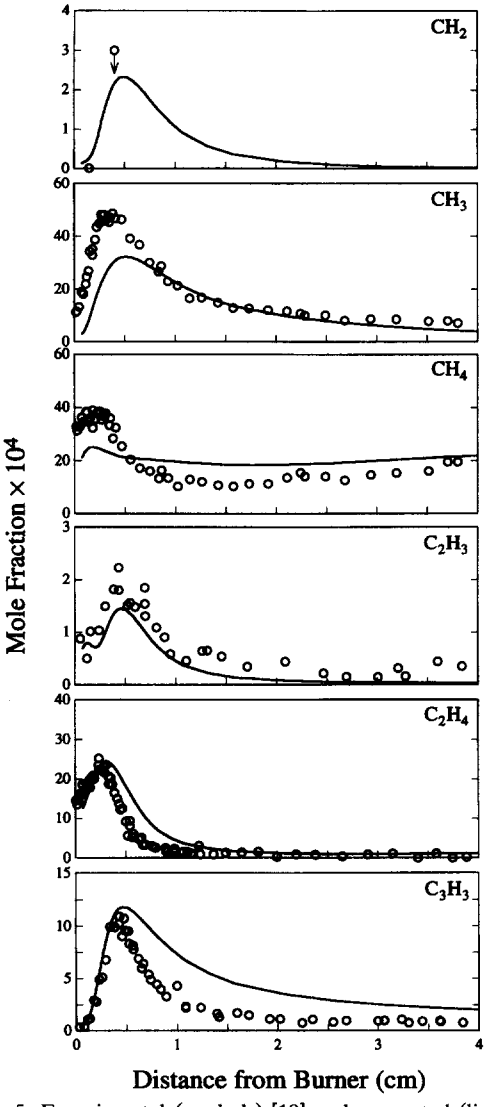

Fig. 5. Experimental (symbols) [19] and computed (lines) mole fraction profiles of selected intermediate species in flame 1.

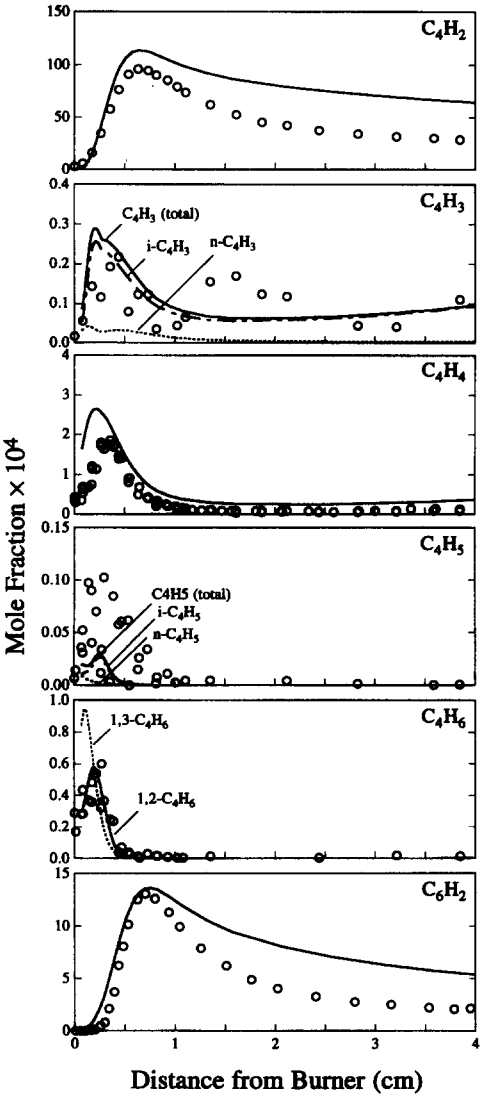

Fig. 6. Experimental (symbols) [19] and computed (lines) mole fraction profiles of selected intermediate species in flame 1.

ble peaks in the predicted OH concentration profile may be related to complex chemical interaction not considered by the model, our analysis does suggest that it is more likely caused by OH radical destruction on the burner surface. It should be noted that the transition from the low-temperature OH peak to the high-temperature peak (at a distance of ~ 0.2 cm from the burner) occurs at a relatively low-temperature region, ~ 1000 K. The predicted secondary OH peak near the burner does not significantly affect aromatics production.

It is seen in Fig. 5 that the concentration profiles of the intermediate C_1, C_2, and C_3 species are well predicted by the present reaction model. It is shown in Fig. 6 that the concentrations of the C_4 species relevant to aromatic formation are also predicted reasonably well. Vinylacetylene concentrations are slightly overpredicted for flames 1 and 3, as seen in Figs. 6 and 8. In the low-temperature,

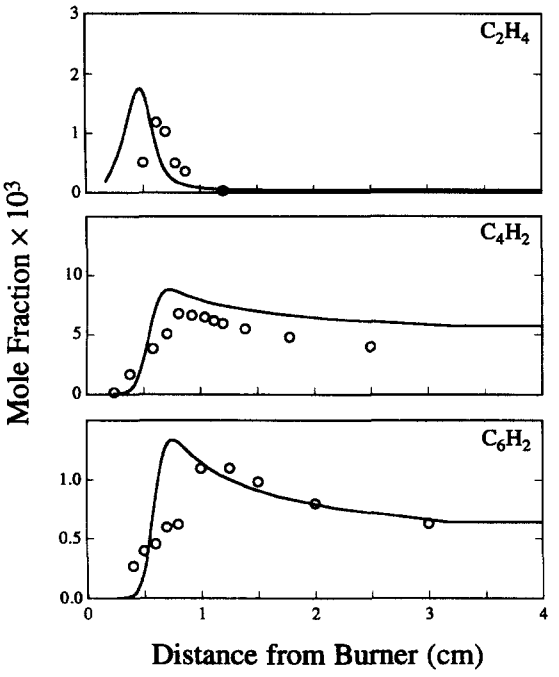

Fig. 7. Experimental (symbols) [3] and computed (lines) mole fraction profiles of selected intermediate species in flame 2.

preheat region of both flames, C_4H_4 is produced by

$$C_2H_3 + C_2H_2 \rightleftharpoons C_4H_4 + H, \qquad \text{(R193)}$$

which quickly reaches partial equilibrium when entering the main reaction zone. As shown in Fig. 6, the model predicts reasonably well the magnitude of the peak C_4H_3 concentration. The present model does predict a significantly lower n-C_4H_3 concentration than i-C_4H_3, which is consistent with Miller and Melius [23]. Double peaks are predicted for the n-C_4H_3 profile, which will be carefully explained later. We note that considering the significant scatter in the C_4H_3 (i-C_4H_3 + n-C_4H_3) experimental data and the fact that i-C_4H_3 concentration is significantly larger than n-C_4H_3, it is not apparent that the predicted double peaks are erroneous. Also shown in Fig. 6 is the comparison between the experimental and computed C_4H_5 profiles. It appears that the model underpredicts C_4H_5 concentrations by a factor of 2 to 3. Again, n-C_4H_5 concentration is significantly lower than i-C_4H_5.

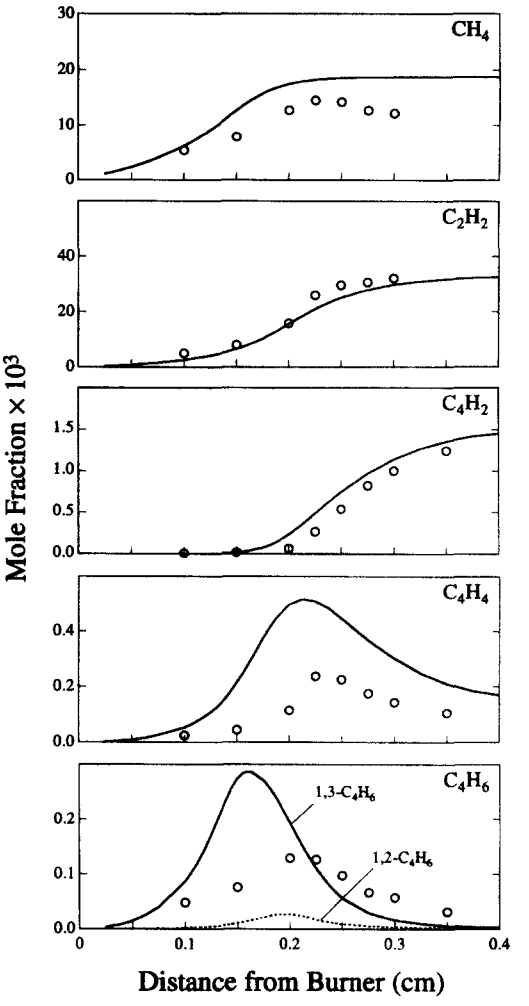

Fig. 8. Experimental (symbols) [16] and computed (lines) mole fraction profiles of selected intermediate species in flame 3.

One-Ring Aromatics

Figures 9–11 present the comparison of experimentally determined and numerically computed concentration profiles of one-ring aromatics for the three flames. Comparing the base case calculation (solid lines) with the experimental data whenever available, it is seen that the peak/maximum benzene concentrations are well reproduced when k_{227} was assigned values of 1×10^{11}, 1×10^{12}, and 2×10^{12} cm^3 mol^{-1} s^{-1} for flames 1, 2, and 3, respectively. For flame 1, it is seen in Fig. 9 that the benzene concentration in the post-flame zone is overpredicted because of the

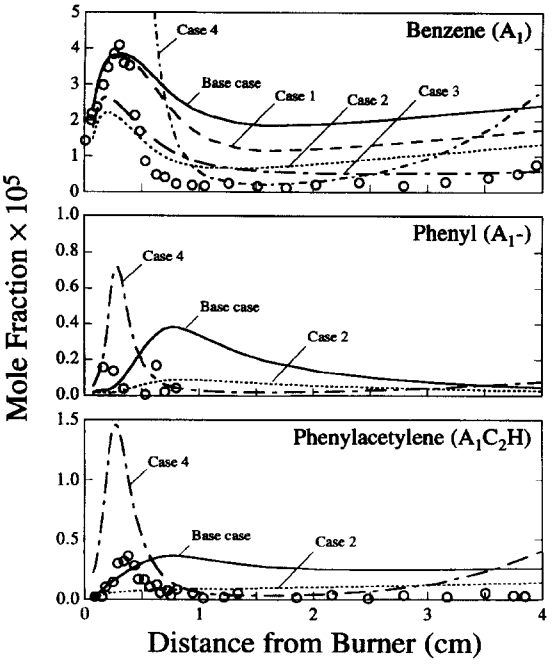

Fig. 9. Experimental (symbols) [19] and computed (lines) mole fraction profiles of one-ring aromatic species in flame 1.

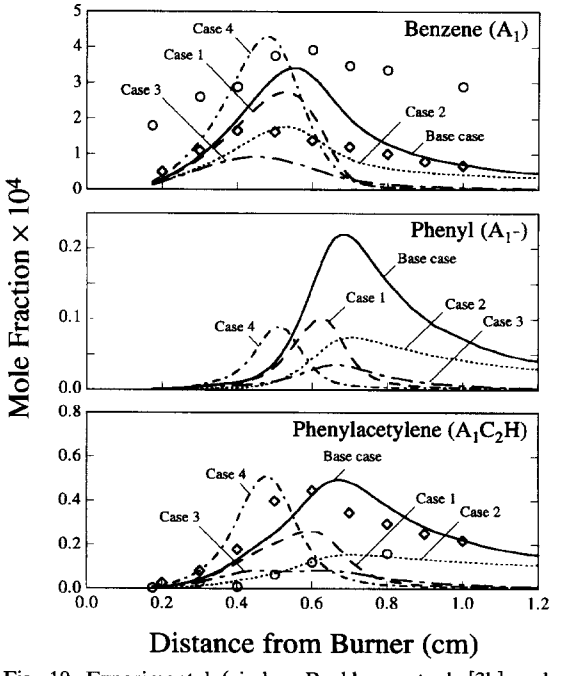

Fig. 10. Experimental (circles: Bockhorn et al. [3b] and Wenz [77]; diamonds: Bockhorn et al. [3a]) and computed (lines) mole fraction profiles of one-ring aromatic species in flame 2.

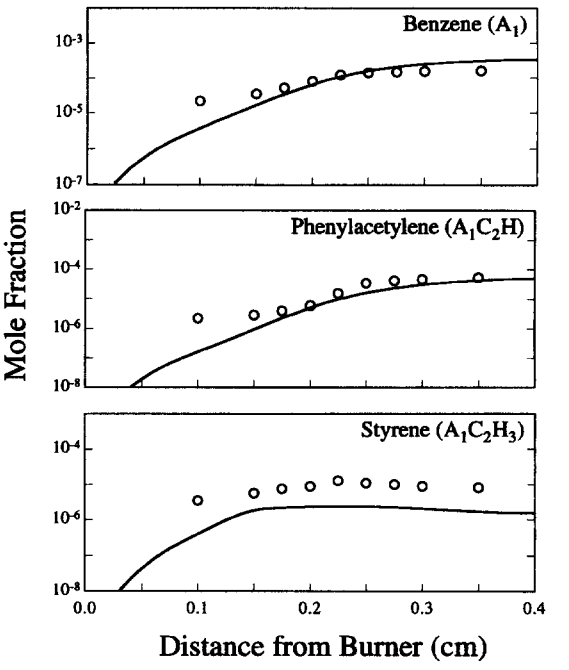

Fig. 11. Experimental (symbols) [16] and computed (lines) mole fraction profiles of aromatic species in flame 3.

persistent production of benzene via the irreversible $C_3H_3 + C_3H_3 \rightarrow$ benzene reaction in the postflame region. We suspect that this problem will be resolved only when the propargyl recombination kinetics becomes better understood. Although the model predicts reasonably well the peak phenylacetylene concentration in flame 1 as seen in Fig. 9, it overpredicts its concentration in the postflame region because the benzene concentrations in the same region are overpredicted.

The circles and diamonds in Fig. 10 represent two sets of data reported by Bockhorn and co-workers [3, 77] for flame 2. The reason for including here both sets is to provide a wider data base for comparison with the model: whereas the more recent results [3b] are presumably more accurate, the older set [3a, 77] has more species reported. It is seen that both benzene and phenylacetylene concentration profiles are well predicted by the reaction model. Figure 11 shows the comparison between the experimentally determined and calculatedbenzene, phenylacetylene, and styrene mole fraction profiles of flame 3. The agreement between model and experiment is again reasonably good. Note that the charac-

teristic difference of the aromatics concentration profiles among flames 1, 2, and 3 is well reproduced by the model, in that while in flames 1 and 2 the aromatics concentrations initially rise and then fall, the aromatics concentrations steadily rise in flame 3.

Polycyclic Aromatic Hydrocarbons

Figure 12 presents the comparison between experiment and numerical prediction for the PAH species of flame 2 up to pyrene. It is seen that the present model reproduces the peak mole fractions for most PAH species within a factor of 3 of the experimental data, which is certainly within the experimental uncertainty and significantly better than the results obtained recently by Castaldi et al. [78] using an alternate route to aromatics growth. The agreement seen in Fig. 12 is remarkable, considering that the only adjustable parameter in the model is the rate coefficient of propargyl recombination leading to benzene, and all aromatic ring growth reactions and their rate coefficients were derived from our previous RRKM calculations without further adjustments. The present results demonstrate that as long as the benzene concentration profile is reasonably well predicted, the H-abstraction–C_2H_2-addition mechanism can accurately account for PAH growth in the tested flames.

DISCUSSION: REACTION PATHWAYS

We focus our discussion on reaction pathways relevant to aromatics formation. The fuel destruction steps, however, determine the formation of intermediate species critical to aromatics production. Therefore, a brief description of the fuel removal pathways in the three flames is given first.

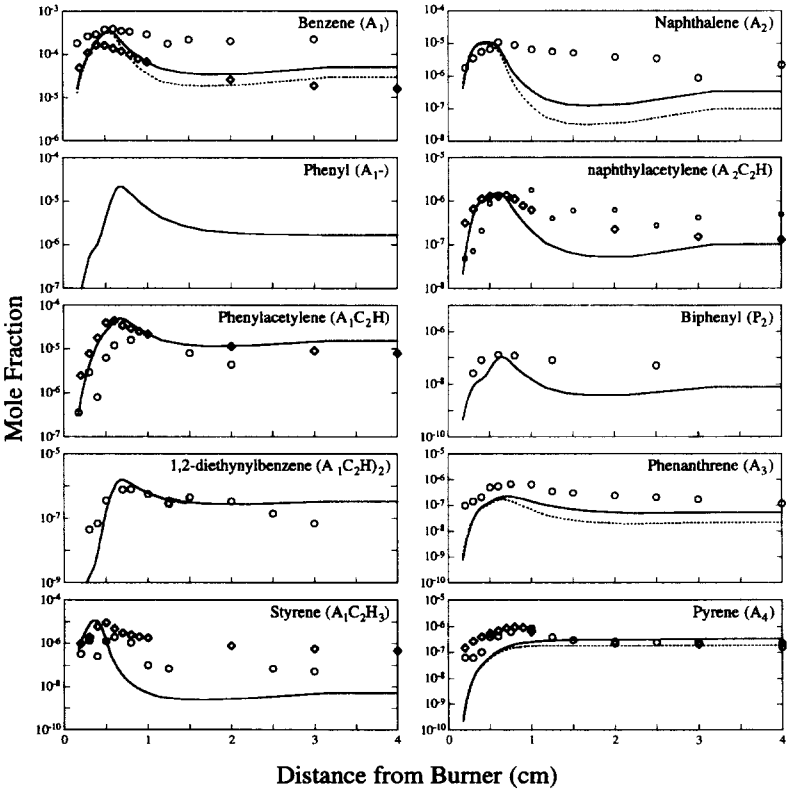

Fig. 12. Comparison of mole fraction profiles of selected aromatic species between experimental data (circles: Bockhorn et al. [3b] and Wenz [77]; diamonds: Bockhorn et al. [3a]) and base case computation (solid lines: base case results; dotted lines: base case results with the entire temperature profile increased by 50 K) for flame 2.

Fuel Destruction

The main reaction pathways leading to fuel destruction in the high-temperature region of the two acetylene flames (flames 1 and 2) are

$$C_2H_2 + O \rightleftharpoons HCCO + H, \quad \text{(R137)}$$

$$C_2H_2 + O \rightleftharpoons CH_2 + CO \quad \text{(R139)}$$

followed by

$$HCCO + H \rightleftharpoons CH_2^* + CO. \quad \text{(R130)}$$

As observed in the work of Frenklach and Warnatz [12], we also see that the reaction

$$C_2H_2 + H(+M) \rightleftharpoons C_2H_3(+M) \quad \text{(R136)}$$

is the dominant channel of C_2H_2 removal in the low-temperature preheat zone of both acetylene flames. The vinyl radicals are oxidized via

$$C_2H_3 + O_2 \rightleftharpoons HCO + CH_2O, \quad \text{(R156)}$$

$$C_2H_3 + O_2 \rightleftharpoons C_2H_3O + O, \quad \text{(R155)}$$

with (R156) being dominant at lower temperatures and (R155) becoming faster at higher temperatures. In the main flame zone, vinyl radicals are produced from C_2H_4 through the H-abstraction reactions by H and OH.

For the ethylene flame (flame 3), the fuel is removed mainly by the H-abstraction reactions

$$C_2H_4 + H \rightleftharpoons C_2H_3 + H_2, \quad \text{(R159)}$$

$$C_2H_4 + OH \rightleftharpoons C_2H_3 + H_2O \quad \text{(R161)}$$

and via oxidation by O atoms,

$$C_2H_4 + O \rightleftharpoons CH_3 + HCO. \quad \text{(R160)}$$

The vinyl radicals dissociate into $C_2H_2 + H$ (−R136) and to a less extent are oxidized via reactions (R155) and (R156).

Formation of C_3H_3 and C_4H_x

For all three flames, the propargyl radicals are produced via the reactions steps

$$C_2H_2 + CH_2 \rightleftharpoons C_3H_3 + H, \quad \text{(R186)}$$

$$C_2H_2 + CH_2^* \rightleftharpoons C_3H_3 + H. \quad \text{(R187)}$$

The relative contribution ranges from (R187) as the dominant step in the lower-pressure acetylene flame (flame 1) to (R186) being the main contributor in the atmospheric ethylene flame (flame 3).

For both acetylene flames, there are two distinct regions, one at lower temperatures and the other at higher temperatures, where the C_4 species are produced by two different reaction pathways. In the main flame zone, the major contributor of vinylacetylene is reaction

$$C_3H_3 + CH_2 \rightleftharpoons C_4H_4 + H, \quad \text{(R224)}$$

in agreement with Miller and Melius [23]. However, in the low-temperature preheat zone, reaction

$$C_2H_3 + C_2H_2 \rightleftharpoons C_4H_4 + H \quad \text{(R193)}$$

is the dominant contributor of vinylacetylene before it reaches partial equilibrium entering the main flame zone. In flame 3 reaction (R224) does not contribute to C_4H_4 production significantly. The major contributor is reaction (R193). In addition, the unimolecular decomposition reactions of n-C_4H_5 and i-C_4H_5 are contributing channels, both leading to $C_4H_4 + H$ at lower temperatures. The C_4H_5 radicals are produced mainly by the reaction sequence

$$C_2H_4 + C_2H_3 \rightleftharpoons 1,3\text{-}C_4H_6 + H, \quad \text{(R197)}$$

$$C_4H_6 + (H, OH) \rightleftharpoons i\text{-}C_4H_5 \text{ and } n\text{-}C_4H_5 + (H_2, H_2O). \quad \text{(R291–294)}$$

Interestingly, the source of C_2H_4 in the main flame zones of flames 1 and 2 is reaction

$$HCCO + CH_3 \rightleftharpoons C_2H_4 + CO \quad \text{(R182)}$$

and to a lesser extent

$$CH_2 + CH_3 \rightleftharpoons C_2H_4 + H. \quad \text{(R92)}$$

To further examine the production and destruction of n-C_4H_3, a probable precursor to the first aromatic ring, we plotted in Fig. 13 its numerically computed concentration profile of flame 1 (solid line). It is seen that there are two distinct peaks, one in the preheat zone and the other close to the main flame zone. As seen in Fig. 6, a similar computational profile

is obtained for the resonantly stabilized isomer i-C_4H_3.

The numerical results show that n-C_4H_3 radicals in flame 1 are produced by reactions

$$C_4H_2 + H \rightleftharpoons n\text{-}C_4H_3, \quad \text{(R241)}$$

$$C_4H_4 + H \rightleftharpoons n\text{-}C_4H_3 + H_2 \quad \text{(R271)}$$

and destroyed by

$$n\text{-}C_4H_3 + H \rightleftharpoons i\text{-}C_4H_3 + H, \quad \text{(R255)}$$

$$n\text{-}C_4H_3 + H \rightleftharpoons C_2H_2 + C_2H_2, \quad \text{(R256)}$$

$$n\text{-}C_4H_3 + H \rightleftharpoons C_4H_2 + H_2, \quad \text{(R260)}$$

$$n\text{-}C_4H_3 \rightleftharpoons C_4H_2 + H, \quad \text{(-R241)}$$

and that the concentrations of n-C_4H_3 can be closely approximated by a steady-state analysis involving the preceding reactions, which gives

$$[n\text{-}C_4H_3]_{ss} = (k_{241}[C_4H_2] + k_{271}[C_4H_4])/D,$$

where $D = k_{255} + k_{256} + k_{260} + k_{-241}/[H]$. A comparison of n-C_4H_3 mole fraction profiles of flame 1 obtained numerically (solid line) and calculated using the foregoing steady-state equation (dashed line) is presented in Fig. 13, which shows the close proximity of the two curves. Examination of the steady-state expression indicates that the first n-C_4H_3 mole fraction peak is produced by H addition to C_4H_2 (R241), i.e., the $k_{241}[C_4H_2]/D$ term, and the second concentration peak is produced from reaction (R271) or the $k_{271}[C_4H_4]/D$ term (see Fig. 13). It will be shown in a later section that it is the first concentration peak where the n-C_4H_3 radicals contribute to the aromatic production in flame 1. Such a low-temperature pathway was not identified in Ref. 23. We note that the destruction of n-C_4H_3 in our reaction model is as significant as that assigned in Ref. 23 because the sum of $k_{255} + k_{256}$ in the denominator D is equal to $\sim 1 \times 10^{14}$ cm^3 mol^{-1} s^{-1} over the entire temperature range of flame 1.

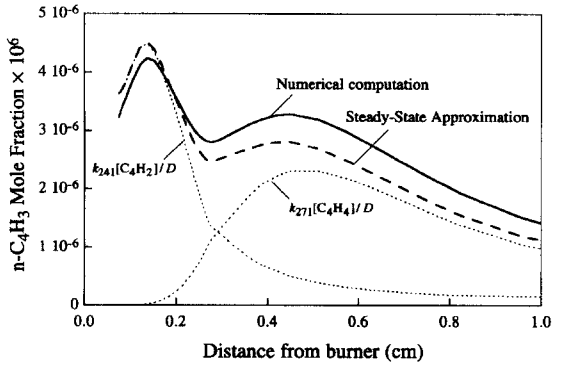

Fig. 13. Analysis of the concentration profiles of n-C_4H_3 in flame 1. $D = k_{255} + k_{256} + k_{260} + k_{-241}/[H]$.

Formation of One-Ring Aromatics

Figures 14 and 15 present the net fluxes of the reactions responsible for benzene and phenyl production and destruction in flames 1 and 2, respectively. In both figures, the rates of the reactions for benzene and phenyl interconversion, i.e.,

$$A_1 + H \rightleftharpoons A_{1^-} + H_2, \quad \text{(R363)}$$

$$A_1 + OH \rightleftharpoons A_{1^-} + H_2O, \quad \text{(R364)}$$

$$A_{1^-} + H(+M) \rightleftharpoons A_1 + (+M) \quad \text{(R365)}$$

are lumped into either a net production rate of A_{1^-} (R363 + R364 − R365) or a net A_{1^-} consumption rate [−(R363 + R364 − R365)]. It is seen in Fig. 14 that in flame 1 benzene is

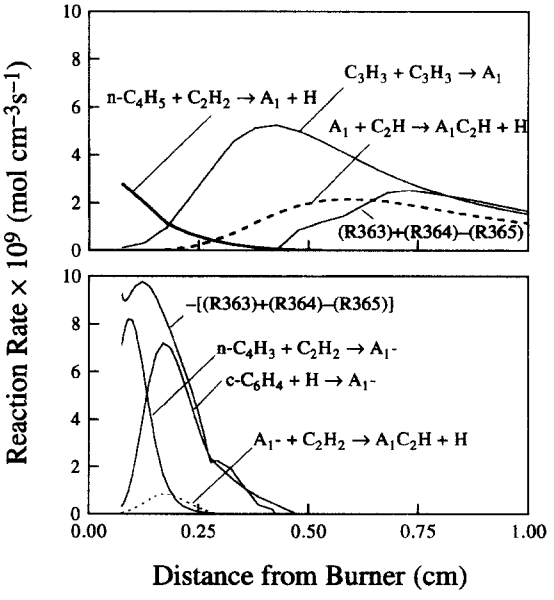

Fig. 14. Computed reaction rate fluxes of benzene and phenyl formation and destruction in flame 1.

produced by four reaction channels, including

$$C_3H_3 + C_3H_3 \rightarrow A_1, \quad \text{(R227)}$$

$$c\text{-}C_6H_4 + H \rightleftharpoons A_1\text{-}, \quad \text{(R326)}$$

$$n\text{-}C_4H_5 + C_2H_2 \rightleftharpoons A_1 + H, \quad \text{(R290)}$$

$$n\text{-}C_4H_3 + C_2H_2 \rightleftharpoons A_1\text{-}. \quad \text{(R267)}$$

It was identified that the temperatures at which the preceding four reactions attain maximum reaction rates are about 1600, 1000, 700, and 600 K, respectively. Hence, although reactions (R267), (R290), and (R326) dominate the production of benzene in the low-temperature, preheat zone of the flame, reaction (R227) is the predominant channel of benzene production in the main reaction zone. Furthermore, because benzyne is produced primarily through reaction

$$n\text{-}C_4H_3 + C_2H_2 \rightleftharpoons c\text{-}C_6H_4 + H, \quad \text{(R268)}$$

(R326) is essentially an extension of the overall path from n-$C_4H_3 + C_2H_2$ to phenyl.

It is important to note that the contributions of the individual channels to benzene formation in flame 1 are of about the same magnitude considering that the rate parameters of the foregoing reactions have at least an uncertainty factor of 2 and that the maximum rates of the foregoing reactions differ by a factor of 4, as shown in Fig. 14. This implies that the benzene concentration of flame 1 can be reasonably well predicted even if reaction (R227) is excluded from the reaction model. Indeed, computations performed for Case 3 of Table 3 show that the peak benzene mole fraction is reduced by less than a factor of 2 when (R227) is excluded from the computation, as seen in Fig. 9. Whereas the destruction of n-C_4H_3 and n-C_4H_5 is significant, as discussed previously, we conclude that a significant amount of one-ring aromatics in flame 1 must be produced via the reactions of $C_4H_x + C_2H_2$.

Contrary to flame 1, it is seen in Fig. 15 that benzene is primarily produced by propargyl recombination (R227). However, the propargyl mole fraction profile was not reported for flame 2 and hence the contribution of the benzene/phenyl production reactions cannot be assessed on rigorous grounds. We note further that when (R227) is excluded from computation (Case 3), the maximum concentration computed for benzene is only a factor of 2 lower than the experimental data reported in Ref. 3a, as seen by comparing the computational result of Case 3 with the diamond symbols shown in Fig. 10. Hence, the contribution of C_2H_2 addition to C_4H_x leading to benzene and phenyl is not insignificant. In addition, the reverse of reaction (R326) is such a dominant phenyl destruction channel in the postflame zone of flame 2 that without including it, the benzene concentration can be seriously overpredicted. This result then further emphasizes that the $C_4H_x + C_2H_2$ reactions are the major contributors of the aromatics kinetics in the flames tested.

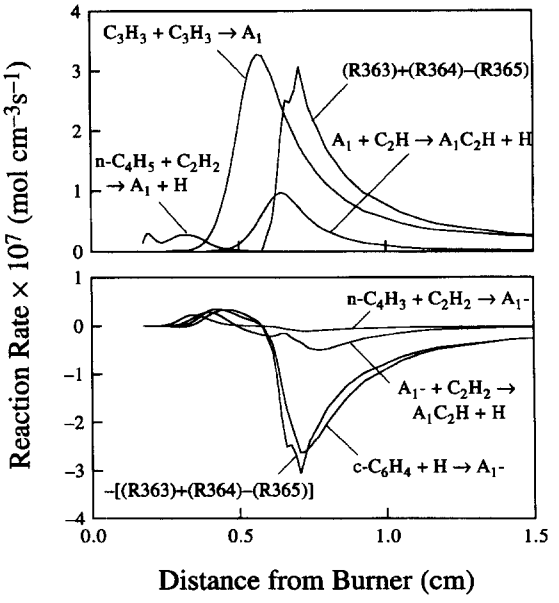

Fig. 15. Computed reaction rate fluxes of benzene and phenyl formation and destruction in flame 2.

In view of the uncertainties associated with the propargyl recombination reaction discussed in the Reaction Model section, we performed several additional tests to determine the effects of these uncertainties on the predicted concentrations of one-ring aromatics. These sensitivity tests are specified in Table 3 as Cases 1, 3, and 4.

In Case 1, reaction (R227) was assumed to be reversible with the forward rate coefficient equal to that of the base case. It is seen in Fig. 9 by comparing the solid and dashed lines that the benzene concentrations computed for flame 1 with Case 1 are slightly lower than the base case results. For flame 2, however, it is seen in Fig. 10 that although the peak benzene concentration is not affected significantly, Case 1 produces a significantly lower benzene concentration in the postflame region (for distances from the burner $x > 0.7$ cm) than both the experimental data and the base case computational results. Furthermore, the unimolecular decomposition of benzene to two propargyl radicals, i.e., the reverse of reaction (R227), becomes the major source of benzene destruction when (R227) is assumed to be reversible. This result is clearly unreasonable considering that if indeed the unimolecular decomposition is the major benzene destruction mode, the predominant channel should be phenyl + H, not $C_3H_3 + C_3H_3$.

In Case 4, the products of reaction (R227) were assigned to be A_1 + H with a rate coefficient of 10^{13} cm^3 mol^{-1} s^{-1}, as in the work of Miller and Melius [23]. It is seen in Fig. 9 that Case 4 overpredicts significantly the peak concentration of benzene in flame 1 (by more than an order of magnitude) and consequently it overpredicts the phenylacetylene concentration as well. In flame 2, Case 4 produces the correct order of magnitude of the peak benzene concentration. Similarly to Case 1, however, it now significantly underpredicts the benzene concentration in the postflame region. The reason is the same as in Case 1, in that the reverse $C_3H_3 + C_3H_3 \rightleftharpoons$ phenyl + H becomes the dominant benzene removal channel. As such, the peak phenyl concentration predicted with Case 4 and shown in the middle panel of Fig. 10 is actually lower than that of the base case prediction, and Case 4 does not predict well the shape of the concentration profiles of both benzene and phenylacetylene.

In their modeling study of benzene formation in the low-pressure acetylene flame of Bastin et al. [18], Miller and Melius [23] assumed reaction (R227′) to be the only route of benzene production. Our sensitivity test performed with Case 4 is very similar to the computation of Miller and Melius, because the large rate coefficient of (R227′) assigned in Case 4 diminishes the contribution of the $C_4 + C_2$ route to benzene. A further sensitivity test by excluding the $C_4 + C_2$ route [more specifically, reactions (R322), (R326), (R327), (R342), (R348), and (R362)] produced benzene concentration profiles almost indistinguishable from those of Case 4.

Analyses presented in the preceding text provide evidence that in flames 1 and 2, (a) the recombination of the propargyl radicals leading to the formation of phenyl and benzene is a global reaction under the conditions of the tested flames and the rate coefficient for such a global reaction is significantly lower than 10^{13} cm^3 mol^{-1} s^{-1} and (b) the fluxes from the reactions of $C_4H_x + C_2H_2$ leading to benzene or phenyl are not negligible for the production and destruction of one-ring aromatics.

For flame 3 the simulation using the base case mechanism predicts that the propargyl recombination leading to benzene is faster by an order of magnitude than the $C_4H_3 + C_2H_2$ channel. However, although the propargyl recombination channel is seen to be important only in the main reaction zone ($x = 0.2$–0.3 cm) of the flame, the $C_4H_3 + C_2H_2$ channel is seen to be important only in the preheat zone (0–0.2 cm) where the temperature is less than 1400 K. Because it is extremely difficult to obtain reliable temperature measurement within such a short distance, i.e., from the burner exit to 2 mm above it, there is a significant uncertainty in the predicted contribution of the $C_4H_3 + C_2H_2$ channel within this preheat zone. In particular, both Harris et al. [15] and the present study found that the computed H-atom concentration is as much as 2 orders of magnitude lower than the experimental data at a distance of, say, 1 mm above the burner. This would certainly make the $C_4H_3 + C_2H_2$ channel unimportant, because the production of n-C_4H_3 requires the presence of H atoms. Hence, the relative contribution of the propargyl recombination and the $C_4H_3 + C_2H_2$ channel leading to one-ring aromatics in flame 3 is not resolved in the present study. We note that the same problem has been observed, analyzed, and reported in our simulation study of soot formation in a similar flame [21].

We performed further sensitivity tests for the rate parameter of phenyl oxidation by molecular oxygen, i.e.,

$$A_1\text{-} + O_2 \rightleftharpoons C_6H_5O + O. \qquad \text{(R462)}$$

When the rate expression of Lin and Lin [60] was adopted in the calculation, i.e., the base case, the oxidation of phenyl by O_2 is not significant as compared to the thermal decomposition of phenyl. However, when k_{462} was assigned with the expression reported by Frank et al. [70] (Case 2), reaction (R462) becomes one of the dominant phenyl removal channels. in the latter test, the predicted benzene mole fractions in flames 1 and 2 are lower than the base case results by about a factor of 2. Because the accuracy of the experimental data is expected to be no better than a factor of 2, even the large uncertainty in the rate coefficient of (R462) appears to be not particularly critical for the predictions of one-ring aromatics in the tested flames.

Aromatics Mass Growth

Based on the present reaction model, the formation of aromatic molecule with an ethynyl side chain is largely governed by partial equilibrium of the reaction

$$A_1\text{-} + C_2H_2 \rightleftharpoons A_1C_2H + H.$$

As demonstrated, respectively, in Figs. 16 and 17 for flames 1 and 2, the forward and reverse reaction fluxes of reaction

$$A_1\text{-} + C_2H_2 \rightleftharpoons A_1C_2H + H \qquad \text{(R369)}$$

are tightly balanced, and both are significantly larger than the rates of other reactions involving A_1C_2H, e.g.,

$$A_1 + C_2H \rightleftharpoons A_1C_2H + H. \qquad \text{(R367)}$$

As such, the peak concentration of phenylacetylene is governed mainly by thermodynamics, specifically the equilibrium constant of reaction (R369), the concentrations of phenyl, C_2H_2, and H, and to a lesser extent by the reaction rate coefficient.

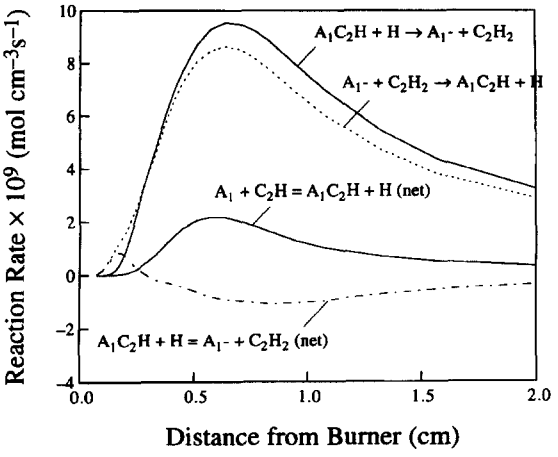

Fig. 16. Computed reaction rate fluxes of phenylacetylene formation and destruction in flame 1.

Figure 18 shows the computed reaction fluxes for the formation and destruction of naphthalene (A_2) in flame 2. It is seen that the dominant reaction channel for A_2 production at $x < 0.6$ cm is via 1-naphthyl (A_2-1) through the reaction between 1, 2-diethynylbenzene, $A_1C_2H)_2$, and the H atom,

$$A_1C_2H)_2 + H \rightleftharpoons A_2\text{-}1, \qquad \text{(R397)}$$

where $A_1C_2H)_2$ is produced from reactions

$$A_1C_2H + H \rightleftharpoons A_1C_2H^* + H_2, \qquad \text{(R372)}$$

$$A_1C_2H^* + C_2H_2 \rightleftharpoons A_1C_2H)_2 + H. \qquad \text{(R398)}$$

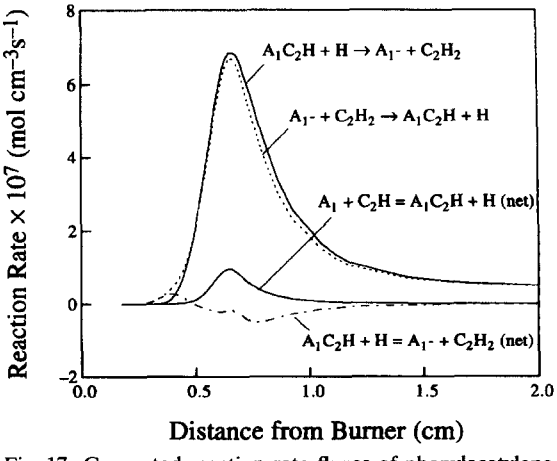

Fig. 17. Computed reaction rate fluxes of phenylacetylene formation and destruction in flame 2.

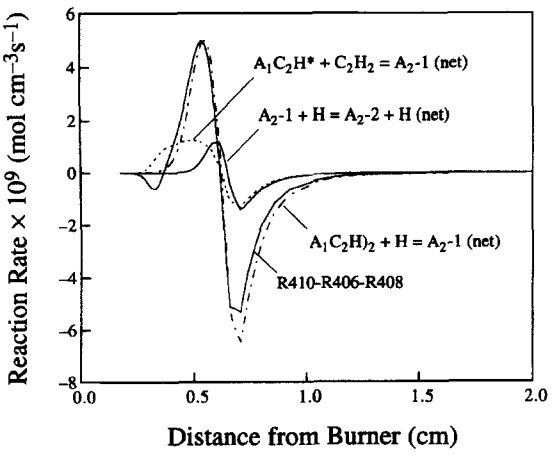

Fig. 18. Computed reaction rate fluxes of naphthyl radicals and naphthalene formation and destruction in flame 2.

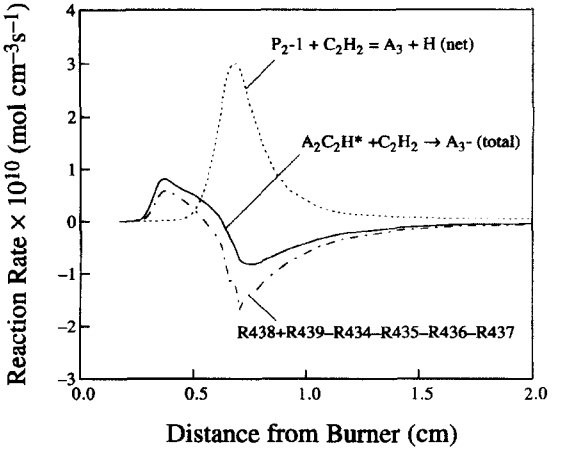

Fig. 19. Computed reaction rate fluxes of phenanthryl radicals and phenanthrene formation and destruction in flame 2.

Hence, reaction (R397) is a direct extension of the H-addition–C_2H_2-addition mechanism. Naphthalene is produced from the H and A_2-1 combination:

$$A_2\text{-}1 + H(+M) \rightleftharpoons A_2(+M). \qquad \text{(R410)}$$

Together with reactions

$$A_2 + H \rightleftharpoons A_2\text{-}1 + H_2, \qquad \text{(R406)}$$

$$A_2 + OH \rightleftharpoons A_2\text{-}1 + H_2O, \qquad \text{(R408)}$$

the net flux of naphthyl to naphthalene interconversion, i.e., the curve marked as R410–R406–R408 in Fig. 18, follows closely that of A_2-1 formation and destruction via reaction (R397). In other words, as soon as the 1-naphthyl radical is produced, it is immediately converted to naphthalene through reactions (R410), (R406), and (R408).

For $x > 0.6$ cm, it is seen in Fig. 18 that the reaction flux of (R397) becomes negative, indicating that this reaction now proceeds in the reverse direction and is responsible for the destruction of the naphthyl radical and naphthalene. Thus, the production of naphthalene is limited by the reversibility of this reaction, which again illustrates the important role of thermodynamics in PAH mass growth as identified previously [12].

Figure 19 presents the rates of reactions relevant to phenanthrene (A_3) formation and destruction. Again, the net conversion rate of phenanthryl radical (A_3-1 and A_3-4) to A_3 is governed by the H abstraction of A_3 by H and OH, and by H addition to A_3-1 and A_3-4, i.e.,

$$A_3 + H \rightleftharpoons A_3\text{-}1, A_3\text{-}4 + H_2, \qquad \text{(R434, R435)}$$

$$A_3 + OH \rightleftharpoons A_3\text{-}1, A_3\text{-}4 + H_2O, \qquad \text{(R436, R437)}$$

$$A_3\text{-}1, A_3\text{-}4 + H(+M) \rightleftharpoons A_3(+M). \qquad \text{(R438, R439)}$$

The corresponding curve in Fig. 19 is marked as R438 + R439 − R434 − R435 − R436 − R437. It is seen that at low temperatures, phenanthryl radicals are produced from two ethynylnaphthyl ($A_2C_2HA^*$ and $A_2C_2HB^*$) isomers:

$$A_2C_2HA^* + C_2H_2 \rightleftharpoons A_3\text{-}4, \qquad \text{(R436)}$$

$$A_2C_2HB^* + C_2H_2 \rightleftharpoons A_3\text{-}1. \qquad \text{(R437)}$$

The flux of the foregoing reactions reverts downstream ($x > 0.6$ cm), which again indicates the importance of thermodynamics in the PAH mass growth process. In the main flame zone, phenanthrene is produced from the reaction between biphenyl radical, P_2-1, and C_2H_2:

$$P_2\text{-}1 + C_2H_2 \rightleftharpoons A_3 + H. \qquad \text{(R459)}$$

This points to a significant contribution of ring–ring condensation reactions in the PAH mass growth process in flame 2, which is con-

sistent with our previous finding for a similar flame [21].

The production of pyrene (A_4) in flame 2 is achieved through the addition of C_2H_2 to the 4-phenanthryl radical,

$$A_3\text{-}4 + C_2H_2 \rightleftharpoons A_4 + H. \qquad \text{(R444)}$$

Because of the large exothermicity ($\Delta H^0 = -56$ kcal/mol), the preceding reaction is virtually irreversible. Hence, the predicted mole fraction profile of pyrene lacks a pronounced peak as seen for other PAH species (Fig. 12).

Figure 20 presents the ranked sensitivity coefficients of the pyrene concentration in flame 2 at a distance of 0.55 cm above the burner. It is seen that a variety of reactions affect the production of pyrene, starting from those which govern the overall flame propagation (e.g., $H + O_2 \rightleftharpoons O + OH$), to fuel consumption ($C_2H_2 + O \rightleftharpoons CH_2 + CO$ and $CH_2 + O_2 \rightleftharpoons CO_2 + 2H$), the production of aromatics precursors (e.g., $C_2H_2 + CH_2 \rightleftharpoons C_3H_3 + H$ and $C_4H_2 + H \rightleftharpoons n\text{-}C_4H_3$), the formation of the first aromatic ring (e.g., $C_3H_3 + C_3H_3 \rightleftharpoons A_1$ and $c\text{-}C_6H_4 + H \rightleftharpoons A_1\text{-}$), the growth of PAHs (e.g., $A_2C_2HA^* + C_2H_2 \rightleftharpoons A_3\text{-}4$ and $P_2\text{-} + C_2H_2 \rightleftharpoons A_3 + H$), and finally the formation of pyrene via $A_3\text{-}4 + C_2H_2 \rightleftharpoons A_4 + H$.

Recognizing the influence of temperature on the aromatics formation and growth in that it determines the reversibility of pertinent reactions, we performed a sensitivity test by increasing the entire temperature profile of flame 2 by 50 K, which is the expected uncertainty in the temperature measurement of Ref. 3. The results are shown for selected aromatic species as dotted lines in Fig. 12. Comparing the solid and dotted lines, we see that such a temperature increase does not affect significantly the predictions of concentrations before they reached their peak values. However, it does affect the aromatics concentrations in the post-flame zone. An increase in the flame temperature reduces the computed aromatics concentrations. Hence, the discrepancy between model prediction and experimental data in the

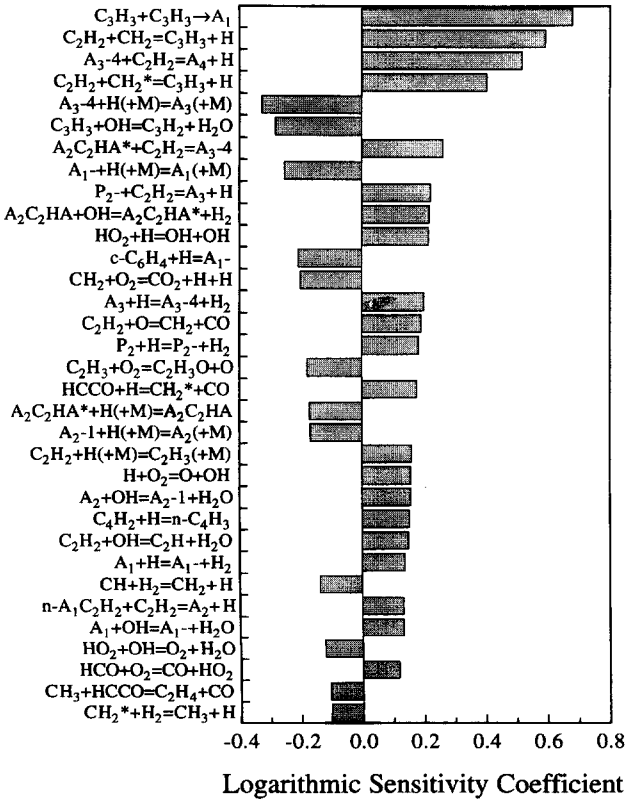

Fig. 20. Logarithmic sensitivity coefficients of pyrene concentration $\partial(\ln[A_4])/\partial(\ln k_i)$ in flame 2 computed at 0.55 cm from the burner surface.

postflame region of flame 2 for species such as styrene, naphthalene, naphthylacetylene, and biphenyl may be caused by the probe cooling affect during sample, which lowers the local temperature of the flame and thus raises the concentrations of the aromatics species at the sampling point. Last, it is noted that in their analysis of aromatics concentration profiles in flame 2, Frenklach and Warnatz [12] showed that uncertainties in the thermochemical data of the PAH species can also affect significantly PAH concentration profiles in the postflame region.

CONCLUDING REMARKS

A detailed reaction mechanism of PAH formation, growth, and oxidation in laminar premixed sooting and near-sooting ethylene and acetylene flames is reported. The reaction mechanism predicts reasonably well the concentration profiles of major and key intermediate species and, most importantly, aromatic molecules in a number of ethylene and acetylene flames available in the literature.

The first aromatic ring formation is analyzed in detail. The results show that the propargyl recombination reaction does not appear to be the unique channel of benzene formation and destruction. Depending on flame conditions, the contribution of the reaction between n-C_4H_3 and C_2H_2 to benzene production may be as significant as the propargyl recombination. Hence, the propargyl recombination is not a complete answer to the kinetic modeling of aromatics formation in flames. Clearly, further quantitative information, both experimental and theoretical, is needed to refine the mechanism of aromatics formation.

The computational results also show that as long as the benzene concentration is reasonably well predicted, the mass growth of PAHs up to pyrene in a 90-torr sooting acetylene flame can be described very well by the H-abstraction–C_2H_2-addition mechanism. The present results show the complex nature underlying the formation and growth of aromatics, which further stresses the importance of the thermodynamic and chemical kinetic coupling of the reaction system, such that an accurate prediction of the aromatics formation and growth in flames is determined not only by accurate reaction kinetics, but also the thermodynamic data.

This work was supported by the Air Force Office of Scientific Research, Air Force Systems Command, USAF, under grant nos. 91-0129 and F49620-94-1-0226, and the Technology Development of the Engine Division of Caterpillar Inc.

REFERENCES

1. Calcote, H. F., *Combust. Flame* 42:215–242 (1981).
2. Bittner, J. D., and Howard, J. B., *Eighteenth Symposium (International) on Combustion*, The Combustion Institute, Pittsburgh, 1981, p. 1105; Bittner, J. D., and Howard, J. B., in *Particulate Carbon Formation During Combustion* (D. Siegla and G. Smith, Eds.), Plenum, New York, 1981, p. 109; Bittner, J. D., Howard, J. B., and Palmer, H. B., in *Soot in Combustion Systems and Its Toxic Properties* (J. Lahaya and G. Prado, Eds.) Plenum, New York, 1983, p. 95.
3. (a) Bockhorn, H., Fetting, F., and Wenz, H. W., *Ber. Bunsenges. Phys. Chem.* 87:1067–1073 (1983); (b) Bockhorn, H. Fetting, F. Heddrich, A., and Reh, Ch. presented at the *Twenty-First Symposium (International) on Combustion*, Munich, Germany, August, 1986, Poster paper P51.
4. Longwell, J. P., *Nineteenth Symposium (International) on Combustion*, The Combustion Institute, Pittsburgh, 1983, p. 1139.
5. Cole, J. A., Bittner, J. D., Longwell, J. P., and Howard, J. B., *Combust. Flame* 56:51–70 (1984).
6. Homann, K. H., *Twentieth Symposium (International) on Combustion*, The Combustion Institute, Pittsburgh, 1985, p. 857.
7. Brezinsky, K., *Prog. Energy Combust. Sci.* 3:1–24 (1986).
8. Stein, S. E., and Fahr, A., *J. Phys. Chem.* 89:3714–3725 (1986).
9. Frenklach, M., Clary, D. W., Gardiner, W. C., Jr., and Stein, S. E., *Twentieth Symposium (International) on Combustion*, The Combustion Institute, Pittsburgh, 1985, p. 887.
10. Frenklach, M., Clary, D. W., Yuan, T., Gardiner, W. C., Jr., and Stein, S. E., *Combust. Sci. Technol.* 50:79–115 (1986).
11. Frenklach, M., Clary, D. W., Gardiner, W. C., Jr., and Stein, S. E., *Twenty-First Symposium (International) on Combustion*, The Combustion Institute, Pittsburgh, 1987, p. 1067.
12. Frenklach, M., and Warnatz, J., *Combust. Sci. Technol.* 51:265–283 (1987).
13. Frenklach, M., Yuan, T., and Ramachandra, M. K., *Energy Fuels* 2:462–480 (1988).
14. Colket, M. B., *Twenty-First Symposium (International) on Combustion*, The Combustion Institute, Pittsburgh, 1987, p. 851.

15. Harris, S. J., Weiner, A. M., Blint, R. J., and Goldsmith, J. E. M., *Twenty-First Symposium (International) on Combustion*, The Combustion Institute, Pittsburgh, 1987, p. 1033.
16. Harris, S. J., Weiner, A. M., and Blint, R. J., *Combust. Flame* 72:91–109 (1988).
17. Frenklach, M., *Twenty-Second Symposium (International) on Combustion*, The Combustion Institute, Pittsburgh, 1989, p. 1075.
18. Bastin, E., Delfau, J.-L., Reuillon, M., Vovelle, C., and Warnatz, J., *Twenty-Second Symposium (International) on Combustion*, The Combustion Institute, Pittsburgh, 1989, p. 313.
19. Westmoreland, P. R., Dean, A. M., Howard, J. B., and Longwell, J. P., *J. Phys. Chem.* 93:8171–8180 (1989); Westmoreland, P. R., Ph.D. Thesis, Massachusetts Institute of Technology, Cambridge, MA 1986.
20. Stein, S. E., Walker, J. A., Suryan, M. M. and Fahr, A., *Twenty-Third Symposium (International) on Combustion*, The Combustion Institute, Pittsburgh, 1991, p. 85.
21. Frenklach, M., and Wang, H., *Twenty-Third Symposium (International) on Combustion*, The Combustion Institute, Pittsburgh, 1991, p. 1559.
22. Frenklach, M., and Wang, H., in *Mechanisms and Models of Soot Formation* (H. Bockhorn, Ed.), Springer-Verlag, Berlin, p. 162.
23. Miller, J. A., and Melius, C. F., *Combust. Flame* 91:21–39 (1992).
24. Wang, H., and Frenklach, M., *J. Phys. Chem.* 98:11465–11489 (1994).
25. Lindstedt, R. P., and Skevis, G., *Combust. Flame* 99:551–561 (1994).
26. Mitchell, T. J., Benson, S. W., and Karra, S. B., *Combust. Sci. Technol.* 107:223–260 (1995).
27. Zhang, H.-Y., and McKinnon, J. T., *Combust. Sci. Technol.* 107:261–300 (1995).
28. Davis, S. G., Wang, H., Brezinsky, K., and Law, C. K., Twenty-Sixth Symposium (International) on Combustion, The Combustion Institute, Pittsburgh, to appear.
29. Kern, R. D., Singh, H. J., and Wu, C. H., *Int. J. Chem. Kinet.* 20:731–747 (1988).
30. Alkemade, U., and Homann, K. H., *Z. Phys. Chem. Neue Folge* 161:19–34 (1989).
31. Weissman, M., and Benson, S. W., *Prog. Energy Combust. Sci.* 15:273–285 (1989).
32. Haynes, B. S., and Wagner, H. Gg. *Prog. Energy Combust. Sci.* 7:229–273 (1981).
33. Wang, H. and Frenklach, M., *J. Phys. Chem.* 97:3867–3874 (1993).
34. Wang, H., and Frenklach, M., *Combust. Flame* 96:163–170 (1994).
35. Frenklach, M., Wang, H., Goldenberg, M., Smith, G. P., Golden, D. M., Bowman, C. T., Hanson, R. K., Gardiner, W. C., and Lissianski, V., *GRI-Mech—An Optimized Detailed Chemical Reaction Mechanism for Methane Combustion*, GRI Technical Report No. GRI-95/0058, November 1, 1995.
36. Koshi, M., Nishida, N., and Matsui, H., *J. Phys. Chem.* 96:5875–5880 (1992); Koshi, M., Fukuda, K., Kamiya, K., and Matsui, H., *J. Phys. Chem.* 96:9839–9843 (1992).
37. Farhat, S. K., Morter, C. L., and Glass, G. P., *J. Phys. Chem.* 97:12789–12792 (1993).
38. Bozzelli, J. W., and Dean, A. M. *J. Phys. Chem.* 97:4427–4441 (1993).
39. Tsang, W., and Hampson, R. F., *J. Phys. Chem. Ref. Data* 15:1087–1279 (1986).
40. Warnatz, J., Bockhorn, H., Möser, A., and Wenz, H. W., *Nineteenth Symposium (International) on Combustion*, The Combustion Institute, Pittsburgh, 1983, p. 197.
41. Böhland, T., Temps, F., and Wagner, H. Gg., *Twenty-First Symposium (International) on Combustion*, The Combustion Institute, Pittsburgh, 1986, p. 841.
42. Dean, A. M., and Westmoreland, P. R., *Int. J. Chem. Kinet.* 19:207–228 (1987).
43. Wang, H., Ph.D. Thesis, The Pennsylvania State University, University Park, PA, 1992.
44. Miller, J. A., and Bowman, C. T., *Prog. Energy Combust. Sci.* 15:287–338 (1989).
45. Homann, K. H., and Wellmann, C., *Ber. Bunsenges. Phys. Chem.* 87:609–614 (1983).
46. Braun-Unkhoff, M., Frank, P., and Just, T., *Twenty-Second Symposium (International) on Combustion*, The Combustion Institute, Pittsburgh, 1989, p. 1053.
47. Wu, C. H., and Kern, R. D., *J. Phys. Chem.* 91:6291–6296 (1987).
48. Hidaka, Y., Nakamura, T., Miyauchi, A., Shiraishi, T., and Kawano, H., *Int. J. Chem. Kinet.* 21:643–666 (1989).
49. Slagle, I. R., and Gutman, D., *Twenty-First Symposium (International) on Combustion*, The Combustion Institute, Pittsburgh, 1988, p. 875.
50. Hammond, B. L., Huang, S.-Y., Lester, W. A., Jr., and Dupuis, M., *J. Phys. Chem.* 94:7969–7972 (1990).
51. Liu, A., Mulac, W., and Jonah, C. D., *J. Phys. Chem.* 92:131–134 (1988).
52. Homann, K. J., and Wellman, Ch., *Ber. Bunsenges. Phys. Chem.* 87:527–533 (1983).
53. Perry, R. A., *Combust. Flame* 58:221–227 (1984).
54. Slagle, I. R., Bernhardt, J. R., and Gutman, D., *Twenty-Second Symposium (International) on Combustion*, The Combustion Institute, Pittsburgh, 1989, p. 953.
55. Gutman, D., Slagle, A., Bencsura, A., and Xing, S.-B., *ACS Preprints, Div. Fuel Chem.* 36:1509–1517 (1991).
56. Tsang, W., *J. Phys. Chem. Ref. Data* 20:221–273 (1991).
57. Kiefer, J. H., Mizerka, L. J., Patel, M. R., and Wei, H.-C., *J. Phys. Chem.* 89:2013–2019 (1985).
58. Baulch, D. L., Cobos, C. J., Cox, R. A., Frank, P., Hayman, G., Just, Th., Kerr, J. A., Murrells, T., Pilling, M. J., Troe, J., Walker, R. W., and Warnatz, J., *J. Phys. Chem. Ref. Data* 21:411–736 (1992).
59. Fahr, A., and Stein, S. E., *Twenty-Second Symposium (International) on Combustion*, The Combustion Institute, Pittsburgh, 1989, p. 1023.
60. Lin, C.-Y., and Lin, M. C., *J. Phys. Chem.* 90:425–431 (1986).
61. He, Y. Z., Mallard, W. G., and Tsang, W., *J. Phys. Chem.* 92:2196–2201 (1988).

62. Emdee, J. L., Brezinsky, K., and Glassman, I., *J. Phys. Chem.* 96:2151–2161 (1992).
63. Kee, R. J., Rupley, F. M., and Miller, J. A., *The Chemkin Thermodynamic Database*, Sandia National Laboratories, Report No. SAND 87-8215, 1987.
64. Burcat, A., McBride, B., and Rabinowitz, M. J., 1990 *Ideal Gas Thermodynamic Data for Compounds Used in Combustion*, Technion Report No. T.A.E. 657, 1990.
65. Stull, D. R., Westrum, E. F., Jr., and Sinke, G. C., *The Chemical Thermodynamics of Organic Compounds*, Wiley, New York, 1969.
66. Troe, J. *Ber. Bunsenges. Phys. Chem.* 87:161–169 (1983).
67. Kiefer, J. H., and Von Drasek, W. A., *Int. J. Chem. Kinet.* 22:747–786 (1990).
68. Colket, M. B., Seery, D. J., and Palmer, H. B., *Combust. Flame* 75:343–366 (1989).
69. Frenklach, M., and Wang, H., *ACS Prep. Div. Fuel Chem.* 36:1509–1517 (1991).
70. Frank, P., Herzler, J., Just, Th., and Wahl, C., *Twenty-Fifth Symposium (International) on Combustion*, The Combustion Institute, Pittsburgh, 1994, p. 833.
71. Yu, T., and Lin, M. C., *J. Am. Chem. Soc.* 116:9571–9576 (1994).
72. Mebel, A. M., and Lin, M. C., *J. Am. Chem. Soc.* 116:9577–9584 (1994).
73. Hsu, D. S. Y., Lin, C. Y., and Lin, M. C., *Twentieth Symposium (International) on Combustion*, The Combustion Institute, Pittsburgh, 1984, p. 623.
74. Kee, R. J., Rupley, F. M., and Miller, J. A., *Chemkin-II: A Fortran Chemical Kinetics Package for the Analysis of Gas Phase Chemical Kinetics*, Sandia National Laboratories Report No. SAND 89-8009B, 1989.
75. Kee, R. J., Grcar, J. F., Smooke, M. D., and Miller, J. A., *A Fortran Program for Modeling Steady Laminar One-Dimensional Premixed Flames*, Sandia National Laboratories Report No. SAND 85-8240, 1985.
76. Kee, R. J., Warnatz, J., and Miller, J. A., *A Fortran Computer Program Package for the Evaluation of Gas-Phase Viscosities, Conductivities, and Diffusion Coefficients*, Sandia National Laboratories, Report No. SAND 83-8209, 1983.
77. Wenz, H. W., Thesis Dissertation, Technische Hochschule Darmstadt, FRG, 1983.
78. Castaldi, M. J., Marinov, N. M., Melius, C. F., Huang, J. Senkan, S. M., Pitz, W. J., and Westbrook, C. K., *Twenty-Sixth Symposium (International) on Combustion*, The Combustion Institute, Pittsburgh, to appear.
79. Gilbert, R. G., and Smith, S. C., *Theory of Unimolecular and Recombination Reactions*, Blackwell, Oxford, 1990.

Received 27 March 1996; accepted 14 October 1996

APPENDIX

RRKM calculations were performed for a number of key reactions included in the reaction mechanism of Table 1. Most of these reactions are chemically activated, involving the stabilization and isomerization of the hot adduct. The computational methodology and

TABLE A1

RRKM Parameters for Reaction $C_2H_4 + C_2H_3 \rightarrow$ Products

Adducts												
n-C_4H_7	ν (cm^{-1})	128	136	339	444	584	732	866	905	943	970	1002
		1055	1197	1212	1247	1274	1333	1355	1414	1791	2868	2934
		3031	3059	3091	3107	3132						
	B_0 (cm^{-1})	0.14 (1, 2)[a] external inactive; 0.93 (1, 1)[a] external active										
	L-J parameters	σ = 5.18 Å; ε/k_B = 357 K										
Transition States												
n-$C_4H_7 \rightarrow C_4H_6 + H$		E_0 = 35.9 kcal/mol										
	ν (cm^{-1})	280	312	471	517	674	914	925	951	1400	964	1010
		1012	1240	1251	1272	1347	1387	1758	1800	3016	3032	3053
		3057	3087	3088								
	B_0 (cm^{-1})	0.14 (1, 2)[a] external inactive; 1.12 (1, 1)[a] external active										
		8.0 (1, 1)[a] internal active										
Reaction path degeneracy		2										
$nC_4H_7 \rightarrow C_2H_4 + C_2H_3$		E_0 = 43.6 kcal/mol										
	ν (cm^{-1})	231	299	338	353	764	794	797	865	886	957	982
		1021	1116	1300	1324	1354	1641	1759	3000	3033	3056	3058
		3062	3084	3206								
	B_0 (cm^{-1})	0.14 (1, 2)[a] external inactive; 0.56 (1, 1)[a] external active										
		1.20 (1, 1)[a] internal active										
Reaction path degeneracy		1										
	$-\langle E_{down} \rangle$	260 kcal/mol for Ar and N_2										

[a] The numbers in the parentheses are for the symmetry number and the dimension of the rotor, in that order.

procedures of the RRKM calculation are documented elsewhere [24]. Here, only a few important points are emphasized. For molecule–radical combination reactions, the transition state was obtained by semiempirical quantum mechanical AM1 calculations. The energy barrier was then obtained by fitting the available experimental data. The vibrational frequencies were systematically adjusted in the same fashion as documented in Ref. 24. For radical–radical combination reactions, the energy barrier is assumed to be equal to zero, and vibrational and rotational properties of the transition state were obtained from the two radical fragments. The rotational constant of the two degenerate, external rotational degrees of freedom was obtained by fitting an assumed rate coefficient at the high-pressure limit. The RRKM parameters for the examined reactions are presented and key points emphasized in the following text.

Reaction $C_2H_4 + C_2H_3 \rightarrow$ Products

The title reaction involves the addition of C_2H_3 to C_2H_4, followed by stabilization of the hot n-C_4H_7 adduct or dissociation of the adduct to 1,3-C_4H_6 + H:

$$C_2H_4 + C_2H_3 \rightleftharpoons [n\text{-}C_4H_7]^* \rightarrow 1,3\text{-}C_4H_6 + H.$$
$$\downarrow$$
$$n\text{-}C_4H_7$$

TABLE A2

RRKM Parameters for Reaction Benzene + Phenyl → Products

Adduct												
P_2-H	υ (cm^{-1})	76	142	211	294	361	394	424	491	479	587	590
		595	625	647	735	769	791	820	847	883	911	923
		934	937	940	958	1012	1050	1064	1112	1118	1119	1125
		1139	1146	1163	1181	1194	1252	1257	1303	1316	1357	1367
		1419	1490	1547	1592	1651	1674	1686	2758	2977	3009	3014
		3018	3021	3022	3027	3030	3038	3042				
	B_0 (cm^{-1})	0.030 (1, 3)[a] external inactive; 0.266 (1, 1)[a] internal active										
	L-J parameters	σ = 6.31 Å; ε/k_B = 677 K										
Transition States												
P_2-H → P_2 + H		E_0 = 20.0 kcal/mol										
	υ (cm^{-1})	114	138	241	313	338	394	398	490	528	529	553
		607	618	625	636	677	750	776	804	846	865	897
		913	936	940	943	958	982	1043	1094	1107	1110	1130
		1132	1139	1164	1171	1199	1217	1248	1251	1300	1393	1470
		1496	1506	1600	1656	1671	1674	1693	3014	3016	3021	3021
		3024	3026	3028	3030	3033	3039					
	B_0 (cm^{-1})	0.030 (1, 3)[a] external inactive; 0.369 (2, 1)[a] internal active										
	Reaction path degeneracy	2										
P_2-H → A_1 + A_1-		E_0 = 22.1 kcal/mol										
	υ (cm^{-1})	141	150	297	394	395	447	575	571	580	611	612
		618	715	729	837	840	844	868	881	934	939	945
		948	969	973	1059	1079	1082	1094	1120	1124	1134	1156
		1162	1183	1218	1219	1242	1257	1290	1447	1478	1488	1493
		1621	1635	1649	1717	2994	3015	3019	3021	3025	3026	3028
		3029	3033	3040	3046							
	B_0 (cm^{-1})	0.029 (1, 3)[a] external inactive; 35.0 (1, 2)[a] internal active 0.24 (1, 1)[a] internal active										
	Reaction path degeneracy	1										
	$-\langle E_{down} \rangle$	260 kcal/mol for Ar and N_2										

[a] The numbers in the parentheses are the symmetry number and the dimension of the rotor, in that order.

The RRKM parameters were estimated in the same fashion as documented in Ref. 24 and are provided in Table A1.

Reaction $A_1 + A_1 \rightarrow$ Products

The title reaction involves the addition of phenyl to benzene, followed by stabilization of the hot phenyl-benzene adduct or dissociation of the adduct to biphenyl + H:

$$A_1 + A_1 \rightleftharpoons [P_2\text{-}H]^* \rightarrow P_2 + H.$$
$$\downarrow$$
$$P_2\text{-}H$$

The RRKM parameters were estimated in the same fashion as documented in Ref. 24 and are provided in Table A2.

Reaction n-$C_4H_3 + H \rightarrow$ Products

The chemically activated reaction of n-C_4H_3 + H is illustrated by

$$C_2H_2 + H_2CC \text{ and } C_4H_2 + H_2$$
$$\uparrow$$
$$n\text{-}C_4H_3 + H \rightleftharpoons [C_4H_4]^* \rightarrow i\text{-}C_4H_3 + H.$$
$$\downarrow$$
$$C_4H_4$$

It is assumed as in the work of Kiefer and Von Drasek [67] that 20% of the $C_2H_2 + H_2CC$ (vinylidene) channel yields $C_4H_2 + H_2$. The energy barrier of C_4H_4 dissociation into $C_2H_2 + H_2CC$ was also taken from Ref. 67. The high-pressure limit rate coefficients of n-$C_4H_3 + H$ and i-$C_4H_3 + H$ were assumed to

TABLE A3

RRKM Parameters for Reaction n-$C_4H_3 + H \rightarrow$ Products

Adduct												
C_4H_4	υ (cm^{-1})	220	300	540	620	620	680	870	930	970	1100	1310
		1410	1600	2110	3030	3070	3120	3330				
	B_0 (cm^{-1})	0.150 (1, 2)[a] external inactive										
	L-J parameters	σ = 5.18 Å; ε/k_B = 357 K										
Transition States												
$C_4H_4 \rightarrow C_2H_2 + H_2CC$		E_0 = 79.5 kcal/mol										
	υ (cm^{-1})	200	300	320	360	360	500	870	930	970	1100	1310
		1410	2110	3030	3070	3120	3330					
	B_0 (cm^{-1})	0.0754 (1, 2)[a] external inactive										
	Reaction path degeneracy	1										
$C_4H_4 \rightarrow i$-$C_4H_3 + H$		E_0 = 101.03 kcal/mol										
	υ (cm^{-1})	149	231	242	364	381	459	763	795	963	1367	1462
		1536	2910	2996	3200							
	B_0 (cm^{-1})	$48.04 - 10.1036T + 1.71 \times 10^{-4}T^2 - 9.29 \times 10^{-8}T^3 + 1.72 \times 10^{-11}T^4$ (1, 2)[a, b] external inactive; 0.14 (1, 2)[a] internal active										
	Reaction path degeneracy	1										
$C_4H_4 \rightarrow n$-$C_4H_3 + H$		E_0 = 109.63 kcal/mol										
	υ (cm^{-1})	222	326	530	584	605	671	762	790	983	1168	1361
		1846	2907	3043	3223							
	B_0 (cm^{-1})	$16.18 - 4.13 \times 10^{-3}T + 2.18 \times 10^{-5}T^2 - 6.70 \times 10^{-9}T^3$ (1, 2)[a, b] external inactive; 0.15 (1, 1)[a] internal active; 0.16 (1,1)[a, b] internal active										
	Reactionary path degeneracy	2										
	$-\langle E_{down} \rangle$	260 cm^{-1} for Ar and N_2										

[a] The numbers in the parentheses are the symmetry number and the dimension of the rotor, in that order.

[b] The rotational constant is fitted as a function of temperature such that the high-pressure limit rate coefficient of the reverse addition reaction is equal to 1×10^{14} cm^3 mol^{-1} s^{-1}.

be equal to 1×10^{14} cm^3 mol^{-1} s^{-1}. The RRKM parameters are provided in Table A3.

Reaction n-C_4H_5 + H → Products

The chemically activated reaction of n-C_4H_5 + H involves the following steps:

$$\begin{array}{ccc} & C_2H_3 + C_2H_3 & \\ & \uparrow & \\ n\text{-}C_4H_5 + H \rightleftharpoons & [1,3\text{-}C_4H_6]^* & \rightarrow i\text{-}C_4H_5 + H. \\ & \downarrow & \\ & C_4H_6 & \end{array}$$

The RRKM calculations are similar to n-C_4H_3 + H reactions just discussed. It is assumed that the high-pressure limit rate coefficients for H addition to both n-C_4H_5 and i-C_4H_5 are equal to 1×10^{14} cm^3 mol^{-1} s^{-1}, and that of the C_2H_3 recombination is 1×10^{13} cm^3 mol^{-1} s^{-1} [39]. The RRKM parameters are provided in Table A4.

Reaction n-$A_1C_2H_2$ + H → Products

The chemically activated reaction of n-$A_1C_2H_2$ + H involves the following steps:

$$\begin{array}{ccc} & A_1\text{-} + C_2H_3 & \\ & \uparrow & \\ n\text{-}A_1C_2H_2 + H \rightleftharpoons & [A_1C_2H_3]^* & \rightarrow i\text{-}A_1C_2H_2 + H. \\ & \downarrow & \\ & A_1C_2H_3 & \end{array}$$

TABLE A4

RRKM Parameters for Reaction n-C_4H_5 + H → Products

Adduct		
1,3-C_4H_6	v (cm^{-1})	167 312 471 517 674 914 925 951 964 1010 1012 1240 1251 1272 1347 1387 1758 1800 3016 3032 3053 3057 3087 3088
	B_0 (cm^{-1})	0.140 (2, 2)[a] external inactive; 1.39 (1, 1)[a] external active
	L-J parameters	σ = 5.18 Å; ε/k_B = 357 K
Transition States		
1,3-C_4H_6 → i-C_4H_5 + H		E_0 = 101.8 kcal/mol
	v (cm^{-1})	232 308 451 540 667 829 900 917 944 1032 1055 1219 1276 1342 1745 2026 2970 2997 3044 3067 3094
	B_0 (cm^{-1})	$1.76 + 1.45 \times 10^{-3}T + 9.58 \times 10^{-7}T^2 - 4.33 \times 10^{-10}T^3$ (1, 2)[a,b] external inactive; 1.53 (1, 1)[a] internal active; 0.14 (1, 2)[a] internal active
Reaction path degeneracy		1
1,3-C_4H_6 → n-C_4H_5 + H		E_0 = 109.6 kcal/mol
	v (cm^{-1})	186 252 417 540 545 765 841 926 941 1015 1136 1188 1268 1340 1778 1795 2988 3045 3060 3089 3319
	B_0 (cm^{-1})	$3.43 + 2.83 \times 10^{-3}T + 2.23 \times 10^{-6}T^2 - 9.87 \times 10^{-10}T^3$ (1, 2)[a,b] external inactive; 1.56 (1, 1)[a] internal active; 0.15 (1,2)[a] internal active
Reaction path degeneracy		2
1,3-C_4H_6 → C_2H_3 + C_2H_3		E_0 = 115.5 kcal/mol
	v (cm^{-1})	738 738 779 779 819 819 956 956 1288 1288 1779 1779 2987 2987 3043 3043 3332 3332
	B_0 (cm^{-1})	$0.153 + 3.94 \times 10^{-4}T + 8.21 \times 10^{-8}T^2 - 5.90 \times 10^{-11}T^3$ (1, 2)[a,c] external inactive; 1.02 (1, 2)[a] internal active; 1.01 (1, 2)[a] internal active; 9.4 (1, 2)[a] internal active
Reaction path degeneracy		1
$-\langle E_{down} \rangle$		260 cm^{-1} for Ar and N_2

[a] The numbers in the parentheses are the symmetry number and the dimension of the rotor, in that order.

[b] The rotational constant is fitted as a function of temperature such that the high-pressure limit rate coefficient, $k_{-,\infty}$, of the reverse addition reaction is equal to 1×10^{14} cm^3 mol^{-1} s^{-1}.

[c] Fitted such that $k_{-,\infty} = 1 \times 10^{13}$ cm^3 mol^{-1} s^{-1}.

The RRKM calculations are similar to n-C_4H_3 + H reactions. It is assumed that the high-pressure limit rate coefficients for H addition to both n-$A_1C_2H_2$ and i-$A_1C_2H_2$ are equal to 1×10^{14} cm^3 mol^{-1} s^{-1}, and that of the A_1- and C_2H_3 combination is 6×10^{12} cm^3 mol^{-1} s^{-1}. The RRKM parameters are provided in Table A5.

Reaction Phenyl + Phenyl → Products

The chemically activated reaction of A_1- + A_1- involves the following steps:

$$A_1\text{-} + A_1\text{-} \rightleftharpoons [P_2]^* \rightarrow P_2\text{-} + H$$
$$\downarrow$$
$$P_2$$

TABLE A5

RRKM Parameters for Reaction n-Styryl + H → Products

Adduct												
$A_1C_2H_3$	υ (cm^{-1})	100	172	240	396	451	471	561	578	631	662	778
		852	853	906	941	948	967	1000	1011	1071	1128	1145
		1150	1186	1248	1272	1330	1336	1400	1504	1570	1690	1709
		1789	3018	3052	3055	3056	3061	3064	3074	3087		
	B_0 (cm^{-1})	0.046 (1, 2)[a] external inactive; 0.17 (1, 1)[a] external active										
	L-J parameters	σ = 6.0 Å; ε/k_B = 546 K										
Transition States												
$A_1C_2H_3 \rightarrow i$-$A_1C_2H_2$ + H		E_0 = 101.9 kcal/mol										
	υ (cm^{-1})	135	176	377	397	421	495	521	622	644	675	783
		795	836	919	927	937	968	978	1044	1116	1135	1152
		1183	1219	1254	1313	1345	1490	1543	1676	1703	2027	2990
		3040	3051	3059	3063	3072	3079					
	B_0 (cm^{-1})	1.94 + 1.29 × 10^{-3}T + 9.09 × 10$^{-7}T^2$ − 4.10 × 10$^{-10}T^3$ (1, 2)[a,b] external inactive; 0.044 (1, 2)[a] internal active; 0.185 (1, 1)[a] internal active										
Reaction path degeneracy		1										
$A_1C_2H_3 \rightarrow n$-$A_1C_2H_2$ + H		E_0 = 109.7 kcal/mol										
	υ (cm^{-1})	148	183	185	398	404	442	470	604	612	631	743
		784	835	858	884	925	951	972	1056	1115	1128	1145
		1153	1178	1258	1322	1374	1503	1572	1690	1708	1795	2978
		3055	3058	3061	3063	3075	3313					
	B_0 (cm^{-1})	2.71 + 3.91 × 10^{-3}T + 1.57 × 10$^{-6}T^2$ − 8.49 × 10$^{-10}T^3$ (1, 2)[a,b] external active; 0.048 (1, 2)[a] internal active; 0.172 (1,1)[a] internal active										
Reaction path degeneracy		2										
$A_1C_2H_3 \rightarrow A_1$- + C_2H_2		E_0 = 113.9 kcal/mol										
	υ (cm^{-1})	779	738	819	956	1288	1779	2987	3043	3332	432	450
		571	614	621	780	886	935	967	983	986	1070	1096
		1145	1148	1234	1238	1309	1465	1514	1633	1766	3072	3078
		3085	3105	3125								
	B_0 (cm^{-1})	0.21 + 4.16 × 10^{-4}T + 8.16 × 10$^{-9}T^2$ − 3.31 × 10$^{-11}T^3$ (1, 2)[a,c] external inactive; 1.01 (1, 2)[a] internal active; 0.135 (1, 2)[a] internal active; 9.64 (1, 1)[a] internal active; 0.213 (2, 1)[a] internal active										
Reaction path degeneracy		1										
	$-\langle E_{down} \rangle$	260 cm^{-1} for Ar and N_2										

[a] The numbers in the parentheses are the symmetry number and the dimension of the rotor, in that order.

[b] The rotational constant is fitted as a function of temperature such that the high-pressure limit rate coefficient, $k_{-,\infty}$, of the reverse addition reaction is equal to 1×10^{14} cm^3 mol^{-1} s^{-1}.

[c] Fitted such that $k_{-,\infty} = 6 \times 10^{12}$ cm^3 mol^{-1} s^{-1}.

It is assumed that the high-pressure limit rate coefficient for H addition to P_2- is equal to 1×10^{14} cm^3 mol^{-1} s^{-1}, and that of the phenyl recombination is 3×10^{12} cm^3 mol^{-1} s^{-1} [59]. The RRKM parameters are provided in Table A6.

Aromatic Radicals + H → Aromatic Molecules

The reactions of H addition to phenyl (A_1-), naphthyl (A_2-), and phenanthryl (A_3-) and the chemically activated process, when applicable, are considered for RRKM analysis. These reactions are

$$A_1\text{-} + H \rightleftharpoons A_1 \qquad \text{(R365)}$$

$$A_2\text{-}1 + H \rightleftharpoons [A_2]^* \rightarrow A_2\text{-}2 + H$$
$$\downarrow$$
$$A_2$$

$$A_3\text{-}4 + H \rightleftharpoons [A_3]^* \rightarrow A_3\text{-}1 + H$$
$$\downarrow$$
$$A_3$$

where A_2-1 and A_2-2 are 1- and 2-naphthyl

TABLE A6

RRKM Parameters for Reaction Phenyl + Phenyl → Products

Adduct												
P_2	υ (cm^{-1})	103	140	243	332	380	390	400	526	500	613	621
		623	627	655	754	785	803	843	847	898	917	937
		940	954	957	980	1041	1095	1107	1113	1133	1135	1138
		1163	1175	1219	1249	1250	1297	1312	1394	1470	1499	1508
		1608	1668	1671	1690	1695	3020	3021	3021	3021	3025	3026
		3029	3030	3038	3039							
	B_0 (cm^{-1})	0.017 (2, 2)[a] external inactive; 0.095 (2, 1)[a] internal active										
		0.38 (2, 1)[a] internal active										
	L-J parameters	σ = 6.31 Å; ε/k_B = 677 K										
Transition States												
$P_2 \rightarrow P_2$-+ H		E_0 = 109.4 kcal/mol										
	υ (cm^{-1})	114	177	238	377	394	408	445	458	501	609	616
		621	632	676	775	803	805	848	878	932	938	948
		966	968	979	1028	1086	1119	1123	1130	1138	1143	1175
		1216	1225	1262	1285	1309	1394	1432	1490	1506	1588	1630
		1668	1689	1764	3015	3025	3028	3032	3036	3038	3043	3049
		3066										
	B_0 (cm^{-1})	$25.07 - 1.02 \times 10^{-2}T + 3.87 \times 10^{-5}T^2 - 1.98 \times 10^{-8}T^3 + 3.13 \times 10^{-12}T^4$ (1, 2)[a,b] external active; 0.017 (1, 2)[a] internal active; 0.098 (1, 1)[a] internal active										
		0.379 (2, 1)[a] internal active										
	Reaction path degeneracy	10										
$P_2 \rightarrow A_1$-+ A_1-		E_0 = 113.2 kcal/mol										
	υ (cm^{-1})	432	450	571	614	621	780	886	935	967	983	986
		1070	1096	1145	1148	1234	1238	1309	1465	1514	1633	1766
		3072	3078	3085	3105	3125	432	450	571	614	621	780
		886	935	967	983	986	1070	1096	1145	1148	1234	1238
		1309	1465	1514	1633	1766	3072	3078	3085	3105	3125	
	B_0 (cm^{-1})	$0.252 + 3.33 \times 10^{-4}T - 4.91 \times 10^{-8}T^2$ (1, 2)[a,c] external active;										
		0.135 (1, 2)[a] internal active; 0.135 (1,2)[a] internal active										
		0.213 (2, 2)[a] internal active										
	Reaction path degeneracy	2										
	$-\langle E_{down} \rangle$	260 cm^{-1} for Ar and N_2										

[a] The numbers in the parentheses are the symmetry number and the dimension of the rotor, in that order.

[b] The rotational constant is fitted as a function of temperature such that the high-pressure limit rate coefficient, $k_{-,\infty}$, of the reverse addition reaction is equal to 1×10^{14} cm^3 mol^{-1} s^{-1}.

[c] Fitted such that $k_{-,\infty} = 3 \times 10^{12}$ cm^3 mol^{-1} s^{-1}.

TABLE A7

RRKM Parameters for Reaction Phenyl + H → Benzene

Adduct												
A_1	υ (cm^{-1})	410	410	606	606	673	703	849	849	975	975	992
		995	1010	1038	1038	1150	1178	1178	1310	1326	1486	1486
		1596	1596	3047	3047	3062	3063	3063	3068			
	B_0 (cm^{-1})	0.190 (1, 2)[a] external inactive; 0.094 (1, 1)[a] external active										
	L-J parameters	σ = 5.29 Å; ε/k_B = 465 K										
Transition States												
$A_1 \rightarrow A_1$-+ H		E_0 = 109.27 kcal/mol										
	υ (cm^{-1})	410	410	606	606	673	703	849	849	975	992	995
		1010	1038	1150	1178	1178	1310	1326	1486	1486	1596	1596
		3047	3047	3062	3063	3068						
	B_0 (cm^{-1})	$7.13 - 0.058T + 1.61 \times 10^{-4}T^2 - 1.72 \times 10^{-7}T^3 + 8.95 \times 10^{-11}T^4 - 2.32 \times 10^{-14}T^5 - 2.38 \times 10^{-18}T^6$ (1, 1)[a,b] external inactive; 0.0197 (1, 2)[a] internal active; 0.098 (1, 1)[a] internal active										
	Reaction path degeneracy	6										
	$-\langle E_{down} \rangle$	300 kcal/mol										

[a] The numbers in the parentheses are the symmetry number and the dimension of the rotor, in that order.

[b] The rotational constant is fitted as a function of temperature such that the high-pressure limit rate coefficient of the reverse addition reaction is equal to 1×10^{14} cm^3 mol^{-1} s^{-1}.

TABLE A8

RRKM Parameters for Reaction Naphthyls + H → Naphthalene

Adduct												
A_2	υ (cm^{-1})	171	173	329	379	417	451	517	517	523	627	712
		738	793	807	846	887	904	912	916	934	946	952
		1104	1110	1126	1142	1144	1145	1215	1249	1256	1380	1385
		1449	1519	1532	1603	1661	1696	1708	3010	3010	3012	3012
		3018	3018	3025	3026							
	B_0 (cm^{-1})	0.035 (2, 2)[a] external inactive; 0.104 (1, 1)[a] external active										
	L-J parameters	σ = 6.18 Å; ε/k_B = 630 K										
Transition States												
$A_2 \rightarrow A_2$-2 + H		E_0 = 109.28 kcal/mol										
	υ (cm^{-1})	180	184	363	385	447	490	516	522	580	624	726
		761	797	858	878	900	912	915	922	936	951	1077
		1106	1111	1134	1145	1182	1241	1261	1348	1382	1444	1502
		1524	1607	1646	1707	1744	3010	3011	3018	3024	3026	3046
		3051										
	B_0 (cm^{-1})	$5.13 - 2.58 \times 10^{-3}T + 8.96 \times 10^{-6}T^2 - 4.58 \times 10^{-9}T^3 + 6.88 \times 10^{-13}T^4$ (1, 2)[a,b] external inactive; 0.036 (1, 2)[a] internal active; 0.104 (1, 1)[a] internal active										
	Reaction path degeneracy	4										
$A_2 \rightarrow A_2$-1 + H		E_0 = 109.70 kcal/mol										
	υ (cm^{-1})	182	208	373	375	422	512	515	526	527	626	713
		787	806	834	899	910	912	946	964	970	995	1089
		1106	1121	1135	1145	1171	1228	1247	1353	1390	1424	1506
		1531	1569	1641	1698	1777	3014	3027	3029	3035	3037	3039
		3063										
	B_0 (cm^{-1})	$4.70 - 1.75 \times 10^{-3}T + 7.71 \times 10^{-6}T^2 - 3.94 \times 10^{-9}T^3 + 5.80 \times 10^{-13}T^4$ (1, 2)[a,b] external inactive; 0.035 (1, 2)[a] internal active; 0.111 (1,1)[a] internal active										
	Reaction path degeneracy	4										
	$-\langle E_{down} \rangle$	260 cm^{-1} for Ar and N_2										

[a] The numbers in the parentheses are the symmetry number and the dimension of the rotor, in that order.

[b] The rotational constant is chosen such that the high-pressure limit rate coefficient of the reverse addition reaction is equal to 1×10^{14} cm^3 mol^{-1} s^{-1}.

radicals, and A_3-1 and A_3-4 are 1- and 4-phenanthryl radicals. All high-pressure limit rate coefficients for H addition to the aromatic radicals are assumed to be equal to 1×10^{14} cm^3 mol^{-1} s^{-1}. The RRKM parameters are provided in Table A7, A8, and A9 for phenyl, naphthyl, and phenanthryl, respectively. The RRKM results obtained for H and phenyl combination were compared to literature data as shown in Fig. A1. It is seen that the experimental data of Hsu et al. [73] (M = Ar) and Kiefer et al. [57] (M = Kr) are well reproduced with reasonable $\langle E_{down} \rangle$ values of 260 and 650 cm^{-1} for argon and krypton, respectively. The RRKM calculations show that the pressure fall-off for the rate coefficient of H and phenyl combination is significant at combustion temperatures. For example, the results show that $k_{365}/k_{365,\infty} = 0.3$ at 1800 K and 90 torr. Therefore, assigning the high-pressure limit rate coefficient for the H and phenyl combination reaction in kinetic modeling of aromatics formation may significantly underpredict the phenyl concentration in flames.

TABLE A9

RRKM Parameters for Reaction Phenanthryls + H → Phanathrene

Adduct												
A_3	υ (cm^{-1})	87	95	200	209	256	336	384	421	445	451	488
		512	513	562	620	647	728	738	747	777	792	822
		862	864	866	899	909	915	930	941	943	1062	1108
		1110	1124	1133	1137	1139	1151	1218	1243	1252	1279	1324
		1370	1396	1417	1482	1488	1554	1575	1617	1646	1680	1685
		1699	2984	2987	2989	2990	2991	2994	2995	2997	3004	3005
	B_0 (cm^{-1})		0.054 (1, 2)[a] external inactive; 0.016 (1, 1)[a] external active									
	L-J parameters		σ = 6.96 Å; ε/k_B = 772 K									
Transition States												
$A_3 \rightarrow A_3$-1 + H			E_0 = 110.7 kcal/mol									
	υ (cm^{-1})	100	121	202	220	232	355	411	420	453	464	507
		508	563	586	617	668	727	750	781	793	806	851
		862	870	890	896	918	929	936	945	1070	1083	1105
		1110	1130	1133	1139	1165	1217	1237	1261	1313	1362	1397
		1421	1470	1491	1564	1572	1591	1638	1679	1691	1757	2986
		2986	2987	2994	2996	2997	3003	3006	3027			
	B_0 (cm^{-1})		$-0.203 + 4.33 \times 10^{-3}T - 1.23 \times 10^{-6}T^2 + 1.22 \times 10^{-9}T^3 - 4.21 \times 10^{-13}T^4$ (1, 2)[a, b] external inactive; 0.016 (1, 2)[a] internal active; 0.055 (1, 1)[a] internal active									
	Reaction path degeneracy		2									
$A_3 \rightarrow A_3$-4 + H			E_0 = 109.7 kcal/mol									
	υ (cm^{-1})	94	103	212	219	253	357	412	423	451	458	505
		516	562	566	620	673	724	740	759	792	827	844
		864	868	888	894	913	930	935	943	1053	1088	1112
		1116	1132	1137	1141	1186	1229	1246	1277	1320	1359	1398
		1421	1476	1489	1542	1566	1593	1634	1684	1693	1757	2986
		2987	2989	2994	2996	2998	3005	3008	3031			
	B_0 (cm^{-1})		$-1.06 + 2.17 \times 10^{-2}T - 5.48 \times 10^{-6}T^2 + 5.50 \times 10^{-9}T^3 - 1.96 \times 10^{-12}T^4$ (1, 2)[a, b] external inactive; 0.016 (1, 2)[a] internal active; 0.054 (1,1)[a] internal active									
	Reaction path degeneracy		8									
	$-\langle E_{down} \rangle$		260 kcal/mol for Ar and N_2									

[a] The numbers in the parentheses are the symmetry number and the dimension of the rotor, in that order.

[b] The rotational constant is chosen such that the high-pressure limit rate coefficient of the reverse addition reaction is equal to 1×10^{14} cm^3 mol^{-1} s^{-1}.

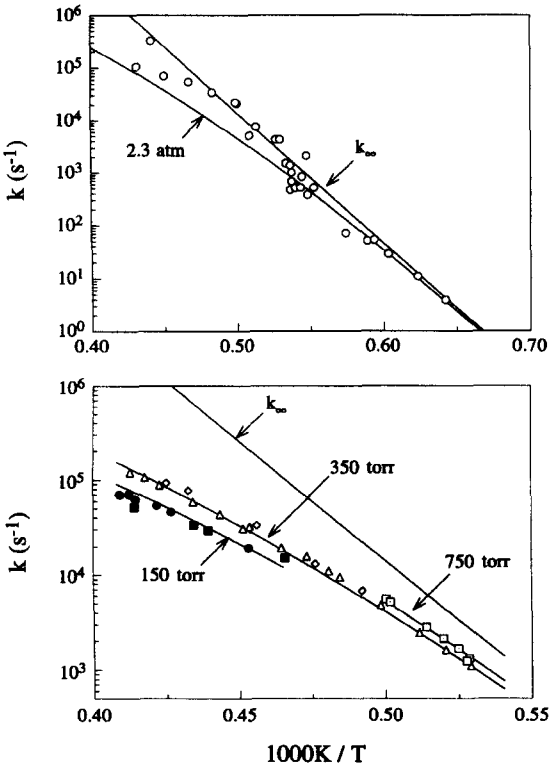

Fig. A1. Experimental (symbols) and calculated (lines) rate coefficient of reaction (R365), A_1- + H(+M) = A_1(+M). Experimental data: top panel, M = argon (Hsu et al. [73]); bottom panel, M = krypton (Kiefer et al. [57]). The calculations in the pressure fall-off region and the low-pressure limit are made with reasonable $\langle E_{down} \rangle$ values of 260 and 650 cm^{-1} for argon and krypton, respectively.